INFORMATION TO USERS

This manuscript has been reproduced from the microfilm master. UMI films the text directly from the original or copy submitted. Thus, some thesis and dissertation copies are in typewriter face, while others may be from any type of computer printer.

The quality of this reproduction is dependent upon the quality of the copy submitted. Broken or indistinct print, colored or poor quality illustrations and photographs, print bleedthrough, substandard margins, and improper alignment can adversely affect reproduction.

In the unlikely event that the author did not send UMI a complete manuscript and there are missing pages, these will be noted. Also, if unauthorized copyright material had to be removed, a note will indicate the deletion.

Oversize materials (e.g., maps, drawings, charts) are reproduced by sectioning the original, beginning at the upper left-hand corner and continuing from left to right in equal sections with small overlaps.

ProQuest Information and Learning
300 North Zeeb Road, Ann Arbor, MI 48106-1346 USA
800-521-0600

University of Alberta

The Nonlinear Fracture Behaviour of Piezoelectric Materials

By

Liying Jiang 

A thesis submitted to the Faculty of Graduate Studies and Research in partial fufillment of the requirements for the degree of **Doctor of Philosophy**

Department of Mechnical Engineering

Edmonton, Alberta

Spring 2005

Abstract

This dissertation presents a comprehensive theoretical study of the plane strain problem of cracked piezoelectric materials. Existing studies indicate that the commonly used electrically impermeable and permeable crack models may be inadequate in evaluating the fracture behaviour of piezoelectric materials in some cases. This is due to the difficulties in describing the electric boundary condition along crack surfaces. In this project, a dielectric crack model based on the 'real' electric boundary condition is proposed to study the nonlinear fracture properties and electromechanical coupling of cracked piezoelectric materials. The electric boundary condition along the crack surfaces is governed by the opening displacement of the crack, which is deformation-dependent and thus nonlinear.

In the current work, the crack is modelled by continuously distributed dislocations involving both displacement and electric potential jumps. The formulation of this nonlinear problem is based on the use of Fourier transform technique and solving the resulting nonlinear singular integral equations. Numerical simulation is conducted to describe the complicated nonlinear fracture behaviour of piezoelectric materials under different electromechanical loads.

The effect of this nonlinear electric boundary condition upon the fracture behaviour of cracked piezoelectric materials is investigated systematically. Multiple deformation modes are observed and discussed, which are governed by geometric and loading conditions. The results obtained from this dielectric crack model demonstrate how

the transition between electrically impermeable and permeable crack surface conditions occurs with the change of the crack opening displacement in response to the applied electromechanical loading. The asymptotic behaviour of cracked piezoelectric media is provided when two limiting cases, permeable and impermeable conditions, are reached. Unlike the results predicted by the traditional crack models, the fracture behaviour and the effective electroelastic property of cracked piezoelectric media are found to be nonlinear and sensitive to loading conditions. Based on theoretical analyses and existing experimental results, a new fracture parameter, crack opening displacement intensity factor K_{COD}, is introduced to predict the effect of applied electric field upon the crack propagation. This work contributes in understanding the nonlinear nature of piezoelectric materials and improving the design and application of this kind of materials in smart structures.

Acknowledgements

The author wishes to express her most sincere and deepest gratitude to her supervisor, Dr. Xiaodong Wang, for his invaluable advice, guidance, support and kind understanding which made this thesis completion as a pleasant and successful experience.

This thesis is supported by the Andrew Stewart Memorial Graduate Prize, ASME OMAE Calgary Chapter Graduate Scholarship and the Dissertation Fellowship.

Last but not least, I would like to thank all my friends for their help in the course of my study. Special thanks to my husband, Duoduo Li and my family, for their love, support and understanding which make it possible to complete this work today.

Table of Contents

List of Tables

List of Figures

List of Symbols

V	Electric potential
D_i	Electric displacement
ϵ_0	Dielectric permittivity of air (or vacuum)
h	Initial crack surface separation
σ_{ij}	Stress
ε_{ij}	Strain
E_i	Electric field intensity
c_{ijkl}	Elastic constant
e_{ijk}	Piezoelectric constant
ϵ_{ij}	Dielectric constant
u_i	Displacement
a	Half of the crack length
θ	Crack orientation
K_I	Stress intensity factor for crack of Mode I
K_{II}	Stress intensity factor for crack of Mode II
K_D	Electric displacement intensity factor
K_{COD}	Crack opening displacement intensity factor
G	Energy release rate
ρ	Crack density

Chapter 1

Introduction

1.1 Piezoelectricity, Its History and Applications

The piezoelectric effect was first discovered by the brothers Pierre and Jacques Curie (1880) in their experiment to demonstrate a connection between macroscopic piezoelectric phenomena and crystallographic structure. By placing a weight on the surface of crystals, they found that a considerable number of crystalline materials (quartz, tourmaline, Rochelle salt, zinc blende, sodium, cane sugar, topaz and tartaric acid etc) generate electric charge proportional to the applied weight. The converse piezoelectric effect, that is the change in dimensions of a crystal on the application of a voltage, was predicted theoretically by Lippman (1881) on the basis of thermodynamics. This converse piezoelectric effect was later experimentally verified by the Curies (1884). Although some of the relations between piezoelectricity and crystal structure were established by the Curies, it was Voigt (1890), who finally completed the rigorous formulation of the piezoelectric principles. The piezoelectric effect remained more or less a scientific curiosity up to World War I.

The first important application of piezoelectric crystal quartz was to generate

acoustic waves, a method developed by Langevin and coworkers in 1917 to locate submerged vessels using piezoelectric quartz plates glued between steel plates. Langevin did not get his device perfected until after the end of the war, but this Langevin-type transducer was extensively used as a sonic depth finder, and similar devices were used in the present war for detecting submarines (Buchanan, 1956). After World War I, several important applications were developed, such as crystal-controlled oscillator (Cady, 1921), acoustic interferometer (Pierce, 1925), high-power ultrasonics (Wood and Loomis, 1927) and selective filter circuits (Mason, 1934). Since then several books on the phenomenon and theory of piezoelectricity have been written. For example, Cady (1946) and Mason (1950) treated the physical properties of piezoelectric crystals and their application in their work; Tiersten (1964) dealt with the linear equations of vibration in piezoelectric materials; Parton and Kudryavtsev (1988) gave a more detailed description of piezoelectricity; Waanders (1991) provided a detailed discussion on the properties and applications of piezoelectric ceramics; Rogacheva (1994) presented the theory of piezoelectric shells and plates.

1.2 Piezoelectric Ceramics

Besides the natural piezoelectric crystals mentioned above, an important group of piezoelectric materials commonly used nowadays are the piezoelectric ceramics, which we will focus on in the current work. These manufactured ceramics, such as lead zirconate titanate, barium titanate and lead titanate, are more versatile with physical, chemical and piezoelectric characteristics able to be tailored to specific applications.

The traditional piezoelectric ceramics can be considered as a mass of minute crystallites. It is found that these materials exhibit permanent polarization below a critical temperature, Curie point, at which the crystal structure changes from a piezoelectric to a non-piezoelectric form. Below the Curie point, the crystallites exhibit tetragonal or rhombohedral symmetry in which the positive and negative charge sites do not coincide, so each elementary cell has a built-in electric dipole. Neighboring dipoles align with each other to form domains of local alignment. Within a domain, therefore, all the dipoles are aligned, giving a net dipole moment to the domain, and hence a net polarization (dipole moment per unit volume). Owing to the random distribution of domains throughout the material, no overall polarization or piezoelectric effect is exhibited.

The ceramic may be made piezoelectric in any chosen direction by a poling treatment which involves exposing the material to a strong electric field at a temperature slightly below the Curie point. Under the action of this field, domains with different polarization directions are re-oriented towards the direction of the applied electric field. When the electric field is removed most of the dipoles are locked into a configuration of near alignment, giving the ceramic material a remanent polarization. The poling treatment is a very important manufacturing process for piezoelectric ceramics, which induces piezoelectric property as well as materials anisotropy in the ceramics. Piezoelectric ceramics can be depolarized when exposed to excessive temperature, strong electric field, or high stress.

Due to their intrinsic coupling effect between electric and mechanical fields, piezoelectric ceramics have been widely used in electromechanical devices (Pohanka and

Smith, 1988), such as actuators, sensors and transducers. They possess a high degree of linearity, high power density, greater efficiency and potential for low cost manufacturability. As a result, piezoceramic materials are being considered for use in active noise and vibration suppression of aircraft wings, control of satellites and space structures, position control of flexible robot arms, smart skin systems for submarines and shape control of advanced structures (Gandhi and Thompson, 1992; Varadan et al., 1993; Ashley, 1995; Dosch et al., 1995). However, these newly developed piezoelectric ceramics are generally brittle and susceptible to the development of critical cracks during manufacturing and service processes. The existence of these cracks will greatly affect the mechanical integrity and electromechanical behaviour of this class of materials (Winzer et al., 1989; Jain and Sirkis, 1994; Barsoum, 1997; Park et al., 1998). Therefore, the evaluation of the fracture behaviour of these piezoelectric materials is of great importance in the design and application of these materials in smart structures.

1.3 Literature Review

The problem of piezoelectric materials containing cracks has been extensively studied by the researchers (Parton and Kudryavtsev, 1988; Freiman and Pohanka, 1989; Mikhailov and Parton, 1990; Suo, 1991; Suo et al., 1992; Zhang et al., 1998; Sunar and Rao, 1999; Qin, 2001). In the following, an attempt is made to summarize the major research outcomes in different aspects of the study of cracks in piezoelectric materials.

1.3.1 Solution techniques and procedures

Piezoelectric materials with cracks can be modelled as linear anisotropic piezoelectric media, containing cracks filled with air (vacuum). From this linearized piezoelectric model and appropriate electromechanical boundary conditions along crack surfaces, the fracture behaviour of cracks in piezoelectric materials can be predicted. Up to date, a number of solution techniques (procedures) have been developed to solve this kind of problems.

For two-dimensional problems in a general anisotropic piezoelectric material, there are two powerful solution procedures in literature. One is the Lekhnitskii's complex function approach (Lekhnitskii, 1963), which was later extended to the electroelastic problems with cracks (e.g., Sosa, 1991; Xu and Rajapakse, 1999; Qin and Mai, 1999) by using both the well-known Lekhnitskii stress function and the induction function. Another one is the generalized Stroh's formalism (Stroh, 1958) for anisotropic media, which is based on the displacement and electric potential, and equilibrium equations to formulate the electroelastic fields in piezoelectric materials. There are several recent studies (Barnett and Lothe, 1975; Park and Sun, 1995a; Chung and Ting, 1996; Park and Carman, 1997) dealing with elliptic voids or cracks in piezoelectric materials using generalized Stroh's formalism.

Distributed dislocation method used for traditional cracked elastic media (Bilby and Eshelby, 1968), in which a crack is modelled by continuously distributed dislocations, was extended to the piezoelectric case by Barnett and Lothe (1975). They used the generalized Stroh's formalism to treat dislocations and line charges in anisotropic

piezoelectric materials. More detailed discussions on this topic can be found in later works (Deeg, 1980; Pak, 1992; Suo et al., 1992; Meguid and Wang, 1998). The Fourier transform technique has also been used in the crack problems of piezoelectric materials (Yu and Qin, 1996a; Meguid and Wang, 2000a; Yang, 2001). Analogue to the classical theory of elasticity, the potential function method with displacements being expressed in terms of potential functions, has been applied to solve the three-dimensional problems of piezoelectric medium with elliptical cracks (Wang and Huang, 1995). The Williams' eigenfunction expansion method (Williams, 1957) for elastic crack problems was extended by Sosa and Park (1990) to study the singular behaviour of cracks in piezoelectric media.

In addition to these solution methods which are mostly based on analytical approaches, numerical methods have also been used to study the problem of cracked piezoelectric materials, such as the finite element method (Allik and Hughes, 1970; Kumar and Singh, 1997a, b) and the boundary element method (Lu and Mahrenholtz, 1994; Ding et al., 1998).

1.3.2 Electric boundary condition

One of the fundamental issues in studying the fracture behaviour of piezoelectric materials is how to deal with the electric boundary condition along the crack surfaces. Most existing investigations in this area are based on two typical crack models. One is the electrically permeable condition proposed by Parton (1976), the perfect contact of crack surfaces is assumed with the electric potential V and normal component of

the electric displacement D_n being continuous across the crack surfaces, i.e.

$$V^+ = V^-, \quad D_n^+ = D_n^- \tag{1.3.1}$$

where superscripts '+' and '−' represents the upper and lower crack surfaces, respectively. This electrically permeable model has been used to study the fracture of piezoelectric materials under both static and dynamic loads (Polovinkina and Ulitko, 1978; Mikhailov and Parton, 1990; Meguid and Wang, 1998; Wang, 2001; Beom, 2003). The perfect contact condition for permeable crack model may not be physically reasonable in some cases, particularly for piezoelectric ceramics with their electric permittivity being 10^3 times higher than that of the air or vacuum filling the crack. Significant potential drop may occur across the crack even for small crack opening.

The other typical crack model is the electrically impermeable one (Deeg, 1980; Pak, 1990), in which the normal component of electric displacement vanishes along the crack surfaces,

$$D_n^+ = D_n^- = 0 \tag{1.3.2}$$

In this model, the electric induction in the medium filling the crack is neglected. This kind of boundary condition has also been extensively used to study the fracture behaviour of piezoelectric materials (Shindo et al., 1990; Pak, 1992; Suo et al., 1992; Park and Sun, 1995a; Wang and Meguid, 2000a). It should be noted that these traditional crack models represent two limiting cases of the physical problem, where the electric permittivity of the crack is assumed to be infinite and zero, respectively.

In most situations, cracks existing in piezoelectric materials are filled with dielectric medium, such as air or vacuum, which may have significant effects upon the

electromechanical behaviour of the cracked media. To evaluate the effect of the dielectric medium filling the crack upon the electric boundary condition, an elliptical crack model has been developed and used to study the electromechanical behaviour of cracked piezoelectric medium (McMeeking, 1989; Sosa, 1991; Dunn, 1994; Sosa and Khutoryansky, 1996; Zhang et al., 1998). By changing the shape of the crack, different electric boundary conditions can be simulated. These studies indicate that the permeable model may underestimate the effect of electric field on the crack initiation, while the impermeable one may overestimate its effect. Another crack model considering the effect of this dielectric medium is the intermediate crack model (Parton and Kudryavtsev, 1988; Dascalu and Homentcovschi, 2002), in which the crack is represented by a dielectric thin layer with thickness h. The electric boundary condition is defined as,

$$D_n^+ = D_n^-, \quad D_n + \frac{\epsilon_0}{h}(V^+ - V^-) = 0 \tag{1.3.3}$$

with ϵ_0 being the permittivity of the dielectric medium filling the crack. This model can be reduced to the permeable and impermeable ones when the thickness of the layer is very small or relatively large, respectively. However, the thickness of the crack (the layer) must be pre-assumed.

It should be mentioned that in both elliptical and intermediate crack models, the electric boundary condition of the crack is independent of the crack deformation since only the original crack profile is considered. For a slit crack without significant initial crack surface separation, these models will result in an electrically permeable boundary condition. However, the electric boundary condition of a slit crack may

be very sensitive to the crack deformation due to the applied loading. The effect of this crack deformation upon the electric boundary condition and fracture behaviour of piezoelectric materials requires further investigation.

1.3.3 Fracture behaviour of piezoelectric materials

A variety of problems of cracked piezoelectric materials have been investigated by researchers using existing crack models and the above-mentioned techniques. In this part, we will give a review on these studies for the fracture behaviour of piezoelectric materials.

(i) Electroelastic fields and crack tip singularity for a single crack problem

Since the study of electroelastic fields around cracks in piezoelectric medium is fundamentally important to the failure analysis of cracked piezoelectric materials, there have been a lot of work investigating the effects of crack geometry, material properties and applied loads upon these fields under a variety of conditions. Parton (1976) and McMeeking (1990) investigated the problem where the crack was filled with conducting medium. Parton and Kudriyavtsev (1988) obtained the solutions of insulated cracks. They derived fully decoupled stress and electric displacement fields near the crack tip. Pak (1990) obtained a closed form solution to the antiplane problem of a finite crack embedded in an infinite piezoelectric medium. The stress and electric fields of an antiplane crack problem of a piezoelectric strip was investigated by Narita and Shindo (1998). The asymptotic expressions of the coupled electroelastic fields at the tip of a crack in an infinite piezoelectric solid were obtained by Sosa (1992). The

electroelastic field solutions for a semi-infinite crack in an infinite piezoelectric body were provided by Sosa and Pak (1990) and Gao and Yu (1998). To show the effect of crack geometry and orientation upon the electroelastic fields, Xu and Rajapakse (1999) derived the analytical solution for a piezoelectric plane with an arbitrarily oriented elliptical void or a crack to examine the crack tip field and fracture criteria.

The interface crack between piezoelectric bimaterials was first studied by Kuo and Barnett (1991) through the generalized Stroh's method, in which various power-type singularities were found for electroelastic fields depending on different boundary conditions. Suo et al. (1992) showed the possibility of the existence of real as well as oscillating singularities at an interface crack tip.

(ii) Crack interaction

Due to the tendency of developing multiple cracks in piezoelectric materials, the interaction among cracks plays an important role in the fracture analysis of this type of materials. Although the interaction between cracks in traditional materials have been extensively investigated (Rubinstein, 1986; Hutchinson, 1987; Kachanov, 1987; Meguid and Wang, 1995), relatively fewer studies have been conducted in analyzing the interaction between multiple cracks in piezoelectric materials.

To understand the multiple crack interaction in piezoelectric solids and their effects on the electroelastic properties, Pak and Goloubeva (1995) derived analytical solutions of interacting cracks for the case of combined antiplane shear load and inplane electrical load. Considering the plain strain problem for a transversely isotropic piezoelectric material, Chen and Han (1999a, b) conducted the analytical and numerical

study for the interacting effect of multiple parallel cracks based on a pseudo-traction electric displacement method initiated from the well-known pseudo-traction method (Horri and Nemat-Nasser, 1987). Based on the single crack solution and the superposition principle, Han and Wang (1999) investigated the effect of locations, orientations and geometries of multiple cracks. Qin (1999) studied the macro- and micro-crack interactions in thermoelectroelastic materials. The interaction of collinear cracks at the interface between dissimilar piezoelectric materials was studied by Gao and Wang (2000).

(iii) Effective electroelastic property of cracked piezoelectric materials

The existence and development of microcracks in solid media exert important influences on various aspects of material properties. The investigation on the effective properties of materials weakened by microcracks is of great importance to assess the integrity of a structure and the failure mechanism of a material. For traditional microcracked solids where boundary conditions along the crack surfaces are well defined, various micromechanics schemes have been established to estimate the effective moduli, including the dilute model (Kachanov, 1992; 1993), in which the interaction among cracks is neglected, the self-consistent method (Budiansky and O'Connel, 1976; Hori and Nemat-Nasser, 1983), the differential method (Norris, 1985; Hashin, 1988; Zimmerman, 1991), the Mori-Tanaka method (Mori and Tanaka, 1973; Benveniste, 1986; Weng, 1990), and the generalized self-consistent method (Aboudi and Benveniste, 1987; Huang et al., 1994).

These micromechanical models mentioned above have been modified and used

to study the effective property of piezoelectric materials, however, relatively fewer studies have been conducted. The effective electroelastic constants of fiber reinforced piezoelectric composites were predicted by using the self-consistent method based on a concentric cylinder model (Grekov et al., 1989). Dunn and Taya (1993a) estimated the effective properties of piezoelectric composites using dilute, self-consistent, Mori-Tanaka and differential micromechanics models. The effective thermo-electro-elastic moduli of mulitphase fibrous composites were studied by Chen (1994). Mori-Tanaka method was used by Dunn and Taya (1993b) to study the electromechanical properties of porous piezoelectric ceramics. Yu and Qin (1996b) evaluated the thermo-electro-elastic properties of microcracked piezoelectric materials using the generalized self-consistent method. Dilute, self-consistent, Mori-Tanaka and differential methods were also modified to study the effective moduli of cracked thermo-piezoelectric materials by Qin et al (1998). It should be noted that existing studies on the effective electroelastic property of cracked piezoelectric materials are limited to the traditional impermeable and permeable crack models. How the electric boundary condition along crack surfaces affect the stiffness variation of cracked piezoelectric materials and the corresponding nonlinear nature are still important issues needed further investigation.

(iv) Dynamic fracture behaviour of cracked piezoelectric materials

In spite of the fact that piezoelectric materials are mostly used or intended to use in situations involving dynamic loading, the dynamic behaviour of cracks in piezoelectric materials has received much less attention than the static problems. This may be due to the complexity of the dynamic formulation and the complicated electromechanical

coupling.

Shindo and Ozawa (1990) first investigated the dynamic behaviour of a cracked piezoelectric medium under incident plane harmonic waves. Shindo et al. (1996) studied the scattering of normally incident longitudinal waves by a finite crack in an infinite dielectric medium under a uniform electric field. The antiplane Yoffe crack in a homogeneous piezoelectric medium was studied by Chen and Yu (1997), indicating that the crack speed has no influence on the electroelastic intensity factors, similar to that predicted by the Yoffe model for traditional elastic media. Gao et al. (2001) investigated the antiplane Yoffe crack between two dissimilar piezoelectric media to show the effect of crack speed upon the dynamic electroelastic fields near the crack tips. Li and Mataga (1996a, b) studied the problem of a semi-infinite crack growth in a piezoelectric material with permeable and impermeable boundary conditions. The dynamic response of an infinite piezoelectric ceramic with a finite crack under arbitrary electro-mechanical impact was studied by Chen and Karihaloo (1999) to show the effect of electric loading upon crack propagation. Wang and Yu (2000; 2001) investigated the transient response of a crack in a piezoelectric strip subjected to electromechanical impacts for Mode III and Mode I crack problems. The transient response of an interface crack in dissimilar piezoelectric materials was studied by Gu et al. (2002).

The dynamic fracture of interacting cracks in piezoelectric materials was investigated by using the self-consistent iteration method (Meguid and Wang, 1998) and pseudo-incident wave method (Wang and Meguid, 2000a, b) under harmonic wave. Chen and Worswick (2000) studied the transient dynamic behaviour of interacting

cracks under combined antiplane mechanical and inplane electric loads. The boundary effect of piezoelectric strip upon the dynamic crack interaction was investigated by Huang et al. (2002).

1.3.4 Fracture criteria

Since the failure event of piezoelectric materials is usually 'sudden' or 'catastrophic', it is mandatory to develop fracture criteria for piezoelectric materials. Unlike traditional materials, the prediction of crack initiation and propagation in piezoelectric materials is much more complicated due to the coupling between mechanical and electric fields. Existing experimental studies indicate that electric field may enhance or retard crack growth depending on its magnitude and direction. This coupled effect should be taken into account in establishing these fracture criteria. In attempt to predict the growth of cracks in piezoelectric materials, various fracture criteria have been developed and examined to determine whether a crack advances or not. There are different kinds of fracture criteria for piezoelectric materials in literature based on the following parameters, energy release rate, strain energy release rate and maximum hoop stress. Most effort has been focused on the use of the energy release rate as the fracture parameter.

Parallel to the J-integral in linear elastic fracture mechanics, many researchers have derived similar path independent integrals to evaluate the energy release rate of cracks in piezoelectric materials. In addition to the general work of Cherepanov (1979), who developed a path-independent Γ integral for piezoelectric materials based on the conservation law of potential energy, there is a lengthy list of theoretical

investigations for the energy release rate of piezoelectric materials using path integrals. Pak and Herrmann (1986) derived a path integral (material momentum) to study the energy release rate. Pak (1990) used the generalized Rice's (Rice, 1968) J-integral to calculate the energy release rate, which is related to the intensity factors through the use of Irwin's (Irwin, 1957) crack closure method. Suo et al. (1992) gave an extensive study for a number of crack problems of piezoelectric materials, introduced the electric displacement intensity factor analogous to the traditional stress intensity factor, and derived the Irwin-type relations connecting energy release rate with stress and electric displacement intensity factors. Using energy release rate as a fracture criterion to predict the propagation of a crack, existing works (Pak, 1990; Suo et al., 1992; Han and Wang, 1999) show that the applied electric field will always impede crack growth when the crack is assumed to be electrically impermeable. On the other hand, the energy release rate is independent of applied electric fields when the crack is assumed to be electrically permeable (McMeeking, 1990; Zhang and Tong, 1996). As pointed out by McMeeking (1999), using the crack tip energy release rate and stress and electric displacement intensity factors based on the assumed unphysical crack boundary conditions are likely misleading.

Park and Sun (1994) performed compact tension tests and indicated that a positive electric field along the poling direction will enhance crack propagation, while a negative one will impede it. Similar observations can be found in the existing experimental work (McHenry and Koepke, 1983; Mehta and Virkar, 1990; Tobin and Pak, 1993). Park and Sun (1994, 1995a, b) verified their experimental results by proposing the mechanical (strain) energy release rate instead of the total energy release rate as

the fracture parameter, based on the consideration that fracture is a pure mechanical process and hence should be controlled only by the mechanical part of energy.

In addition to these generally used fracture criteria, Kumar and Singh (1996), by using the criterion of maximum hoop stress, predicted that cracks introduced by indentation propagate less under a positive electric field, whereas the crack propagation is enhanced under a negative one. Their result is consistent with the previous experimental observation (Singh and Wang, 1995). This fracture criterion also indicated that applying larger electric field increased the tendency for crack to deviate from its path and propagate at an oblique direction. Such a crack skewing or turning in piezoelectric materials was early experimentally observed by McHenry and Koepke (1983).

In order to overcome the trouble of controversial results in both experimental and theoretical studies, people are aware of the fact that nonlinear behaviour associated with crack opening should be introduced. How to describe this nonlinearity is the focus of this dissertation by using a dielectric crack model.

1.4 Objectives and Dissertation Overview

The main objective of this dissertation is to present a comprehensive theoretical study on the nonlinear fracture behaviour of piezoelectric materials with slit cracks. Specifically, attention will be focused on: (i) proposing a new dielectric crack model with the electric boundary condition along crack surfaces being governed by the deformed crack geometry to study the effect of dielectric medium inside the crack upon the

electromechanical coupling of piezoelectric materials; (ii) conducting theoretical and numerical simulations to investigate different aspects of the nonlinear fracture behaviour of cracked piezoelectric materials due to the dielectric condition of the crack; (iii) deriving both classic and newly defined fracture parameters to predict the fracture behaviour of piezoelectric materials; (iv) investigating the transition between different crack models under various loading and crack geometry conditions.

The main content of this study is covered in Chapter 2 through Chapter 7. It is organized as follows. In Chapter 2, the electromechanical coupling of cracked piezoelectric materials is modelled and formulated through a new dielectric crack model with the electric boundary condition along crack surfaces being governed by crack deformation. The fundamental solutions of a single dislocation involving both mechanical displacement and electric potential jumps are derived. Chapter 3 provides a theoretical study associated with a plain strain problem of a finite crack embedded in an infinite piezoelectric medium. The effects of electric boundary condition, crack orientation and applied loads upon the fracture behaviour of the piezoelectric medium are investigated. Attention is also paid to crack deformation modes and the transition between traditional crack models. The coupled fracture behaviour of multiple cracks is presented in Chapter 4. The effects of the location, orientation and geometry of cracks upon the nonlinear fracture behaviour of interacting dielectric cracks are discussed. Chapter 5 focuses on the evaluation of effective electroelastic properties of cracked piezoelectric materials. A dilute model of distributed cracks and the solution of a single dielectric crack are used to show the nonlinearity of the effective electroelastic properties. The comparison between existing crack models and the current model is

discussed and concluded in Chapter 6. Chapter 7 summarizes the contributions and conclusions of this research and proposes some suggestions for the future work.

Chapter 2

Formulation of the Problem and Fundamental Solutions

In this Chapter, linearized piezoelectricity formulations are used to describe the electromechanical coupling of piezoelectric materials. Since the electric boundary condition along crack surfaces may be very sensitive to the crack surface deformation, attention will be paid to develop a dielectric crack model with the electric boundary condition along crack surfaces being governed by crack opening displacements. In this model, the effects of both the normal and tangential displacements upon the electric boundary condition are taken into account to formulate the electric boundary condition. This deformation-dependent electric boundary condition will result in the nonlinearity of the fracture behaviour of cracked piezoelectric materials. As a mathematical model, the crack in the piezoelectric medium can be modelled by continuously distributed dislocations involving both displacement and electric potential jumps. Therefore, another objective of this chapter is to derive the fundamental solutions of a single dislocation through Fourier transform technique.

2.1 Basic Equations of Linear Piezoelectric Materials

The materials considered are modelled as linear anisotropic piezoelectric media (Cady, 1946; Tiersten, 1964; Parton and Kudryavtsev, 1988). To present the general behaviour of piezoelectric materials, a three-dimensional Cartesian coordinate system $oxyz$ is adopted where the position vector is denoted by (x, y, z). In the absence of free charges and body forces, the electromechanical behavior of the piezoelectric medium is governed by the equilibrium equation and the Gauss' law,

$$\sigma_{ij,j} = 0; \; D_{i,i} = 0 \tag{2.1.1}$$

in which σ_{ij} and D_i are stress and electric displacement, a comma followed by arguments denotes partial differentiation with respect to the arguments. The summation convention over repeated Latin indices has been used in this equation and will be used in the entire thesis, with $i, j = 1, 2, 3$ corresponding to x, y, z, respectively. It is well known that piezoelectric materials produce an electric field when deformed, while undergoing deformation when subjected to an electric field. This electromechanical coupling property can be described by the constitutive equations, as

$$\sigma_{ij} = c_{ijkl}\varepsilon_{kl} - e_{kij}E_k; \; D_i = e_{ikl}\varepsilon_{kl} + \epsilon_{ij}E_j \tag{2.1.2}$$

where c_{ijkl}, e_{ikl} and ϵ_{ij} are elastic, piezoelectric and dielectric constants, respectively, with the following symmetry,

$$\begin{cases} c_{ijkl} = c_{ijlk} = c_{jikl} = c_{klij} \\ e_{kij} = e_{kji} \\ \epsilon_{ij} = \epsilon_{ji} \end{cases} \tag{2.1.3}$$

and ε_{kl} and E_k are strain and electric field intensity defined by

$$\varepsilon_{kl} = \frac{1}{2}(\frac{\partial u_k}{\partial x_l} + \frac{\partial u_l}{\partial x_k});\ E_k = -\frac{\partial V}{\partial x_k} \tag{2.1.4}$$

with u_k and V being the displacement and electric potential. Historically, the so-called two-index notation is extensively used for describing linear piezoelectricity, in place of the tensor notation. It replaces ij or kl by p or q, where i, j, k, l take the values $1, 2, 3$, whereas p and q take the values $1, 2, 3, 4, 5, 6$. When this convention is applied to material constants, the constitutive equation (2.1.2) can be rewritten accordingly in the following matrix notation,

$$\begin{Bmatrix} \sigma_{11} \\ \sigma_{22} \\ \sigma_{33} \\ \sigma_{23} \\ \sigma_{31} \\ \sigma_{21} \end{Bmatrix} = \begin{bmatrix} c_{11} & c_{12} & c_{13} & c_{14} & c_{15} & c_{16} \\ c_{21} & c_{22} & c_{23} & c_{24} & c_{25} & c_{26} \\ c_{31} & c_{32} & c_{33} & c_{34} & c_{35} & c_{36} \\ c_{41} & c_{42} & c_{43} & c_{44} & c_{45} & c_{46} \\ c_{51} & c_{52} & c_{53} & c_{54} & c_{55} & c_{56} \\ c_{61} & c_{62} & c_{63} & c_{64} & c_{65} & c_{66} \end{bmatrix} \begin{Bmatrix} \varepsilon_{11} \\ \varepsilon_{22} \\ \varepsilon_{33} \\ 2\varepsilon_{23} \\ 2\varepsilon_{31} \\ 2\varepsilon_{21} \end{Bmatrix} - \begin{bmatrix} e_{11} & e_{21} & e_{31} \\ e_{12} & e_{22} & e_{32} \\ e_{13} & e_{23} & e_{33} \\ e_{14} & e_{24} & e_{34} \\ e_{15} & e_{25} & e_{35} \\ e_{16} & e_{26} & e_{36} \end{bmatrix} \begin{Bmatrix} E_1 \\ E_2 \\ E_3 \end{Bmatrix} \tag{2.1.5}$$

and

$$\begin{Bmatrix} D_1 \\ D_2 \\ D_3 \end{Bmatrix} = \begin{bmatrix} e_{11} & e_{21} & e_{31} \\ e_{12} & e_{22} & e_{32} \\ e_{13} & e_{23} & e_{33} \\ e_{14} & e_{24} & e_{34} \\ e_{15} & e_{25} & e_{35} \\ e_{16} & e_{26} & e_{36} \end{bmatrix}^T \begin{Bmatrix} \varepsilon_{11} \\ \varepsilon_{22} \\ \varepsilon_{33} \\ 2\varepsilon_{23} \\ 2\varepsilon_{31} \\ 2\varepsilon_{21} \end{Bmatrix} + \begin{bmatrix} \epsilon_{11} & \epsilon_{12} & \epsilon_{13} \\ \epsilon_{21} & \epsilon_{22} & \epsilon_{23} \\ \epsilon_{31} & \epsilon_{32} & \epsilon_{33} \end{bmatrix} \begin{Bmatrix} E_1 \\ E_2 \\ E_3 \end{Bmatrix} \tag{2.1.6}$$

with the superscript 'T' representing the matrix/vector transpose.

The poled piezoelectric ceramics are often characterized as piezoelectric materials with transverse symmetry in the poling direction. This direction is established by a poling treatment during manufacturing process, which involves applying a strong electric field between a pair of electrodes to induce the piezoelectricity (Waanders, 1991). If z-axis is assumed to be parallel to the material poling direction, this piezoelectric medium exhibits isotropic behaviour within the oxy plane. Accordingly, constitutive equations (2.1.5) and (2.1.6) can be reduced to (Suo et al., 1992),

$$\begin{Bmatrix} \sigma_{11} \\ \sigma_{22} \\ \sigma_{33} \\ \sigma_{23} \\ \sigma_{31} \\ \sigma_{21} \end{Bmatrix} = \begin{bmatrix} c_{11} & c_{12} & c_{13} & 0 & 0 & 0 \\ c_{12} & c_{11} & c_{13} & 0 & 0 & 0 \\ c_{13} & c_{13} & c_{33} & 0 & 0 & 0 \\ 0 & 0 & 0 & c_{44} & 0 & 0 \\ 0 & 0 & 0 & 0 & c_{44} & 0 \\ 0 & 0 & 0 & 0 & 0 & c_{55} \end{bmatrix} \begin{Bmatrix} \varepsilon_{11} \\ \varepsilon_{22} \\ \varepsilon_{33} \\ 2\varepsilon_{23} \\ 2\varepsilon_{31} \\ 2\varepsilon_{21} \end{Bmatrix} - \begin{bmatrix} 0 & 0 & e_{31} \\ 0 & 0 & e_{31} \\ 0 & 0 & e_{33} \\ 0 & e_{15} & 0 \\ e_{15} & 0 & 0 \\ 0 & 0 & 0 \end{bmatrix} \begin{Bmatrix} E_1 \\ E_2 \\ E_3 \end{Bmatrix} \tag{2.1.7}$$

and

$$\begin{Bmatrix} D_1 \\ D_2 \\ D_3 \end{Bmatrix} = \begin{bmatrix} 0 & 0 & e_{31} \\ 0 & 0 & e_{31} \\ 0 & 0 & e_{33} \\ 0 & e_{15} & 0 \\ e_{15} & 0 & 0 \\ 0 & 0 & 0 \end{bmatrix}^T \begin{Bmatrix} \varepsilon_{11} \\ \varepsilon_{22} \\ \varepsilon_{33} \\ 2\varepsilon_{23} \\ 2\varepsilon_{31} \\ 2\varepsilon_{21} \end{Bmatrix} + \begin{bmatrix} \epsilon_{11} & 0 & 0 \\ 0 & \epsilon_{11} & 0 \\ 0 & 0 & \epsilon_{33} \end{bmatrix} \begin{Bmatrix} E_1 \\ E_2 \\ E_3 \end{Bmatrix} \tag{2.1.8}$$

where $c_{55} = \dfrac{c_{11} - c_{12}}{2}$.

2.2 A Dielectric Crack Model

In this dissertation, the cracks in piezoelectric materials are considered as slit cracks. A slit crack is assumed to have perfect contact profile, i.e., no pre-separation of crack surfaces before subjected to applied loading. When undergoing electromechanical loads, crack opening occurs and the dielectric medium (air or vacuum) filling the crack may significantly affect the electric boundary condition along crack surfaces. Existing crack models, electrically impermeable and permeable models, ignore the effect of this dielectric medium and may not be able to accurately evaluate the fracture behaviour of cracked piezoelectric materials. As a result, the crack deformation shows no effect on the resulting electroelastic fields around the crack tip. In the intermediate dielectric layer model defined by Equation (1.3.3), the effect of crack deformation has also been neglected. Since for a slit crack the electric boundary condition may be very sensitive to the crack deformation caused by applied electromechanical loads, how to describe the 'real' electric boundary condition along crack surfaces is of great importance in studying the fracture behaviour of piezoelectric materials. An 'ideal' model should combine both the crack deformation and the effect of the dielectric medium inside the crack in formulating the electric boundary condition along crack surfaces.

Similar to the traditional crack problems where the mechanical modulii of air (or vacuum) filling the crack are negligible, the crack is assumed to satisfy the traction free condition along the crack surfaces, i.e.,

$$\sigma_n = 0, \quad \tau_n = 0 \tag{2.2.1}$$

where σ_n and τ_n represent the normal and shear stress components along the crack surfaces.

When the slit crack is deformed, the thickness of the dielectric medium filling the crack will be changed, which will influence the overall dielectric property of the crack. As a result, the apparent electric boundary condition of the crack will be deformation-dependent, unlike the existing crack models where only the original dimension of the crack is used (Parton and Kudryavtsev, 1988; McMeeking, 1989; Dunn, 1994; Sosa and Khutoryansky, 1996; Zhang and Tong, 1996; Dascalu and Homentcovschi, 2002). For cases where crack opening is much smaller than the crack length, it is assumed that the normal electric field intensity E_n and the normal electric displacement D_n in the dielectric medium are uniform across the thickness of the deformed crack. The electric boundary condition along the crack surfaces needs to be determined based on the deformed crack geometry.

For a typical crack, the final position of a point of the crack surface after deformation is determined by both normal and tangential displacements of the crack surface as shown in Figure 2.1, in which the crack is described by the Cartesian coordinate system oxy with x-axis being parallel with crack surface line. At any point $x = x_0$ along the crack surface, the opening displacement after deformation is given by $u_n^+(\xi, 0) - u_n^-(\eta, 0)$ where u_n is the normal displacement, superscripts $+$ and $-$ represent the upper and lower surfaces of the crack, ξ and η are two points at the upper and lower surfaces of the crack, respectively, in the undeformed configuration, which move to $x = x_0$ after deformation. Similarly, the electric potential difference across the crack at $x = x_0$ after deformation is $V^+(\xi, 0) - V^-(\eta, 0)$, with V being the

electric potential.

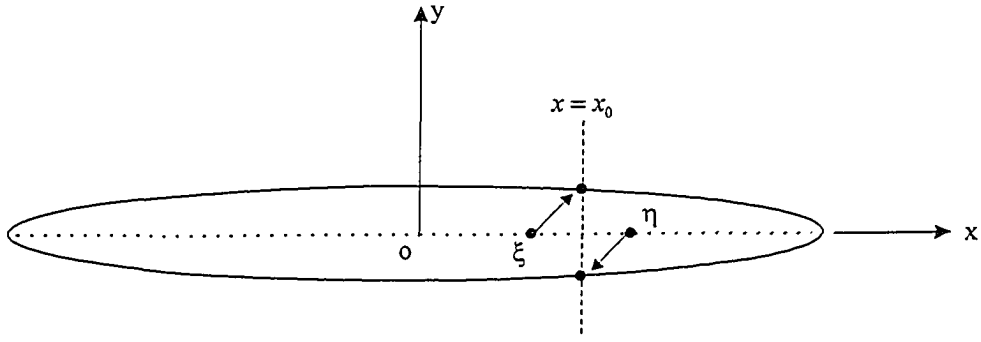

Figure 2.1: Crack surface deformation scheme

Accordingly, the electric boundary condition along the deformed crack surfaces can be expressed as,

$$D_n = \epsilon_0 E_n(x) = -\epsilon_0 \frac{V^+(\xi,0) - V^-(\eta,0)}{u_n^+(\xi,0) - u_n^-(\eta,0)} \tag{2.2.2}$$

where $\epsilon_0 = 8.85 \times 10^{-12} C/Vm$ is the dielectric constant of air inside the crack. It is clearly indicated in Equation (2.2.2) that the electric boundary condition is deformation-dependent, which will cause the nonlinearity of the problem.

2.3 Fundamental Solution for a Single Dislocation

In this dissertation, we will focus on studying the plain strain problem of cracks in an infinite piezoelectric medium, in which all electroelastic fields depends on the inplane coordinates only. The interested plane containing crack is assumed to be xy plane,

in which a Cartesian coordinate system oxy is used to describe the crack with crack line along x-axis, as shown in Figure 2.1. Assuming that the poling direction of the piezoelectric medium is in xy plane, the anisotropic behaviour of the material can be determined from Equations (2.1.5) and (2.1.6) as,

$$\begin{Bmatrix} \sigma_{11} \\ \sigma_{22} \\ \sigma_{21} \end{Bmatrix} = \begin{bmatrix} c_{11} & c_{12} & c_{16} \\ c_{12} & c_{22} & c_{26} \\ c_{16} & c_{26} & c_{66} \end{bmatrix} \begin{Bmatrix} \varepsilon_{11} \\ \varepsilon_{22} \\ 2\varepsilon_{21} \end{Bmatrix} - \begin{bmatrix} e_{11} & e_{21} \\ e_{12} & e_{22} \\ e_{16} & e_{26} \end{bmatrix} \begin{Bmatrix} E_1 \\ E_2 \end{Bmatrix} \tag{2.3.1}$$

and

$$\begin{Bmatrix} D_1 \\ D_2 \end{Bmatrix} = \begin{bmatrix} e_{11} & e_{21} \\ e_{12} & e_{22} \\ e_{16} & e_{26} \end{bmatrix}^T \begin{Bmatrix} \varepsilon_{11} \\ \varepsilon_{22} \\ 2\varepsilon_{21} \end{Bmatrix} + \begin{bmatrix} \epsilon_{11} & \epsilon_{12} \\ \epsilon_{12} & \epsilon_{22} \end{bmatrix} \begin{Bmatrix} E_1 \\ E_2 \end{Bmatrix} \tag{2.3.2}$$

Substituting equations (2.3.1) and (2.3.2) into (2.1.1) results in the governing equation of this problem,

$$(\mathbf{Q}X^2 + (\mathbf{R} + \mathbf{R}^T)XY + \mathbf{T}Y^2)\mathbf{v} = 0 \tag{2.3.3}$$

with $X = \dfrac{\partial}{\partial x}$, $Y = \dfrac{\partial}{\partial y}$ and

$$\mathbf{Q} = \begin{bmatrix} c_{11} & c_{16} & e_{11} \\ c_{16} & c_{66} & e_{16} \\ e_{11} & e_{16} & -\epsilon_{11} \end{bmatrix}, \mathbf{T} = \begin{bmatrix} c_{66} & c_{26} & e_{26} \\ c_{26} & c_{22} & e_{22} \\ e_{26} & e_{22} & -\epsilon_{22} \end{bmatrix}, \mathbf{R} = \begin{bmatrix} c_{16} & c_{12} & e_{21} \\ c_{66} & c_{26} & e_{26} \\ e_{16} & e_{12} & -\epsilon_{12} \end{bmatrix} \tag{2.3.4}$$

$\mathbf{v}$ is displacements and electric potential field defined as,

$$\mathbf{v} = \{u_1 \; u_2 \; V\}^T \tag{2.3.5}$$

Bold-face letters will be used in this thesis to represent matrices and/or vectors.

As a mathematical model, the crack can be modelled as the superposition of continuously distributed dislocations along crack line $y = 0$. Therefore, the solution of a single dislocation is essential in determining the electroelastic fields of cracked piezoelectric medium. A generalized dislocation involving both displacement and electric potential jumps at $(x, 0)$ along crack line is defined as,

$$\mathbf{d}(x) = \mathbf{v}^{+}(x,0) - \mathbf{v}^{-}(x,0) = \mathbf{d}_0 H(x) \tag{2.3.6}$$

with superscripts $+$ and $-$ representing upper and lower crack surfaces. $\mathbf{d}_0 = \{\triangle u_1^0,\ \triangle u_2^0,\ \triangle V^0\}^T$ is a constant vector representing the applied displacement and electric potential jumps and $H(x)$ is the Heaviside step function.

To solve the governing equation (2.3.3), Fourier transform pairs are introduced,

$$\widetilde{f}(s,y) = \frac{1}{2\pi}\int_{-\infty}^{\infty} f(x,y)e^{isx}dx, \quad f(x,y) = \int_{-\infty}^{\infty} \widetilde{f}(s,y)e^{-isx}ds \tag{2.3.7}$$

with $\sim$ representing Fourier transform. Applying Fourier transform with respect to x, Equation (2.3.3) can be deduced to,

$$-s^2\mathbf{Q}\widetilde{\mathbf{v}} - is(\mathbf{R} + \mathbf{R}^T)\frac{\partial \widetilde{\mathbf{v}}}{\partial y} + \mathbf{T}\frac{\partial^2 \widetilde{\mathbf{v}}}{\partial y^2} = 0 \tag{2.3.8}$$

The solution of Equation (2.3.8) can be obtained by considering eigenfunction of the form,

$$\widetilde{\mathbf{v}} = \mathbf{a}e^{-i\eta y} \tag{2.3.9}$$

substituting Equation (2.3.9) into Equation (2.3.8) results in,

$$(\mathbf{Q} + p(\mathbf{R} + \mathbf{R}^T) + p^2\mathbf{T})\mathbf{a} = 0 \tag{2.3.10}$$

with $p = \eta/s$. To obtain a nontrivial solution for $\mathbf{a}$ we should let the following determinant vanish, i.e.

$$\|\mathbf{Q} + p(\mathbf{R} + \mathbf{R}^T) + p^2\mathbf{T}\| = 0 \tag{2.3.11}$$

Where $\|\bullet\|$ denotes the determinant. It has been proved (Suo et al., 1992) that this equation has no real roots. Let p_α ($\alpha = 1, 2, 3$) be the eigenvalues with positive imaginary parts, $\mathbf{a}_\alpha$ the corresponding eigenvectors, and $\overline{p}_\alpha$ and $\overline{\mathbf{a}}_\alpha$ the conjugates of p_α and $\mathbf{a}_\alpha$ in Equation (2.3.11). Introducing the definition,

$$\eta_\alpha = \begin{cases} p_\alpha s, & s > 0 \\ \overline{p}_\alpha s, & s < 0 \end{cases}, \quad \overline{\eta}_\alpha = \begin{cases} \overline{p}_\alpha s, & s > 0 \\ p_\alpha s, & s < 0 \end{cases} \quad (\alpha = 1, 2, 3) \tag{2.3.12}$$

it is obvious that $\mathrm{Im}\,\eta_\alpha > 0$. With such a definition, the general solution of Equation (2.3.8) can be obtained from a linear combination of those determined eigenvalues and eigenvectors, as

$$\widetilde{\mathbf{v}}(s, y) = (\mathbf{A}\mathbf{F}\mathbf{f}^r + \overline{\mathbf{A}}\mathbf{G}\mathbf{g}^r)H(s) + (\overline{\mathbf{A}}\mathbf{F}\mathbf{f}^l + \mathbf{A}\mathbf{G}\mathbf{g}^l)H(-s) \tag{2.3.13}$$

where $\mathbf{f}$ and $\mathbf{g}$ are unknown vectors to be determined with the superscripts r and l representing the right ($s > 0$) and left ($s < 0$) half-planes, H is the Heaviside step function and the bar denotes the conjugate of a complex number/matrix. $\mathbf{A} = [\mathbf{a}_1\ \mathbf{a}_2\ \mathbf{a}_3\ \mathbf{a}_4]$, $\overline{\mathbf{A}} = [\overline{\mathbf{a}}_1\ \overline{\mathbf{a}}_2\ \overline{\mathbf{a}}_3\ \overline{\mathbf{a}}_4]$, $\mathbf{F}(s, y) = diag[e^{-i\eta_1 y}, e^{-i\eta_2 y}, e^{-i\eta_3 y}, e^{-i\eta_4 y}]$ and $\mathbf{G}(s, y) = diag[e^{-i\overline{\eta}_1 y}, e^{-i\overline{\eta}_2 y}, e^{-i\overline{\eta}_3 y}, e^{-i\overline{\eta}_4 y}]$.

From Equation (2.1.4) and constitutive equations (2.3.1) and (2.3.2), the corresponding stress and electric displacement fields can be expressed as,

$$\mathbf{t} = \mathbf{R}^T\frac{\partial \mathbf{v}}{\partial x} + \mathbf{T}\frac{\partial \mathbf{v}}{\partial y} \tag{2.3.14}$$

$$\mathbf{s} = \mathbf{Q}\frac{\partial \mathbf{v}}{\partial x} + \mathbf{R}\frac{\partial \mathbf{v}}{\partial y} \tag{2.3.15}$$

with $\mathbf{t} = \{\sigma_{12}\ \sigma_{22}\ D_2\}^T$ and $\mathbf{s} = \{\sigma_{11}\ \sigma_{21}\ D_1\}^T$. Based on Equation (2.3.13), applying Fourier transform with respect to x to equations (2.3.14) and (2.3.15) results in,

$$\widetilde{\mathbf{t}}(s,y) = -is(\mathbf{B}\mathbf{F}\mathbf{f}^r + \overline{\mathbf{B}}\mathbf{G}\mathbf{g}^r)H(s) - is(\overline{\mathbf{B}}\mathbf{F}\mathbf{f}^l + \mathbf{B}\mathbf{G}\mathbf{g}^l)H(-s) \tag{2.3.16}$$

$$\widetilde{\mathbf{s}}(s,y) = -is(\mathbf{C}\mathbf{F}\mathbf{f}^r + \overline{\mathbf{C}}\mathbf{G}\mathbf{g}^r)H(s) - is(\overline{\mathbf{C}}\mathbf{F}\mathbf{f}^l + \mathbf{C}\mathbf{G}\mathbf{g}^l)H(-s) \tag{2.3.17}$$

where the matrices $\mathbf{B}$ and $\mathbf{C}$ are given by,

$$\mathbf{B} = \mathbf{R}^T\mathbf{A} + \mathbf{T}\mathbf{A}\mathbf{P}, \quad \mathbf{C} = \mathbf{Q}\mathbf{A} + \mathbf{R}\mathbf{A}\mathbf{P} \tag{2.3.18}$$

with $\mathbf{P} = diag[p_1, p_2, p_3]$.

Using inverse Fourier transform defined in (2.3.7), the corresponding displacement, electric potential, stress and electric displacement fields can be derived as,

$$\mathbf{v}(x,y) = \int_0^\infty (\mathbf{A}\mathbf{F}\mathbf{f}^r + \overline{\mathbf{A}}\mathbf{G}\mathbf{g}^r)e^{-isx}ds + \int_{-\infty}^0 (\overline{\mathbf{A}}\mathbf{F}\mathbf{f}^l + \mathbf{A}\mathbf{G}\mathbf{g}^l)e^{-isx}ds \tag{2.3.19}$$

$$\mathbf{t}(x,y) = -i\int_0^\infty s(\mathbf{B}\mathbf{F}\mathbf{f}^r + \overline{\mathbf{B}}\mathbf{G}\mathbf{g}^r)e^{-isx}ds - i\int_{-\infty}^0 s(\overline{\mathbf{B}}\mathbf{F}\mathbf{f}^l + \mathbf{B}\mathbf{G}\mathbf{g}^l)e^{-isx}ds \tag{2.3.20}$$

$$\mathbf{s}(x,y) = -i\int_0^\infty s(\mathbf{C}\mathbf{F}\mathbf{f}^r + \overline{\mathbf{C}}\mathbf{G}\mathbf{g}^r)e^{-isx}ds - i\int_{-\infty}^0 s(\overline{\mathbf{C}}\mathbf{F}\mathbf{f}^l + \mathbf{C}\mathbf{G}\mathbf{g}^l)e^{-isx}ds \tag{2.3.21}$$

Since these solutions must be bounded as $|y| \to \infty$, the unknown coefficient vectors in these electroelastic fields must satisfy

$$\begin{cases} \mathbf{f}^r = \mathbf{f}^l = 0, & y > 0 \\ \mathbf{g}^r = \mathbf{g}^l = 0, & y < 0 \end{cases} \tag{2.3.22}$$

Correspondingly, the electromechanical fields in equations (2.3.13), (2.3.16) and (2.3.17) can be rewritten as,

$$\begin{cases} \widetilde{\mathbf{v}}^{+}(s,y) = \overline{\mathbf{A}}\mathbf{g}^{r}H(s) + \mathbf{A}\mathbf{g}^{l}H(-s) \\ \\ \widetilde{\mathbf{v}}^{-}(s,y) = \mathbf{A}\mathbf{f}^{r}H(s) + \overline{\mathbf{A}}\mathbf{f}^{l}H(-s) \end{cases} \tag{2.3.23}$$

$$\begin{cases} \widetilde{\mathbf{t}}^{+}(s,y) = -is\overline{\mathbf{B}}\mathbf{G}\mathbf{g}^{r}H(s) - is\mathbf{B}\mathbf{G}\mathbf{g}^{l}H(-s) \\ \\ \widetilde{\mathbf{t}}^{-}(s,y) = -is\mathbf{B}\mathbf{F}\mathbf{f}^{r}H(s) - is\overline{\mathbf{B}}\mathbf{F}\mathbf{f}^{l}H(-s) \end{cases} \tag{2.3.24}$$

$$\begin{cases} \widetilde{\mathbf{s}}^{+}(s,y) = -is\overline{\mathbf{C}}\mathbf{G}\mathbf{g}^{r}H(s) - is\mathbf{C}\mathbf{G}\mathbf{g}^{l}H(-s) \\ \\ \widetilde{\mathbf{s}}^{-}(s,y) = -is\mathbf{C}\mathbf{F}\mathbf{f}^{r}H(s) - is\overline{\mathbf{C}}\mathbf{F}\mathbf{f}^{l}H(-s) \end{cases} \tag{2.3.25}$$

where superscripts '+' and '−' represents $y > 0$ and $y < 0$ respectively. In addition, the continuity condition ($\mathbf{t}^{+} = \mathbf{t}^{-}$) at $y = 0$ will result in,

$$\overline{\mathbf{B}}\mathbf{g}^{r} = \mathbf{B}\mathbf{f}^{r}, \quad \mathbf{B}\mathbf{g}^{l} = \overline{\mathbf{B}}\mathbf{f}^{l} \tag{2.3.26}$$

Applying Fourier transform with respect to x to Equation (2.3.6) results in

$$\widetilde{\mathbf{d}}(s) = \widetilde{\mathbf{v}}^{+} - \widetilde{\mathbf{v}}^{-} = -\frac{1}{2\pi}\frac{\mathbf{d}_0}{is} \tag{2.3.27}$$

Substituting Equation (2.3.23) into (2.3.27), the unknown vectors $\mathbf{f}^{r}, \mathbf{f}^{l}, \mathbf{g}^{r}$ and $\mathbf{g}^{l}$ in the electroelastic fields are then expressed in terms of this unknown dislocation, as

$$\begin{cases} \mathbf{f}^{r} = \dfrac{\mathbf{d}_0}{2\pi s}\mathbf{B}^{-1}\mathbf{H}^{-1} \\ \\ \mathbf{f}^{l} = -\dfrac{\mathbf{d}_0}{2\pi s}\overline{\mathbf{B}}^{-1}\mathbf{H}^{-1} \\ \\ \mathbf{g}^{r} = \dfrac{\mathbf{d}_0}{2\pi s}\overline{\mathbf{B}}^{-1}\mathbf{H}^{-1} \\ \\ \mathbf{g}^{l} = -\dfrac{\mathbf{d}_0}{2\pi s}\mathbf{B}^{-1}\mathbf{H}^{-1} \end{cases} \tag{2.3.28}$$

where

$$\mathbf{H} = -2\,\mathrm{Im}\,(\mathbf{A}\mathbf{B}^{-1}) \tag{2.3.29}$$

with 'Im' standing for the imaginary part of a complex number and the superscript $'-1'$ representing the inverse of matrix.

Substituting Equation (2.3.28) into (2.3.20) and (2.3.21), the electroelastic fields caused by the existence of this single dislocation can be determined, as

$$\mathbf{t}(x,y) = -\Big[\mathbf{B}_1(\frac{1}{x+p_\alpha y}) + \mathbf{B}_2(\frac{1}{x+\overline{p}_\alpha y})\Big]\mathbf{H}^{-1}\mathbf{d}_0 \tag{2.3.30}$$

$$\mathbf{s}(x,y) = -\Big[\mathbf{C}_1(\frac{1}{x+p_\alpha y}) + \mathbf{C}_2(\frac{1}{x+\overline{p}_\alpha y})\Big]\mathbf{H}^{-1}\mathbf{d}_0 \tag{2.3.31}$$

where

$$\mathbf{B}_1(\frac{1}{x+p_\alpha y}) = \begin{cases} -\dfrac{i}{2\pi}\displaystyle\int_{-\infty}^{0} \mathbf{B}\mathbf{G}\mathbf{B}^{-1}e^{-isx}ds & y>0 \\ \dfrac{i}{2\pi}\displaystyle\int_{0}^{\infty} \mathbf{B}\mathbf{F}\mathbf{B}^{-1}e^{-isx}ds & y<0 \end{cases} \tag{2.3.32}$$

$$\mathbf{B}_2(\frac{1}{x+\overline{p}_\alpha y}) = \begin{cases} \dfrac{i}{2\pi}\displaystyle\int_{0}^{\infty} \overline{\mathbf{B}}\mathbf{G}\overline{\mathbf{B}}^{-1}e^{-isx}ds & y>0 \\ -\dfrac{i}{2\pi}\displaystyle\int_{-\infty}^{0} \overline{\mathbf{B}}\mathbf{F}\overline{\mathbf{B}}^{-1}e^{-isx}ds & y<0 \end{cases} \tag{2.3.33}$$

$$\mathbf{C}_1(\frac{1}{x+p_\alpha y}) = \begin{cases} -\dfrac{i}{2\pi}\displaystyle\int_{-\infty}^{0} \mathbf{C}\mathbf{G}\mathbf{B}^{-1}e^{-isx}ds & y>0 \\ \dfrac{i}{2\pi}\displaystyle\int_{0}^{\infty} \mathbf{C}\mathbf{F}\mathbf{B}^{-1}e^{-isx}ds & y<0 \end{cases} \tag{2.3.34}$$

$$\mathbf{C}_2(\frac{1}{x+\overline{p}_\alpha y}) = \begin{cases} \dfrac{i}{2\pi}\displaystyle\int_{0}^{\infty} \overline{\mathbf{C}}\mathbf{G}\overline{\mathbf{B}}^{-1}e^{-isx}ds & y>0 \\ -\dfrac{i}{2\pi}\displaystyle\int_{-\infty}^{0} \overline{\mathbf{C}}\mathbf{F}\overline{\mathbf{B}}^{-1}e^{-isx}ds & y<0 \end{cases} \tag{2.3.35}$$

This general solution for a single generalized dislocation will be used to formulate the electroelastic fields caused by the existence of cracks in piezoelectric materials.

Chapter 3

Nonlinear Fracture Behaviour of Piezoelectric Materials with an Oriented Dielectric Crack

This chapter presents a theoretical study of the plane strain problem of an infinite piezoelectric medium with an arbitrarily oriented slit dielectric crack. The deformed crack geometry is used for formulating the nonlinear electric boundary condition along crack surfaces. Solving the resulting nonlinear singular integral equations, the fracture behaviour of the cracked piezoelectric medium is discussed in detail. Multiple deformation modes are observed according to different geometric and loading conditions. The effects of the crack orientation, the electric boundary condition and the applied loads upon the fracture behaviour of cracked piezoelectric materials are studied. Attention is also focused on the relation between the current crack model and the commonly used permeable and impermeable models.

3.1 Statement of the Problem

As discussed in the previous chapter, existing studies on the crack problem of piezoelectric materials are mostly based on the electrically impermeable and permeable crack models. These models ignore the effect of dielectric medium inside the crack and crack deformation upon the electric boundary condition and, therefore, can not accurately predict the fracture behaviour of cracked piezoelectric materials. The dielectric crack model proposed in Chapter 2 will be used to study the nonlinear fracture behaviour of an arbitrarily oriented crack to evaluate the effect of deformation-dependent electric boundary condition.

Consider a plane problem of a slit crack in an infinite piezoelectric medium subjected to mechanical and electric loads $(\mathrm{t}^{\infty}, \mathrm{s}^{\infty})$ with $\mathrm{t}^{\infty} = \{\sigma_{21}^{\infty}\ \sigma_{22}^{\infty}\ D_2^{\infty}\}^T$ and $\mathrm{s}^{\infty} = \{\sigma_{11}^{\infty}\ \sigma_{21}^{\infty}\ D_1^{\infty}\}^T$. The piezoelectric medium has a poling direction along y'-axis of the global coordinate system $o'x'y'$, as shown in Figure 3.1. The crack length is $2a$ and the crack orientation is measured by angle θ between the direction of the crack surface and x'-axis. The original problem (a) in Figure 3.1 can be decomposed into two sub-problems (b) and (c). Sub-problem (b) contains a uniform medium under the same external electromechanical loading as the original problem. In problem (c), which will be solved in this chapter, the cracked medium is subjected to both electric and mechanical loads $\mathrm{t}^0 = \{\sigma_{21}^0\ \sigma_{22}^0\ D_2^0\}^T$ along the crack surfaces, which can be deduced from the original loading. A local coordinate system oxy is used to describe the crack with its origin being at the centre of the crack and x-axis along the crack surfaces.

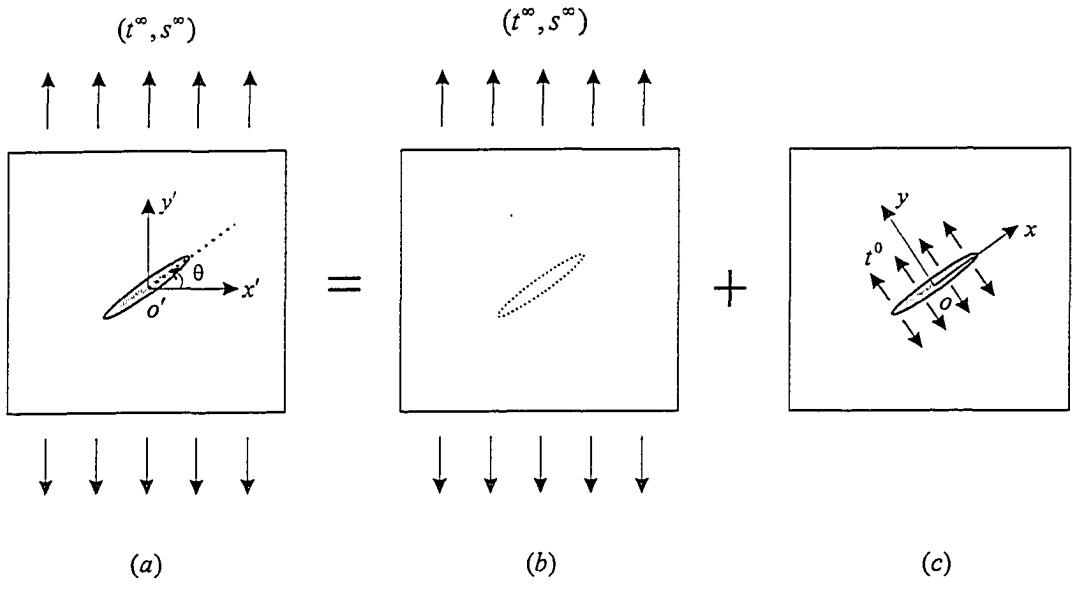

Figure 3.1: Crack model and the decomposition of the problem

In sub-problem (c), according to the deformed geometry, the crack should satisfy the following conditions, which are consistent with the original boundary conditions given in Equations (2.2.1) and (2.2.2),

$$\sigma_{2i}^{+} = \sigma_{2i}^{-} = -\sigma_{2i}^{0} \quad (i = 1, 2) \tag{3.1.1}$$

$$D_2^{+} = D_2^{-} = D_2; \quad D_2 + \epsilon_0 \frac{V^{+}(\xi, 0) - V^{-}(\eta, 0)}{u_2^{+}(\xi, 0) - u_2^{-}(\eta, 0)} = -D_2^{0} \tag{3.1.2}$$

where $(\xi, 0)$ and $(\eta, 0)$ are points at the upper and lower surfaces of the crack, respectively, which move to $(x, 0)$ after the deformation, as discussed in Chapter 2. It should be mentioned that the deformed geometry will only be used in the electric boundary condition given in Equation (3.1.2). For the electroelastic field inside the piezoelectric medium, analysis will be based on the original configuration.

3.2 General Solution of a Single Crack

A crack can be regarded as distributed dislocations (Bilby and Eshelby, 1968; Barnett and Lothe, 1975; Meguid and Wang, 1998). Therefore, the electroelastic fields caused by a crack can be expressed by the superposition of the electroelastic fields of these dislocations. Based on the single dislocation solution, the general electroelastic fields caused by the existence of a crack can then be derived in the local coordinate system by integrating (2.3.30) and (2.3.31) over the crack length $2a$, as,

$$\mathbf{t}(x,y) = -\int_{-a}^{a} \left[\mathbf{B}_1\left(\frac{1}{x+p_\alpha y-w}\right) + \mathbf{B}_2\left(\frac{1}{x+\overline{p}_\alpha y-w}\right)\right]\mathbf{H}^{-1}\mathbf{d}'(w)dw \tag{3.2.1}$$

$$\mathbf{s}(x,y) = -\int_{-a}^{a} \left[\mathbf{C}_1\left(\frac{1}{x+p_\alpha y-w}\right) + \mathbf{C}_2\left(\frac{1}{x+\overline{p}_\alpha y-w}\right)\right]\mathbf{H}^{-1}\mathbf{d}'(w)dw \tag{3.2.2}$$

where $\mathbf{d}'$ is the dislocation intensity function defined as,

$$\mathbf{d}'(x) = \frac{\partial[\mathbf{v}^+(x,0) - \mathbf{v}^-(x,0)]}{\partial x}, \quad |x| \le a \tag{3.2.3}$$

and $\mathbf{B}_1$, $\mathbf{B}_2$, $\mathbf{B}_3$ and $\mathbf{B}_4$ are derived from equations (2.3.32)-(2.3.35),

$$\mathbf{B}_1\left(\frac{1}{x+p_\alpha y-w}\right) = \begin{cases} -\dfrac{i}{2\pi}\displaystyle\int_{-\infty}^{0} \mathbf{B}\mathbf{G}\mathbf{B}^{-1}e^{-is(x-w)}ds & y>0 \\ \dfrac{i}{2\pi}\displaystyle\int_{0}^{\infty} \mathbf{B}\mathbf{F}\mathbf{B}^{-1}e^{-is(x-w)}ds & y<0 \end{cases} \tag{3.2.4}$$

$$\mathbf{B}_2\left(\frac{1}{x+\overline{p}_\alpha y-w}\right) = \begin{cases} \dfrac{i}{2\pi}\displaystyle\int_{0}^{\infty} \overline{\mathbf{B}}\mathbf{G}\overline{\mathbf{B}}^{-1}e^{-is(x-w)}ds & y>0 \\ -\dfrac{i}{2\pi}\displaystyle\int_{-\infty}^{0} \overline{\mathbf{B}}\mathbf{F}\overline{\mathbf{B}}^{-1}e^{-is(x-w)}ds & y<0 \end{cases} \tag{3.2.5}$$

$$\mathbf{C}_1\left(\frac{1}{x+p_\alpha y-w}\right) = \begin{cases} -\dfrac{i}{2\pi}\displaystyle\int_{-\infty}^{0} \mathbf{C}\mathbf{G}\mathbf{B}^{-1}e^{-is(x-w)}ds & y>0 \\ \dfrac{i}{2\pi}\displaystyle\int_{0}^{\infty} \mathbf{C}\mathbf{F}\mathbf{B}^{-1}e^{-is(x-w)}ds & y<0 \end{cases} \tag{3.2.6}$$

$$\mathbf{C}_2\left(\frac{1}{x+\overline{p}_\alpha y-w}\right)=\begin{cases}\dfrac{i}{2\pi}\displaystyle\int_0^\infty \overline{\mathbf{C}}\mathbf{G}\overline{\mathbf{B}}^{-1}e^{-is(x-w)}ds & y>0\\[2ex] -\dfrac{i}{2\pi}\displaystyle\int_{-\infty}^0 \overline{\mathbf{C}}\mathbf{F}\overline{\mathbf{B}}^{-1}e^{-is(x-w)}ds & y<0\end{cases} \tag{3.2.7}$$

with all quantities p_α, $\mathbf{B}$, $\mathbf{C}$, $\mathbf{F}$, $\mathbf{G}$ and $\mathbf{H}$ being defined in Chapter 2.

It should be noted that eigenvalues p_α, matrices $\mathbf{B}$, $\mathbf{C}$ and $\mathbf{H}$ are all related to material constants of piezoelectric materials and derived in the coordinate system attached to the crack surface, i.e., the local coordinate system *oxy* in this case. These quantities depend on the orientation of the crack (or the poling direction of the material). The dependence can, however, be represented in terms of θ explicitly (Suo et al., 1992), as

$$p_\alpha=\frac{p'_\alpha\cos\theta-\sin\theta}{p'_\alpha\sin\theta+\cos\theta},\ \mathbf{B}=\mathbf{S}\mathbf{B}',\ \mathbf{C}=\mathbf{S}\mathbf{C}',\ \mathbf{H}=\mathbf{S}\mathbf{H}'\mathbf{S}^T \tag{3.2.8}$$

where the superscript $'$ represent the corresponding quantities in the global coordinate system $o'x'y'$ and the transformation matrix $\mathbf{S}$ is given by

$$\mathbf{S}=\begin{bmatrix}\cos\theta & \sin\theta & 0\\ -\sin\theta & \cos\theta & 0\\ 0 & 0 & 1\end{bmatrix} \tag{3.2.9}$$

For the specific case where the poling direction is perpendicular to the crack surfaces, i.e. $\theta=0$, $\mathbf{H}$ is symmetric with only the last element being negative (Suo et al., 1992), for example,

$$\mathbf{H}'=\begin{bmatrix}h'_{11} & 0 & 0\\ 0 & h'_{22} & h'_{23}\\ 0 & h'_{32} & h'_{33}\end{bmatrix} \tag{3.2.10}$$

Once these material constant matrix $\mathbf{B},\mathbf{C}$ and $\mathbf{H}$ are calculated out in the local coordinate system, the electroelastic fields of a single crack problem can be expressed

in terms of the unknown dislocation intensity function. Correspondingly, the stress and electric displacement fields $\mathbf{t}(x,0)$ along the crack line in sub-problem (c) can be deduced from Equation (3.2.1) as,

$$\mathbf{t}(x,0) = -\frac{\mathbf{H}^{-1}}{\pi}\int_{-a}^{a}\frac{\mathbf{d}'(w)}{x-w}dw \tag{3.2.11}$$

It is observed from Equation (3.2.11) that the electroelastic field is governed by one unknown dislocation density function $\mathbf{d}'$, which will be determined from the boundary conditions along crack surfaces. Using the boundary conditions for problem (c), as described by equations (3.1.1) and (3.1.2), the following singular integral equations can be obtained,

$$\frac{1}{\pi}\int_{-a}^{a}\frac{\mathbf{\Gamma}'(w)}{w-x}dw + \left\{\begin{array}{c} 0 \\ 0 \\ \dfrac{\epsilon_0(V^+(\xi,0)-V^-(\eta,0))}{u_2^+(\xi,0)-u_2^-(\eta,0)} \end{array}\right\} = -\mathbf{t}^0 \tag{3.2.12}$$

where $\mathbf{t}^0$ is the electromechanical load acting on the crack surfaces in problem (c), which can be deduced from the applied external loading $(\mathbf{t}^\infty, \mathbf{s}^\infty)$ as,

$$\mathbf{t}^0 = \cos\theta\mathbf{S}\mathbf{t}^\infty - \sin\theta\mathbf{S}\mathbf{s}^\infty \tag{3.2.13}$$

and

$$\mathbf{\Gamma} = \mathbf{H}^{-1}\mathbf{d} \tag{3.2.14}$$

The singular integral equation (3.2.12) can be solved using Chebyshev polynomials,

$$\mathbf{\Gamma}'(\xi) = \mathbf{c}T_1(\frac{\xi}{a})/\sqrt{1-\frac{\xi^2}{a^2}} \tag{3.2.15}$$

where $\mathbf{c}^T = \{c_1, c_2, c_3\}$ is a vector to be determined and $T_1(\xi/a)$ is the first order Chebyshev polynomial of the first kind. From Equation (3.2.14), the jumps of displacement and electric potential crossing crack surfaces can be derived by integrating Equation (3.2.15) as,

$$\mathbf{d}(x) = \mathbf{v}^+(x) - \mathbf{v}^-(x) = \mathbf{H}\boldsymbol{\Gamma} = -\mathbf{H}\mathbf{c}\sqrt{a^2 - x^2} \tag{3.2.16}$$

It is interesting to note that the solution given by (3.2.16) will result in $E_2(x)$ in the dielectric medium filling the crack being a constant, i.e.

$$E_2(x) = -\frac{V_0}{d_0}\frac{(\sqrt{a^2-\xi^2} - \sqrt{a^2-\eta^2})}{(\sqrt{a^2-\xi^2} - \sqrt{a^2-\eta^2})} = -\frac{h_{31}c_1 + h_{32}c_2 + h_{33}c_3}{h_{21}c_1 + h_{22}c_2 + h_{23}c_3} \tag{3.2.17}$$

with $h_{ij}(i,j = 1,2,3)$ being the elements of matrix $\mathbf{H}$. Correspondingly, the singular integral equation (3.2.12) can be rewritten as,

$$\frac{1}{\pi}\int_{-a}^{a}\frac{\boldsymbol{\Gamma}'}{w-x}dw + \left\{\begin{array}{c} 0 \\ 0 \\ \dfrac{\epsilon_0(h_{31}c_1 + h_{32}c_2 + h_{33}c_3)}{h_{21}c_1 + h_{22}c_2 + h_{23}c_3} \end{array}\right\} = -\mathbf{t}^0 \tag{3.2.18}$$

Substituting (3.2.15) into (3.2.18) results in the following nonlinear algebraic equations,

$$\left\{\begin{array}{l} c_1 = -\sigma_{21}^0 \\ \\ c_2 = -\sigma_{22}^0 \\ \\ c_3 = -D_2^0 - \epsilon_0\dfrac{h_{31}c_1 + h_{32}c_2 + h_{33}c_3}{h_{21}c_1 + h_{22}c_2 + h_{23}c_3} \end{array}\right. \tag{3.2.19}$$

from which, c_1, c_2 and c_3 can be determined. In addition, the property of Chebyshev polynomials (Erdogan, 1975) given by,

$$\int_{-1}^{1}\frac{T_n(u)du}{(u-x)\sqrt{1-u^2}} = \left\{\begin{array}{ll} -\pi\dfrac{|x|}{x\sqrt{x^2-1}}\left[x - \dfrac{|x|\sqrt{x^2-1}}{x}\right]^n & |x| > 1 \\ \\ \pi U_{n-1}(x) & |x| \le 1 \end{array}\right. \tag{3.2.20}$$

are used with $U_n(x)$ being the second kind Chebyshev polynomial of the nth order.

3.3 Crack Deformation Modes

Since the nonlinear electric boundary condition results in a quadratic equation in (3.2.19), multiple solutions (real or complex) can be determined, predicting multiple deformation modes of the crack physically. In this section, attention will be focused on the evaluation of deformation modes in response to different crack orientation and applied loads. Due to the symmetry of the problem, the crack orientation is limited to the range of $\theta \in [0°, 90°]$.

From Equation (3.2.19), two general solutions of c_3 are deduced,

$$c_3^{(1)} = \frac{1}{2h_{23}}(A_1 + B);\ c_3^{(2)} = \frac{1}{2h_{23}}(A_1 - B) \tag{3.3.1}$$

and the corresponding jumps of tangential and normal displacements along crack surfaces can be derived from Equation (3.2.16) as,

$$\begin{cases} d_1^{(1)} = \left[h_{11}\sigma_{21}^0 + h_{12}\sigma_{22}^0 - \dfrac{h_{13}}{2h_{23}}(A_1 + B)\right]\sqrt{a^2 - x^2} \\ \\ d_1^{(2)} = \left[h_{11}\sigma_{21}^0 + h_{12}\sigma_{22}^0 - \dfrac{h_{13}}{2h_{23}}(A_1 - B)\right]\sqrt{a^2 - x^2} \end{cases} \tag{3.3.2}$$

$$\begin{cases} d_2^{(1)} = \dfrac{1}{2}(A_2 - B)\sqrt{a^2 - x^2} \\ \\ d_2^{(2)} = \dfrac{1}{2}(A_2 + B)\sqrt{a^2 - x^2} \end{cases} \tag{3.3.3}$$

where

$$\begin{cases} A_1 = h_{21}\sigma_{21}^0 + h_{22}\sigma_{22}^0 - h_{23}D_2^0 - \epsilon_0 h_{33} \\ A_2 = h_{21}\sigma_{21}^0 + h_{22}\sigma_{22}^0 + h_{23}D_2^0 + \epsilon_0 h_{33} \\ C = 4\epsilon_0\left[(h_{23}^2 - h_{22}h_{33})\sigma_{22}^0 + (h_{23}h_{31} - h_{21}h_{33})\sigma_{21}^0\right] \\ B = \sqrt{A_2^2 + C} \end{cases} \tag{3.3.4}$$

Following results can be predicted from equations (3.3.1)-(3.3.4),

(i) $C > 0$, which results in $B > |A_2|$. There exists two solutions corresponding to open crack $d_2^{(2)} > 0$ and closed crack $d_2^{(1)} < 0$ respectively.

(ii) $C \leq 0$ and $A_2^2 + C \geq 0$, which results in $B \leq |A_2|$. For the case where $A_2 > 0$, there exists two solutions corresponding to open cracks with $d_2^{(1)} > 0$ and $d_2^{(2)} > 0$. When $A_2 \leq 0$, only closed crack is predicted with $d_2^{(1)} \leq 0$ and $d_2^{(2)} \leq 0$.

(iii) $C < 0$ and $A_2^2 + C < 0$. There is no real solution, which corresponds to a closed crack $d_2^{(1)} = d_2^{(2)} = 0$.

In the following discussion, these mathematical results will be used to predict different deformation modes of the crack under different loading conditions.

3.3.1 A tensile normal load and a shear load

Firstly, we will consider the case where the cracked body is subjected to remotely applied electromechanical loads $(\mathrm{t}^\infty, \mathrm{s}^\infty)$, which can be represented in the local coordinate system oxy as $\sigma_{21}^0, \sigma_{22}^0$ and D_2^0, with $\sigma_{22}^0 > 0$ and $1, 2$ corresponding to x and y, respectively. It should be noted that in this case, local coordinate axes x and

y are always parallel and perpendicular, respectively, to the crack surfaces. For the case of $\sigma_{21}^0 \geq 0$, a positive $C(> 0)$ is predicted. Equation (3.2.19), therefore, has two different solutions as given in (3.3.1) irrespective of the applied electric loading conditions. It can be determined from Equation (3.3.3) that $d_2^{(1)} < 0$ and $d_2^{(2)} > 0$, which correspond to overlapping and opening of the crack surfaces, respectively. Since crack surface overlapping contradicts with the original crack model, for this loading case, only one open mode exists with $d_2^{(2)} > 0$. It should be noted that for cases where the poling direction is not perpendicular to the crack surfaces, shear deformation of the crack ($d_1^{(2)} \neq 0$) will be generated even for pure normal loading condition ($\sigma_{21}^0 = 0, D_2^0 = 0$). This coupling effect is illustrated in Figure 3.2 for the case where piezoelectric medium is taken as $PZT-4$ with materials properties being given in the Appendix and $\sigma_{22}^0 = 20MPa$ and $a = 1mm$. It is shown that the crack opening deformation decreases with increasing θ, while the shear deformation reaches its maximum value when $\theta = 45°$.

For $\sigma_{21}^0 < 0$, more complicated deformation modes exist. When the applied mechanical loads satisfy $\left|\frac{\sigma_{22}^0}{\sigma_{21}^0}\right| > \frac{h_{23}h_{31} - h_{21}h_{33}}{h_{23}^2 - h_{22}h_{33}}$, which results in $C > 0$, there are still two solutions for c_3 as given in Equation (3.3.1), with $c_3^{(2)}$ being the solution corresponding to the opening crack mode $d_2^{(2)} > 0$. However, when the mechanical loading ratio reduces to $\left|\frac{\sigma_{22}^0}{\sigma_{21}^0}\right| < \frac{h_{23}h_{31} - h_{21}h_{33}}{h_{23}^2 - h_{22}h_{33}}$, which corresponds to $C < 0$, the crack deformation modes will depend on the level of electric loading, identified by

two critical values of D_2^0,

$$D_2^{(1)} = \frac{1}{h_{23}}\Big\{ - h_{21}\sigma_{21}^0 - h_{22}\sigma_{22}^0 - h_{33}\epsilon_0 + 2\sqrt{\epsilon_0\left[(h_{22}h_{33} - h_{23}^2)\sigma_{22}^0 - (h_{23}h_{31} - h_{21}h_{33})\sigma_{21}^0\right]}\Big\} \tag{3.3.5}$$

$$D_2^{(2)} = \frac{1}{h_{23}}\Big\{ - h_{21}\sigma_{21}^0 - h_{22}\sigma_{22}^0 - h_{33}\epsilon_0 - 2\sqrt{\epsilon_0\left[(h_{22}h_{33} - h_{23}^2)\sigma_{22}^0 - (h_{23}h_{31} - h_{21}h_{33})\sigma_{21}^0\right]}\Big\} \tag{3.3.6}$$

When the applied electric displacement satisfies $D_2^0 > D_2^{(1)}$, which is identified by condition (ii) with $A_2 > 0$, there are two solutions for c_3 resulting in positive crack opening, indicating that the deformation of crack is an unstable process with two different possible profiles, $d_2^{(1)} > 0, d_2^{(2)} > 0$, which are given in Equation (3.3.3). For $D_2^0 = D_2^{(1)}$, a unique solution exists with $d_2^{(1)} = d_2^{(2)} > 0$. When $D_2^{(2)} < D_2^0 < D_2^{(1)}$, this loading condition results in $A_2^2 + C < 0$ as described in condition (iii), which corresponds to a closed crack. While for $D_2^0 \leq D_2^{(2)}$, two solutions with crack surface overlapping are found with these solutions being the same when $D_2^0 = D_2^{(2)}$. This case is identified by condition (ii) with $A_2 < 0$ and corresponds to a closed crack.

3.3.2 A compressive normal load and a shear load

When the normal load mentioned in the previous discussion is replaced by a compressive one ($\sigma_{22}^0 < 0$), the crack deformation modes will depend on the direction of the shear load and the ratio between normal and shear loads. For the case where $\sigma_{21}^0 \leq 0$ or $\sigma_{21}^0 > 0$ with $\left|\frac{\sigma_{22}^0}{\sigma_{21}^0}\right| > \frac{h_{23}h_{31} - h_{21}h_{33}}{h_{23}^2 - h_{22}h_{33}}$, two critical values for D_2^0 as shown in equations (3.3.5) and (3.3.6) can also be found. These loading conditions correspond to

$C < 0$. The solutions for these cases are similar to the case of $\sigma_{22}^0 > 0, \sigma_{21}^0 < 0$ with $\left|\frac{\sigma_{22}^0}{\sigma_{21}^0}\right| < \frac{h_{23}h_{31} - h_{21}h_{33}}{h_{23}^2 - h_{22}h_{33}}$ as discussed before. But in this case, since the normal loading is compressive, a closed crack is also a possible solution of the problem. Therefore, there are two open modes and one closed mode for $D_2^0 > D_2^{(1)}$, one open and one closed modes for $D_2^0 = D_2^{(1)}$ and one closed mode for $D_2^0 < D_2^{(1)}$. It should be mentioned that although complicated modes are observed for $D_2^0 < D_2^{(2)}$, since overlapping of the crack surfaces is meaningless for the current problem, these are considered as a unique mode of a closed crack. When the loading ratio reduces to $\left|\frac{\sigma_{22}^0}{\sigma_{21}^0}\right| < \frac{h_{23}h_{31} - h_{21}h_{33}}{h_{23}^2 - h_{22}h_{33}}$ with $\sigma_{21}^0 > 0$, $C > 0$ is predicted, which satisfies condition (i). There are, therefore, one open and one closed deformation modes for the crack in this case.

For a specific case where the crack is perpendicular to the poling direction ($\theta = 0°$), the typical crack opening displacement (COD) at the centre of the crack in $PZT-4$ is shown in Figure 3.3 under a pure compressive load $\sigma_{22}^0 = -0.5MPa$. The existence of two open modes in this figure indicates that the deformation of the crack is an unstable process with different possible profiles. Although the multiple deformation modes are governed by an unstable process, they may be achieved by using different loading processes. For example, an applied compressive stress σ_{22}^0 followed by $D_2^0 = D^* > D_2^{(1)}$ may result in zero crack opening only. However, for the same applied $D_2^0 = D^*$, if a tensile stress is applied first to induce a crack opening, then changed back to the corresponding compressive stress σ_{22}^0, a non-zero crack opening displacement may be generated. To illustrate this process, let us consider a specific example. Figure 3.4 shows the variation of the opening displacement at the

centre of the crack with the applied stress σ_{22}^0. A tensile stress $\sigma_{22}^0 = 10MPa$ and an electric displacement $D_2^0 = D^* = 0.1C/m^2$ are applied first, which result in an initial opening deformation of the crack. Without changing D_2^0, the applied stress is then reduced and the deformation of the crack will follow the path shown in this figure, according to the current solution. When the applied normal stress becomes a compressive one, $\sigma_{22}^0 = -10MPa$ for example, the crack is still open. This example clearly shows the effect of the loading sequence.

3.3.3 Pure shear loading

When the crack is subjected to a pure shear load $\sigma_{21}^0 > 0$ ($\sigma_{22}^0 = 0$), C is positive as discussed in (i). Two solutions of c_3 can be found, which are independent of electric loading. These two solutions result in overlapping and opening of the crack surfaces, respectively, i.e. $d_2^{(1)} < 0, d_2^{(2)} > 0$. Figure 3.5 shows both the opening and shear displacement at the centre of the crack under pure shear loading $\sigma_{21}^0 = 20MPa$ for different crack orientation θ. The crack opening displacement approaches its maximum value when $\theta = 45°$, while shear deformation increases with increasing crack orientation. Considering the fact that the applied shear load is always parallel to the crack surfaces, this coupling effect is significant with the crack opening displacement being 11% of the shear deformation at $\theta = 45°$.

More complicated deformation modes can be observed for $\sigma_{21}^0 < 0$. When the electric displacement applied satisfies $D_2^0 > D_2^{(1)}$, there are two open crack modes. While for $D_2^0 < D_2^{(1)}$, a closed crack mode exists.

3.3.4 Summary of crack deformation modes

The crack deformation modes under different loading conditions are summarized in Table 3.1, in which $\gamma = \left|\frac{\sigma_{22}^0}{\sigma_{21}^0}\right|$, $\gamma_0 = \left|\frac{h_{23}h_{31} - h_{21}h_{33}}{h_{23}^2 - h_{22}h_{33}}\right|$ and $D_2^{(1)}$, $D_2^{(2)}$ are given by equations (3.3.5) and (3.3.6). Only physically possible deformation modes are included in this table.

Table 3.1: Crack deformation modes under different electromechanical loads

Mechanical loading	Electric loading	Number of solutions	Deformation modes
$\sigma_{22}^0 > 0, \sigma_{21}^0 \geq 0$	any D_2^0	2	Open
$\sigma_{22}^0 \geq 0, \sigma_{21}^0 < 0$ $\gamma < \gamma_0$	$D_2^0 > D_2^{(1)}$	2	Open
	$D_2^0 = D_2^{(1)}$	1	Open
	$D_2^0 < D_2^{(2)}$	2	Closed
	$D_2^0 = D_2^{(2)}$	1	Closed
	$D_2^{(2)} < D_2^0 < D_2^{(1)}$	1	Closed
$\sigma_{22}^0 > 0, \sigma_{21}^0 < 0$ $\gamma > \gamma_0$	any D_2^0	2	Open
$\sigma_{22}^0 < 0, \sigma_{21}^0 \leq 0$	$D_2^0 > D_2^{(1)}$	2	Open and Closed
	$D_2^0 = D_2^{(1)}$	1	Open and Closed
	$D_2^0 < D_2^{(2)}$	2	Closed
	$D_2^0 = D_2^{(2)}$	1	Closed
	$D_2^{(2)} < D_2^0 < D_2^{(1)}$	1	Closed
$\sigma_{22}^0 < 0, \sigma_{21}^0 > 0$ $\gamma > \gamma_0$	$D_2^0 > D_2^{(1)}$	2	Open and closed
	$D_2^0 = D_2^{(1)}$	1	Open and Closed
	$D_2^0 < D_2^{(2)}$	2	Closed
	$D_2^0 = D_2^{(2)}$	1	Closed
	$D_2^{(2)} < D_2^0 < D_2^{(1)}$	1	Closed
$\sigma_{22}^0 \leq 0, \sigma_{21}^0 > 0$ $\gamma < \gamma_0$	any D_2^0	2	Open and closed

3.4 Nonlinear Fracture Behaviour

In this section, the fracture behaviour of a piezoelectric medium with an arbitrarily oriented crack, subjected to remotely applied $(\mathbf{t}^{\infty}, \mathbf{s}^{\infty})$, is studied numerically using traditional stress intensity factors and electric displacement intensity factor, energy release rate and crack opening displacement (COD) intensity factor. The effect of the electric boundary condition is also demonstrated. $PZT-4$ ceramic is taken as the cracked medium for numerical simulation.

3.4.1 Fracture parameters

Based on electroelastic fields provided in section 3.2, the stress and electric displacement field $\mathbf{t}$, at a distance $r = |x| - a$ ahead of the crack tip, can be expressed in terms of stress and electric displacement intensity factor $\mathbf{k}$,

$$\mathbf{t}(r) = \frac{\mathbf{k}}{\sqrt{2\pi r}} \tag{3.4.1}$$

where $\mathbf{k} = \{K_{II}, K_I, K_D\}^T$, with K_I, K_{II} and K_D being the stress intensity factors of modes I and II and the electric displacement intensity factor, respectively. From equations (3.2.11), (3.2.14), (3.2.15) and (3.2.20), $\mathbf{k}$ can be derived as,

$$\mathbf{k} = -\sqrt{\pi a}\mathbf{c} \tag{3.4.2}$$

The corresponding jumps of displacements and electric potential across the crack surfaces can also be expressed explicitly as,

$$\mathbf{d}(x,0) = \sqrt{\frac{2(a-x)}{\pi}}\mathbf{H}\mathbf{k}, \quad |x| \leq a \tag{3.4.3}$$

Parallel to the crack closure integral derived by Irwin (1957) for cracks in traditional elastic materials, the energy release rate of a crack in piezoelectric materials was derived by Suo et al. (1992). From equations (3.4.1) and (3.4.3), this energy release rate is expressed, as

$$G = \lim_{\delta \to 0+} (\frac{1}{2\delta} \int_a^{a+\delta} \mathbf{t}^T(x)\mathbf{d}(x-\delta)dx) = \frac{1}{4}\mathbf{k}^T\mathbf{H}\mathbf{k} \tag{3.4.4}$$

in which the following identity is used,

$$\int_0^1 t^{1/2}(x-t)^{-1/2}dt = \frac{\pi}{2} \tag{3.4.5}$$

According to existing experimental results (Park and Sun, 1994; 1995a, b), the energy release rate may not be a suitable fracture criterion for cracks in piezoelectric materials. To describe the mechanical deformation, it is interesting to consider the property of crack opening displacement (COD), the jump of displacement across crack surfaces. A COD intensity factor K_{COD}, which can be used to describe the opening deformation of the crack surfaces, is introduced to evaluate the fracture behaviour, defined as,

$$K_{COD} = \lim_{x \to a} \frac{d_2}{\sqrt{a-x}} = \sqrt{\frac{2}{\pi}}\{h_{21}\ h_{22}\ h_{23}\}\mathbf{k} \tag{3.4.6}$$

3.4.2 Effect of electric field

Firstly, we will restrict our attention on the effect of electric field upon the fracture behaviour of cracked piezoelectric materials. Figure 3.6 shows the effect of the applied electric field intensity E_2^∞ on the energy release rate G for the case where the poling direction of the piezoelectric medium is perpendicular to crack surfaces ($\theta = 0°$) and

the medium is subjected to a tensile stress $\sigma_{22}^{\infty} = 20MPa$. If the energy release rate is used as a criterion to predict crack propagation, it is clearly indicated in this figure that the presence of electric loading always reduces this energy release rate implying that the electric field will impede crack propagation. Comparison with the energy release rate for an electrically impermeable crack, G^I, and the permeable result, G^p, is also provided. In the current case, a significant discrepancy between G and G^p can be observed, indicating the importance of considering the crack opening for formulating electric boundary condition along crack surfaces.

As argued by Park and Sun (1994; 1995a, b) that fracture is a mechanical process, energy release rate may not be a suitable fracture criterion for cracks in piezoelectric materials. It is interesting to consider the mechanical deformation of crack directly, a COD intensity factor is used to evaluate the effect of electric field upon the crack propagation. The variation of K_{COD} for a tensile crack with applied electric field intensity E_2^{∞} for $\sigma_{22}^{\infty} = 20MPa$ is shown in Figure 3.7 when the crack orientation $\theta = 0^o$. The corresponding results using impermeable (K_{COD}^I) and permeable(K_{COD}^P) crack models are also provided in this figure for comparison. It can be observed that K_{COD} for both the current and impermeable crack models increases monotonically with increasing electric field, while keeps constants for permeable crack model. If K_{COD} is used as a fracture parameter and it is assumed that the crack will propagate when K_{COD} reaches a critical value, the corresponding critical stress $\sigma_{22}^{cr}(E_2^{\infty})$ for different applied electric fields can be predicted. The normalized critical stress $\sigma^* = \sigma_{22}^{cr}(E_2^{\infty})/\sigma_{22}^{cr}(0)$ is depicted in Figure 3.8. It can be concluded from this figure that an applied positive electric field tends to reduce the critical stress, while an applied

negative electric field will increase it. This conclusion agrees with the experimental results given by Park and Sun (1994; 1995a, b).

3.4.3 Effect of crack orientation

Figure 3.9 shows the variation of normalized intensity factors $k_I = K_I/K_I^0$, $k_{II} = K_{II}/K_I^0$ and $k_D = K_D/K_D^0$ with the change of crack orientation, in which superscript '0' represents the case where the poling direction is perpendicular to crack surfaces ($\theta = 0$). Regardless of the applied electric and mechanical loads, the variation of k_I and k_{II} with crack orientation is always the same as that for a crack in a traditional isotropic elastic medium. However, the relation of k_D with the crack orientation will vary for different applied electromechanical loads as shown in Figure 3.9, in which $k_D^{(1)}$ and $k_D^{(2)}$ correspond to $\sigma_{22}^{\infty} = 20MPa$ and $\sigma_{22}^{\infty} = 30MPa$, respectively, with $D_2^{\infty} = 0.001C/m^2$. It should be noted that under this tensile loading condition, only the open crack mode is considered.

To predict the combined effect of crack orientation and applied electric field upon crack deformation, the behaviour of the COD intensity factor is considered. For an applied mechanical load $\sigma_{22}^{\infty} = 20MPa$, the variation of K_{COD} with an applied electric field intensity E_2^{∞} along poling direction is depicted in Figure 3.10 for different crack orientations. It can be observed that K_{COD} increases monotonically with increasing electric field for small θ. However, with the increase of angle of crack orientation, this effect becomes insignificant. If K_{COD} is regarded as a fracture parameter, current result predicts that a positive electric field will enhance the crack initiation, while a negative electric field will impede it for $\theta < 90°$.

3.4.4 Effect of electric boundary condition

The effect of electric boundary conditions upon the fracture parameter K_D has been investigated by Xu and Rajapakse (2001) for the case where relatively low mechanical loads are applied, i.e. a tensile stress $\sigma_{22}^{\infty} = 0.6MPa$ was used for numerical simulation. The resulting K_D for the crack based on the 'real' electric boundary condition is found nearly identical to that from the permeable crack model. However, the results given in that paper can not be used to study the transition between permeable and impermeable crack models and the property of multiple deformation modes of the crack with increasing loading level, which are the fundamental features of this nonlinear crack problem. The understanding on the nonlinear fracture behaviour of oriented cracks in piezoelectric materials is still very limited and needs to be further studied. For an oriented crack both normal and tangential deformation of the crack surface may affect the electric boundary condition. This important issue has not been discussed in the previous studies.

The current study indicates that with increasing applied loading level, the crack opening increases and may result in significant discrepancy between the current dielectric model and the permeable model. This phenomenon is illustrated in Figure 3.11, which shows the effect of electric boundary conditions upon K_D under different applied electric field intensity E_2^{∞} for a higher mechanical load $\sigma_{22}^{\infty} = 50MPa$ for the case where the poling direction is perpendicular to crack surfaces. To show the transition between the permeable and impermeable crack models under different mechanical loads, the variation of the electric displacement intensity factor K_D with

σ_{22}^{∞} from different crack models are plotted in Figure 3.12 for $E_2^{\infty} = 500V/mm$ and $\theta = 45°$. It is observed that K_D from the current dielectric crack model is always between the predictions from impermeable (K_D^I) and permeable (K_D^P) models. K_D approaches the corresponding results from permeable and impermeable models for low and high stress levels, respectively.

The effect of the boundary condition upon K_{COD} is shown in Figure 3.13 for evaluating the crack surface deformation based on the impermeable, permeable and current dielectric crack models for $\sigma_{22}^{\infty} = 1MPa$ and $D_2^{\infty} = 0.001C/m^2$. At this low stress level, K_{COD} is very close to the result from the permeable model. But significant discrepancy between predictions on K_{COD} from impermeable and permeable models can be observed. Figure 3.14 provides the corresponding results for a higher applied stress level, $\sigma_{22}^{\infty} = 80MPa$, showing the significant difference between the permeable model and the current model. Figure 3.14 further indicates that with the increase of crack orientation, the discrepancy among these three models decreases. When $\theta = 90°$, i.e. the crack is parallel to the poling direction, these three models predict unique K_{COD} as expected. The transition between the permeable and impermeable crack models is also evidenced by the variation of crack opening displacement intensity factor K_{COD} with applied tensile stress σ_{22}^{∞} for the case where the applied electric field $E_2^{\infty} = 500V/mm$ and crack orientation $\theta = 0°$, as shown in Figure 3.15. Similar results to Figure 3.12 are observed.

3.5 Conclusions

It is observed from the current study that the crack opening has a significant effect on the electric boundary condition along the crack surfaces. The electromechanical behaviour of a dielectric slit crack is deformation-dependent. Unlike the results from the traditional crack models, nonlinear response and multiple deformation modes of the crack are predicted. It can be concluded from the numerical results that both crack orientation (or poling direction) and electric boundary condition along the crack surfaces may play significant roles in determining the fracture behaviour of this kind of materials. The transition between the permeable and impermeable crack models is clearly demonstrated with the increase of applied loading level.

Appendix

In this dissertation, PZT-4 ceramic is taken as the piezoelectric medium for the numerical simulation. In the global Cartesian coordinate system $o'x'y'$, the material constants for PZT-4 piezoceramics are

$$
\begin{aligned}
c'_{11} &= 13.9 \times 10^{10} N/m^2 \\
c'_{12} &= 7.43 \times 10^{10} N/m^2 \\
c'_{22} &= 11.5 \times 10^{10} N/m^2 \\
c'_{66} &= 2.56 \times 10^{10} N/m^2 \\
e'_{21} &= -5.2 C/m^2 \\
e'_{22} &= 15.1 C/m^2 \\
e'_{16} &= 12.7 C/m^2 \\
\epsilon'_{11} &= 6.45 \times 10^{-9} C/Vm \\
\epsilon'_{22} &= 5.62 \times 10^{-9} C/Vm
\end{aligned}
$$

and the other parameters are 0 according to constitutive equations (2.3.1) and (2.3.2) (Park and Sun, 1994). The corresponding elements of material matrix $\mathbf{H}'$ in Equation (3.2.10) are derived as,

$$
\begin{aligned}
h'_{11} &= 3.67901 \times 10^{-11} m^2/N \\
h'_{22} &= 3.54442 \times 10^{-11} m^2/N \\
h'_{23} &= 4.41997 \times 10^{-2} m^2/C \\
h'_{32} &= 4.41997 \times 10^{-2} m^2/C \\
h'_{33} &= -1.76691 \times 10^{8} Vm/C
\end{aligned}
$$

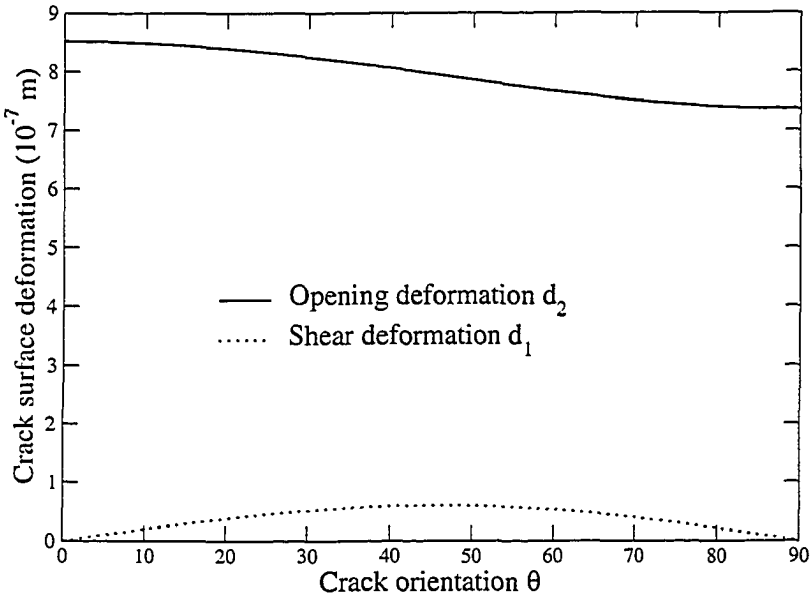

Figure 3.2: Crack surface deformation at the central point under a pure tensile load ($\sigma_{22}^0 = 20MPa$)

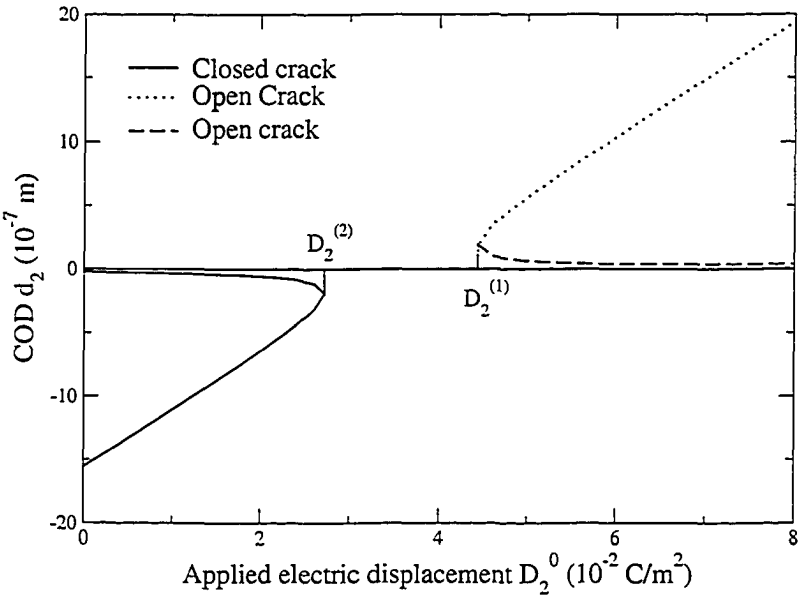

Figure 3.3: Deformation modes for the crack subjected to a compressive stress $\sigma_{22}^0 = -0.5MPa$

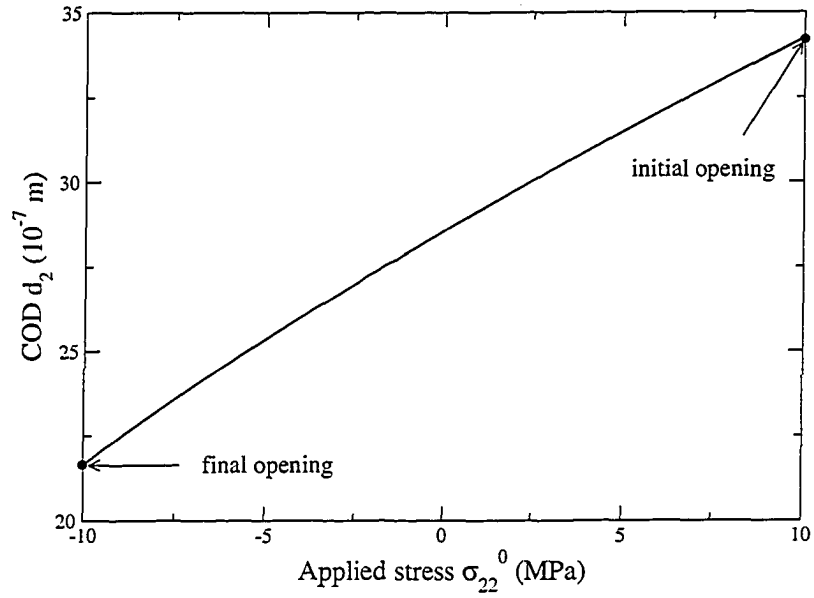

Figure 3.4: Effects of the loading sequence

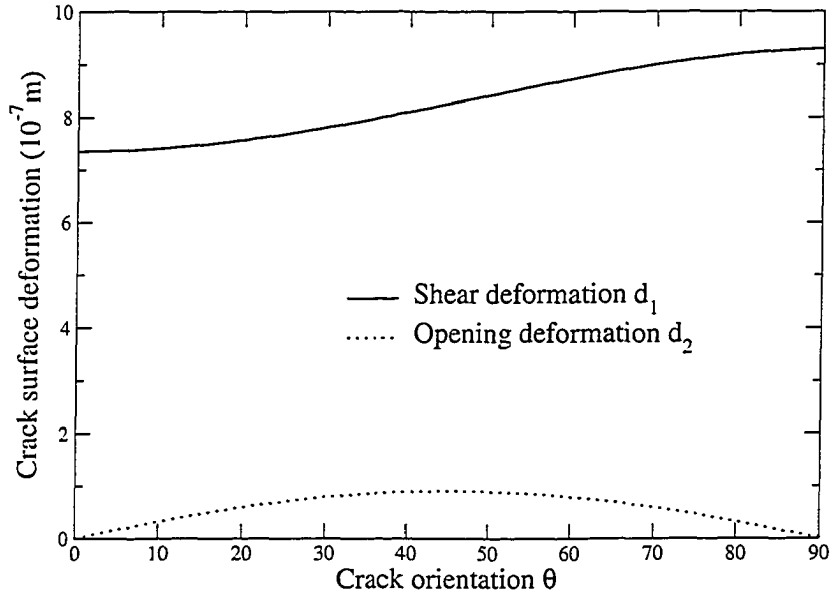

Figure 3.5: Crack surface deformation at the central point under a pure shear load ($\sigma_{21}^0 = 20MPa$)

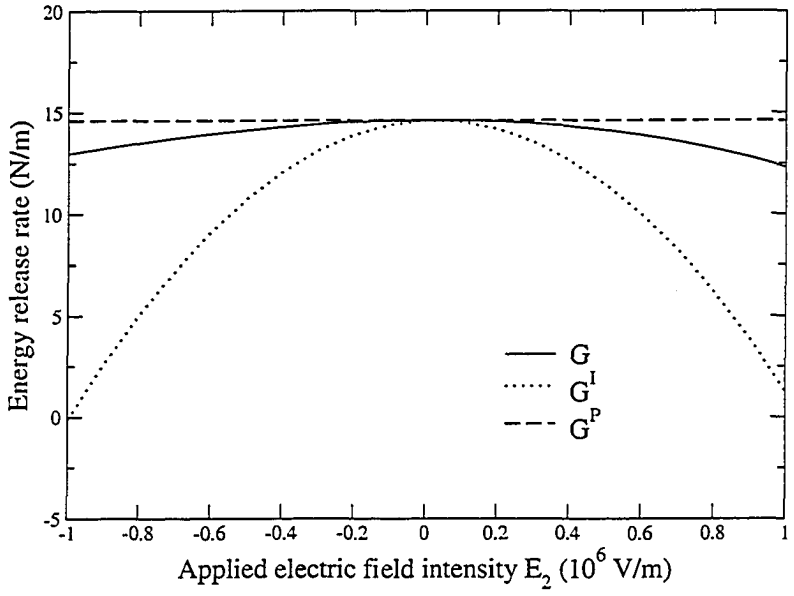

Figure 3.6: Energy release rate of a crack subjected to a tensile stress $\sigma_{22}^{\infty} = 20MPa$

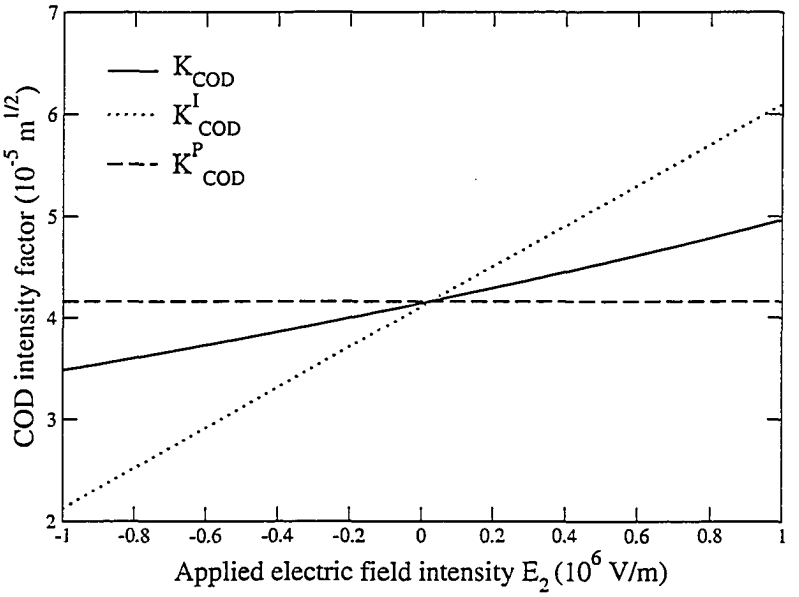

Figure 3.7: COD intensity factor of a crack subjected to a tensile stress $\sigma_{22}^{\infty} = 20MPa$

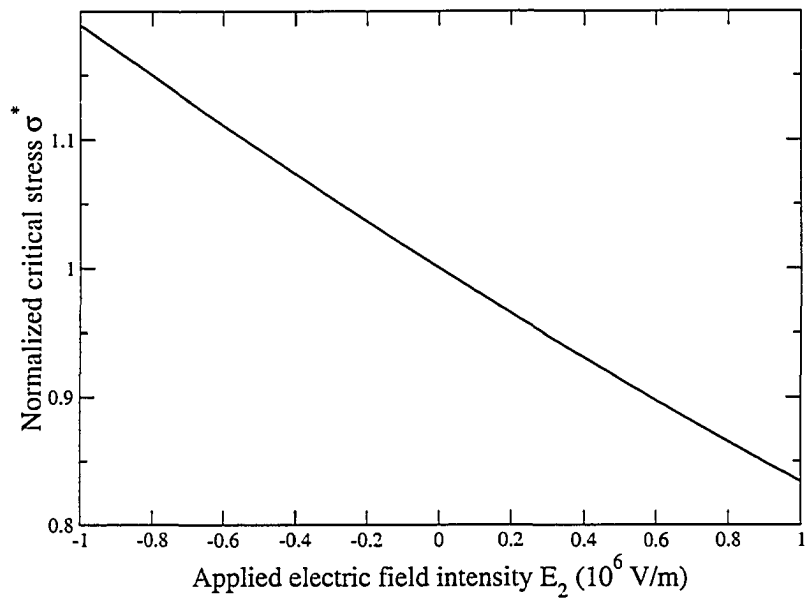

Figure 3.8: The variation of the normalized fracture load of a crack with the applied electric field

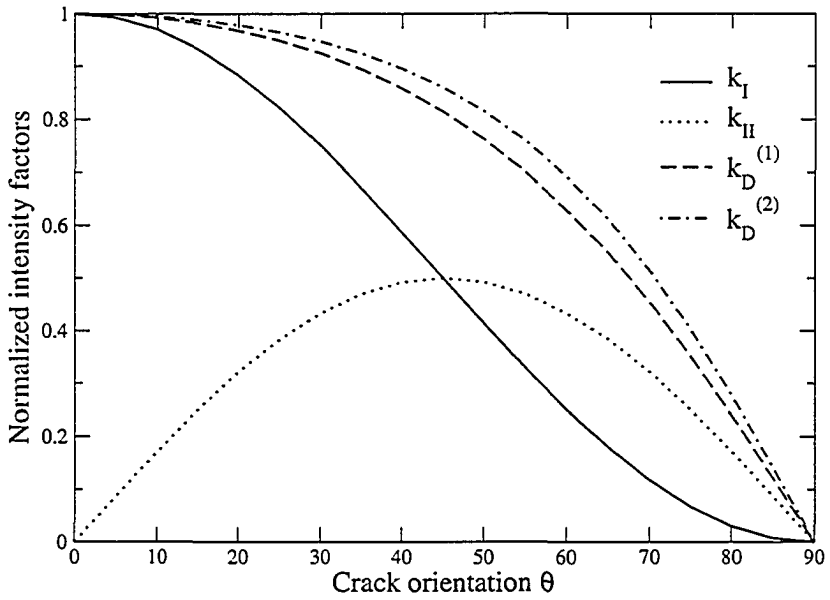

Figure 3.9: The variation of normalized intensity factors with the crack orientation

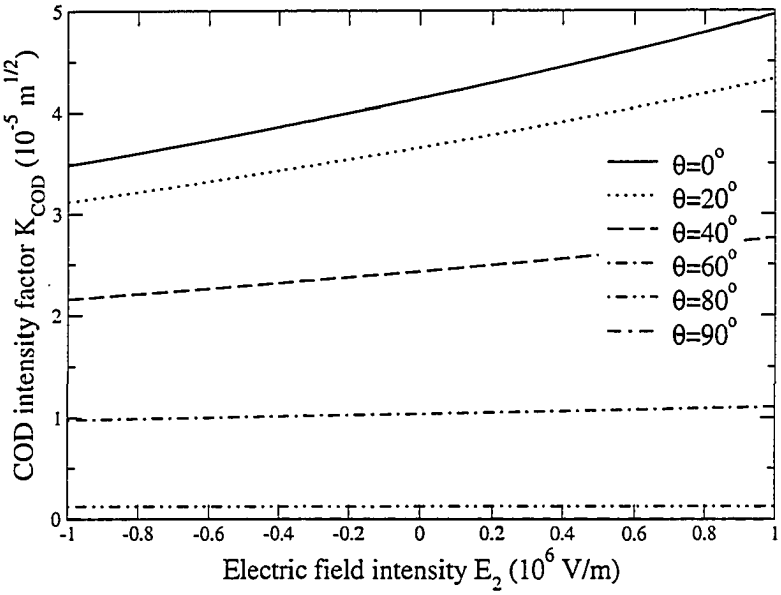

Figure 3.10: The variation of K_{COD} with applied electric field for different crack orientations

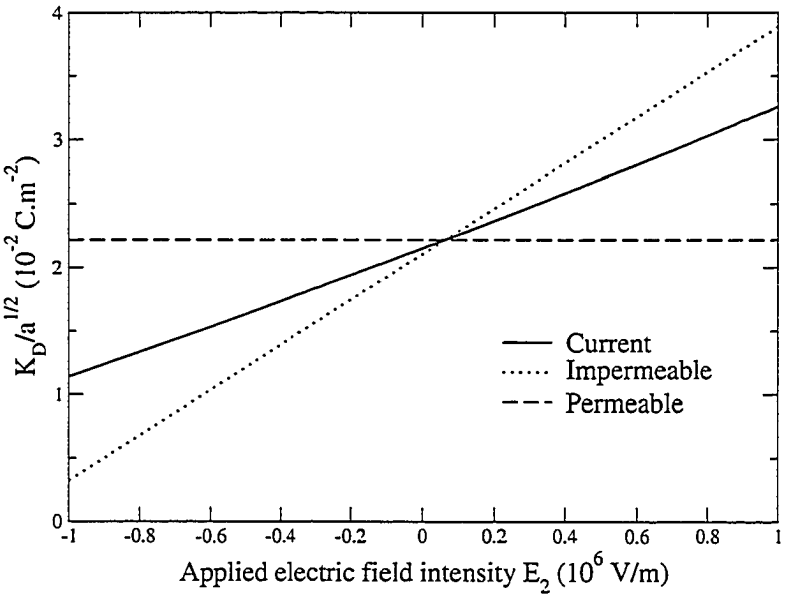

Figure 3.11: The variation of electric displacement intensity factor with the applied electric field ($\theta = 0°$)

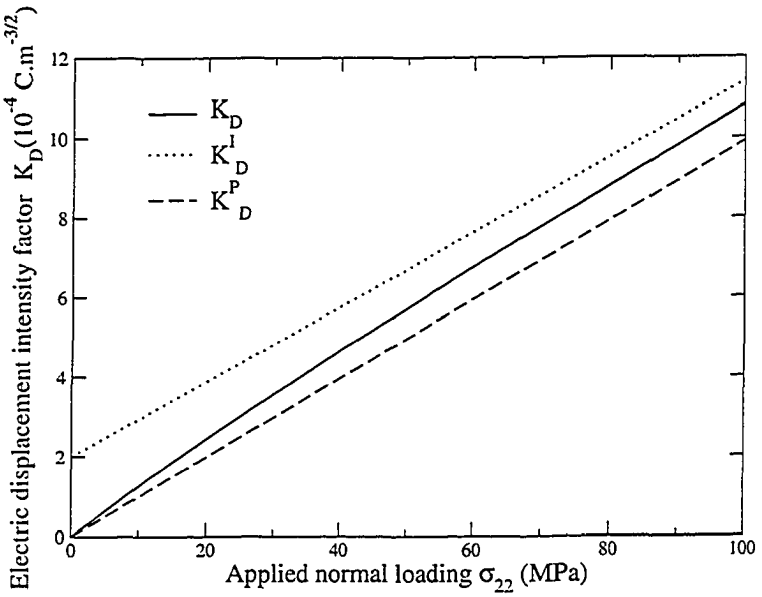

Figure 3.12: The variation of K_D with the applied normal loading for different crack models ($\theta = 45°$)

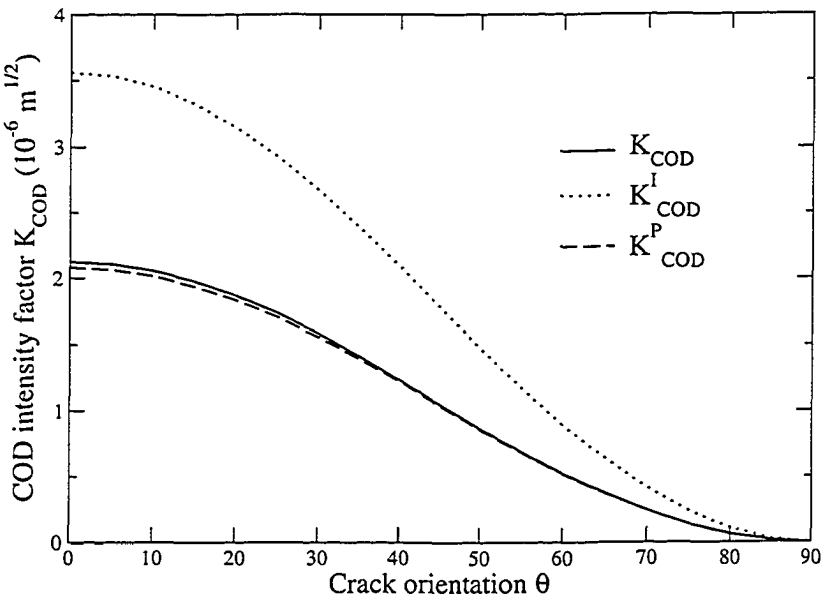

Figure 3.13: The variation of COD intensity factor with the crack orientation for different crack models ($\sigma^{\infty}_{22} = 1MPa$)

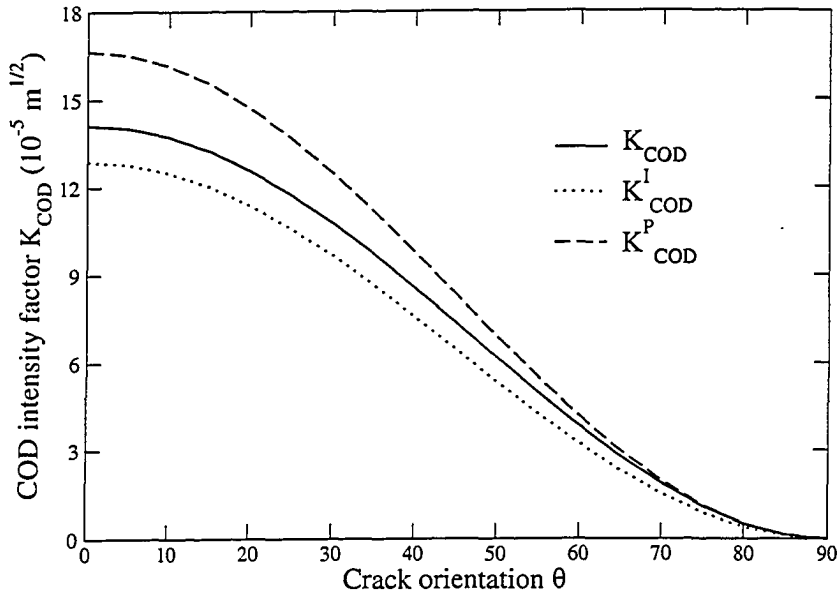

Figure 3.14: The variation of COD intensity factor with the crack orientation for different crack models ($\sigma_{22}^{\infty} = 80MPa$)

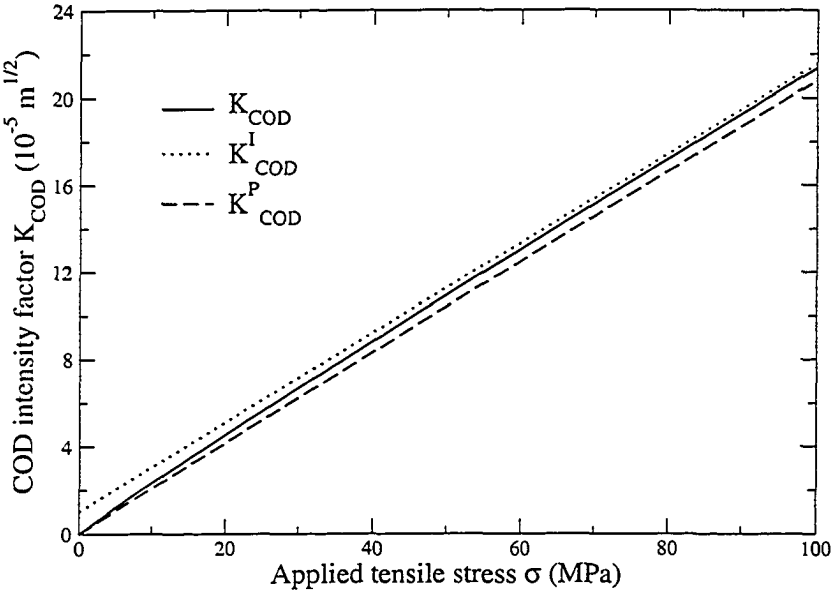

Figure 3.15: The variation of COD intensity factor with the applied normal loading for different crack models ($\theta = 0°$)

Chapter 4

Interacting Dielectric Cracks in Piezoelectric Materials

This chapter presents a study on the electromechanical behaviour of interacting dielectric cracks in piezoelectric materials. The cracks are filled with dielectric media and, as a result, the electric boundary condition along the crack surfaces is governed by the opening displacement of the cracks. The interaction between cracks is formulated by modelling the cracks using distributed dislocations and solving the resulting nonlinear singular integral equations using Chebyshev polynomials. Multiple deformation modes are predicted. A solution technique is developed to determine the desired deformation mode of the interacting cracks. Numerical simulation is conducted to study the effect of location, orientation and geometry of cracks upon the nonlinear fracture behaviour of the cracked medium. Special attention is paid to the effect of the electric boundary condition along crack surfaces upon the crack interaction. The discrepancy between different crack models in predicting the fracture behaviour is clearly observed.

4.1 Statement of the Problem

Commonly used piezoelectric ceramics have a tendency to develop multiple cracks during manufacturing and service processes. These interacting cracks will result in shielding/amplification effects, which play an important role in the fracture of these materials. Existing studies on crack interaction in piezoelectric materials are limited to two limiting cases, the electrically impermeable and permeable conditions. How the dielectric medium inside the crack affects the crack interaction is still unknown and needs to be investigated. It is, therefore, the objective of this chapter to treat the interaction among multiple cracks using a dielectric crack model, which contains the effects of the dielectric property of the crack and the crack opening deformation.

Consider the plane strain problem of N arbitrarily distributed interacting cracks in an infinite piezoelectric medium, as shown in Figure 4.1. The centre of crack k is located at (X_k, Y_k) in a global Cartesian coordinate system oxy. This piezoelectric medium is assumed to be transversely isotropic with the poling direction parallel to the y-axis. The medium is subjected to external electromechanical loads $(\mathrm{t}^{\infty}, \mathrm{s}^{\infty})$ at infinity, with $\mathrm{t}^{\infty} = \{\sigma_{21}^{\infty}\ \sigma_{22}^{\infty}\ D_2^{\infty}\}^T$ and $\mathrm{s}^{\infty} = \{\sigma_{11}^{\infty}\ \sigma_{21}^{\infty}\ D_1^{\infty}\}^T$. A set of local coordinate systems $o_k x_k y_k$ $(k = 1, 2, ...N)$ are used to describe these cracks, with the origin of (x_k, y_k) being at the centre of crack k and x_k-axis parallel to its surface. The length of the kth crack is $2a_k$ and its orientation θ_k is measured from x-axis to x_k-axis. These cracks are assumed to be filled with a dielectric medium with negligible elastic constants (air or vacuum).

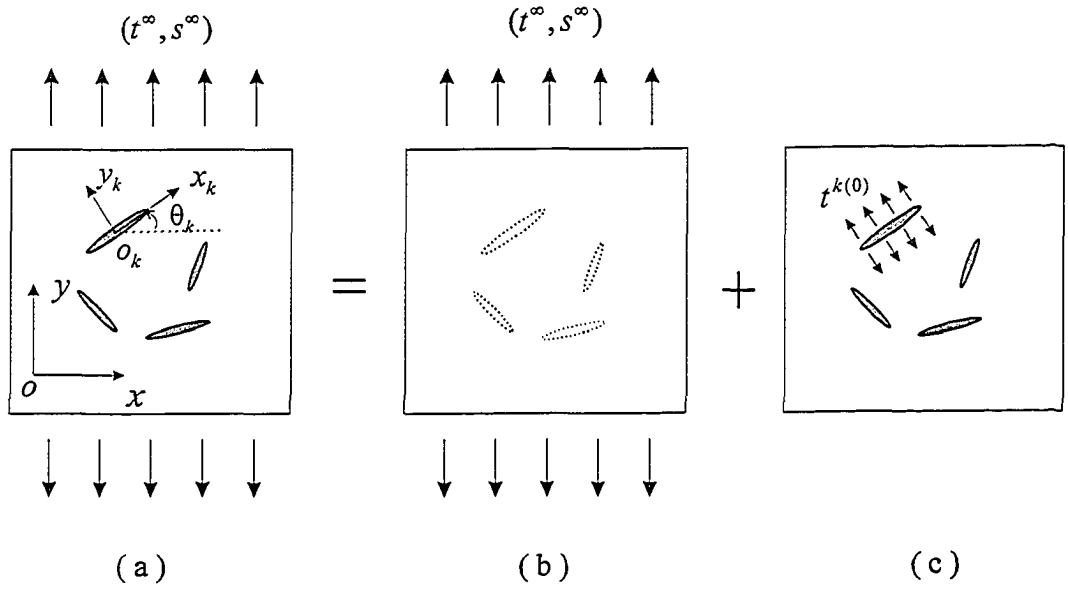

Figure 4.1: Interacting cracks and the decomposition of the problem

Similar to the single crack problem discussed in Chapter 3, the mechanical boundary condition for each crack is traction free,

$$\overline{\sigma}^k_{2i}(x_k, 0) = 0 \tag{4.1.1}$$

where $i = 1, 2$ with $1, 2$ corresponding to x_k and y_k in the local coordinate system and " $-$ " stands for the quantities in the original problem (a).

The dielectric crack model discussed in Chapter 2 will be used to represent the electric boundary condition along crack surfaces. When the effect of the tangential deformation of crack surfaces is ignored, the electric boundary condition for crack k

can be expressed as,

$$\overline{E}_2^k = -\frac{\overline{V}^{k+} - \overline{V}^{k-}}{d_2^k} \tag{4.1.2}$$

$$\overline{D}_2^k = \epsilon_0 \overline{E}_2^k \text{ or } \overline{D}_2^k = -\epsilon_0 \frac{\overline{V}^{k+} - \overline{V}^{k-}}{d_2^k} \tag{4.1.3}$$

where $\overline{E}_2^k$, $\overline{D}_2^k$ and $\overline{V}^k$ are electric field intensity, electric displacement and electric potential with superscripts $+$ and $-$ representing the upper and lower surfaces of crack k, respectively. $d_2^k = u_2^{k+}(x_k, 0) - u_2^{k-}(x_k, 0)$ is the crack opening displacement, which depends on the applied electromechanical load.

4.2 Formulation of Interacting Cracks

4.2.1 General formulation

The original problem shown in Figure 4.1(a) is decomposed into a sub-problem (b) with the undamaged medium subjected to the same remotely applied electromechanical loading as problem (a), and a sub-problem (c) containing N dielectric cracks with electromechanical loading acting along crack surfaces, i.e. $\mathbf{t}^{k(0)}$ along the surfaces of crack k.

Based on the single crack solution provided in Equations (3.2.1) and (3.2.2), the stress and electric displacement fields $(\mathbf{t}^k, \mathbf{s}^k)$ caused by the kth crack can be expressed in the local coordinate system (x_k, y_k) as,

$$\mathbf{t}^k(x_k, y_k) = -\int_{-a_k}^{a_k} \left[\mathbf{B}_1^k\left(\frac{1}{x_k + p_\alpha^k y_k - w}\right) + \mathbf{B}_2^k\left(\frac{1}{x_k + \overline{p}_\alpha^k y_k - w}\right)\right] \mathbf{\Gamma}^{k'}(w) dw \tag{4.2.1}$$

$$\mathbf{s}^k(x_k, y_k) = -\int_{-a_k}^{a_k} \left[\mathbf{C}_1^k\left(\frac{1}{x_k + p_\alpha^k y_k - w}\right) + \mathbf{C}_2^k\left(\frac{1}{x_k + \overline{p}_\alpha^k y_k - w}\right)\right] \mathbf{\Gamma}^{k'}(w) dw \tag{4.2.2}$$

with

$$\mathbf{B}_1^k\left(\frac{1}{x_k+p_\alpha^k y_k-w}\right)=\begin{cases}-\dfrac{i}{2\pi}\displaystyle\int_{-\infty}^{0}\mathbf{B}^k\mathbf{G}^k(\mathbf{B}^k)^{-1}e^{-is(x_k-w)}ds & y_k>0\\[2ex] \dfrac{i}{2\pi}\displaystyle\int_{0}^{\infty}\mathbf{B}^k\mathbf{F}^k(\mathbf{B}^k)^{-1}e^{-is(x_k-w)}ds & y_k<0\end{cases} \tag{4.2.3}$$

$$\mathbf{B}_2^k\left(\frac{1}{x_k+\overline{p}_\alpha^k y_k-w}\right)=\begin{cases}\dfrac{i}{2\pi}\displaystyle\int_{0}^{\infty}\overline{\mathbf{B}}^k\mathbf{G}^k(\overline{\mathbf{B}}^k)^{-1}e^{-is(x_k-w)}ds & y_k>0\\[2ex] -\dfrac{i}{2\pi}\displaystyle\int_{-\infty}^{0}\overline{\mathbf{B}}^k\mathbf{F}^k(\overline{\mathbf{B}}^k)^{-1}e^{-is(x_k-w)}ds & y_k<0\end{cases} \tag{4.2.4}$$

$$\mathbf{C}_1^k\left(\frac{1}{x_k+p_\alpha^k y_k-w}\right)=\begin{cases}-\dfrac{i}{2\pi}\displaystyle\int_{-\infty}^{0}\mathbf{C}^k\mathbf{G}^k(\mathbf{B}^k)^{-1}e^{-is(x_k-w)}ds & y_k>0\\[2ex] \dfrac{i}{2\pi}\displaystyle\int_{0}^{\infty}\mathbf{C}^k\mathbf{F}^k(\mathbf{B}^k)^{-1}e^{-is(x_k-w)}ds & y_k<0\end{cases} \tag{4.2.5}$$

$$\mathbf{C}_2^k\left(\frac{1}{x_k+\overline{p}_\alpha^k y_k-w}\right)=\begin{cases}\dfrac{i}{2\pi}\displaystyle\int_{0}^{\infty}\overline{\mathbf{C}}^k\mathbf{G}^k(\overline{\mathbf{B}}^k)^{-1}e^{-is(x_k-w)}ds & y_k>0\\[2ex] -\dfrac{i}{2\pi}\displaystyle\int_{-\infty}^{0}\overline{\mathbf{C}}^k\mathbf{F}^k(\overline{\mathbf{B}}^k)^{-1}e^{-is(x_k-w)}ds & y_k<0\end{cases} \tag{4.2.6}$$

where $\mathbf{\Gamma}^k=(\mathbf{H}^k)^{-1}\mathbf{d}^k$ with $\mathbf{d}^k$ being the jumps of displacements and electric potential across the surfaces of crack k defined in the local system (x_k, y_k). The material-related quantities, eigenvalues $p_\alpha^k, \overline{p}_\alpha^k$ and matrices $\mathbf{B}^k, \overline{\mathbf{B}}^k, \mathbf{C}^k, \overline{\mathbf{C}}^k$ and $\mathbf{H}^k$ can be similarly derived from the corresponding $p_\alpha, \overline{p}_\alpha, \mathbf{B}, \overline{\mathbf{B}}, \mathbf{C}, \overline{\mathbf{C}}$ and $\mathbf{H}$ in Chapter 3. It should be noted that in the crack solution provided in Chapter 3, $\mathbf{B}$, $\mathbf{C}$, $\mathbf{H}$ and p_α depend on the orientation of the crack. As a result, for cracks with different orientations, these quantities are different. It has been proved, however, that if these quantities are determined in the simple case where the crack is perpendicular to the poling

direction as $\mathbf{B}$, $\mathbf{C}$, $\mathbf{H}$ and p_α, the corresponding quantities for an oriented crack can be obtained directly by the following transformation (Suo et al., 1992),

$$\mathbf{B}^k = \mathbf{S}^k\mathbf{B},\ \mathbf{C}^k = \mathbf{S}^k\mathbf{C},\ \mathbf{H}^k = \mathbf{S}^k\mathbf{H}(\mathbf{S}^k)^T,\ p_\alpha^k = \frac{p_\alpha\cos\theta_k - \sin\theta_k}{p_\alpha\sin\theta_k + \cos\theta_k} \tag{4.2.7}$$

with the transformation matrix $\mathbf{S}^k$ being given by,

$$\mathbf{S}^k = \begin{bmatrix} \cos\theta_k & \sin\theta_k & 0 \\ -\sin\theta_k & \cos\theta_k & 0 \\ 0 & 0 & 1 \end{bmatrix} \tag{4.2.8}$$

where θ_k is the orientation of crack k.

In problem (c) of Figure 4.1, the stresses and the electric displacement $\mathbf{t}^{l(0)}$ acting on the surfaces of crack l caused by the applied external electromechanical loading $(\mathbf{t}^\infty, \mathbf{s}^\infty)$ can be expressed as,

$$\mathbf{t}^{l(0)} = \cos\theta_l\mathbf{S}^l\mathbf{t}^\infty - \sin\theta_l\mathbf{S}^l\mathbf{s}^\infty \tag{4.2.9}$$

with $\mathbf{S}^l$ being given by replacing θ_k by θ_l in Equation (4.2.8). The stresses and the electric displacement along the lth crack surfaces caused by crack k can be obtained using (4.2.1) and (4.2.2) as,

$$\mathbf{t}^{lk} = \cos\theta_{lk}\mathbf{S}^{lk}\mathbf{t}^k - \sin\theta_{lk}\mathbf{S}^{lk}\mathbf{s}^k \tag{4.2.10}$$

with $\theta_{lk} = \theta_l - \theta_k$ and $\mathbf{S}^{lk}$ being determined by replacing θ_k in Equation (4.2.8) by θ_{lk}. According to the deformed geometry, each crack in sub-problem (c) should satisfy the following boundary conditions, which are consistent with the original boundary conditions (4.1.1)-(4.1.3),

$$\sum_{k=1}^{N}\mathbf{t}^{lk} + \mathbf{t}^{l(0)} + \mathbf{K}^l(\mathbf{v}^{l+} - \mathbf{v}^{l-}) = 0\ (l = 1, 2...N) \tag{4.2.11}$$

where $\mathbf{K}^l$ is a matrix with the only nonvanishing element being $k^l_{33} = \frac{\epsilon_0}{d^l_2}$. d^l_2 is the crack opening displacement of crack l. By substituting (4.2.1), (4.2.2), (4.2.9) and (4.2.10) into (4.2.11), the general boundary conditions (4.2.11) result in the following nonlinear singular integral equations,

$$\frac{1}{\pi}\int_{-a_l}^{a_l}\frac{\mathbf{\Gamma}^{l'}(w)}{w-x_l}dw + \sum_{k\neq l}^{N}\Bigg\{\cos\theta_{lk}\mathbf{S}^{lk}\Bigg[\int_{-a_k}^{a_k}\Big(\mathbf{B}^k_1\Big(\frac{1}{w-(x_l+x_{lk}+p^k_\alpha y_{lk})}\Big)+ \mathbf{B}^k_2\Big(\frac{1}{w-(x_l+x_{lk}+\overline{p}^k_\alpha y_{lk})}\Big)\Big)\mathbf{\Gamma}^{k\prime}(w)dw\Bigg] - \sin\theta_{lk}\mathbf{S}^{lk}\Bigg[\int_{-a_k}^{a_k}\Big(\mathbf{C}^k_1\Big(\frac{1}{w-(x_l+x_{lk}+p^k_\alpha y_{lk})}\Big) + \mathbf{C}^k_2\Big(\frac{1}{w-(x_l+x_{lk}+\overline{p}^k_\alpha y_{lk})}\Big)\Big)\mathbf{\Gamma}^{k\prime}(w)dw\Bigg]\Bigg\} + \mathbf{t}^{l(0)}(x_l) + \mathbf{K}^l\mathbf{H}^l\mathbf{\Gamma}^l(x_l) = 0, \quad (l = 1, 2...N) \tag{4.2.12}$$

where $x_{lk} = X_l - X_k$ and $y_{lk} = Y_l - Y_k$. The integral equations given in (4.2.12) are characterized by square root singularity and, therefore, the general solution of them can be expressed as,

$$\mathbf{\Gamma}^{l'}(w) = \sum_{m=0}^{\infty}\mathbf{c}^l_m T_m(\frac{w}{a_l})/\sqrt{1-\frac{w^2}{a_l^2}} \tag{4.2.13}$$

where $\mathbf{c}^l_m = \{c^l_{1m}, c^l_{2m}, c^l_{3m}\}^T$ are unknown vectors to be determined and $T_m(\frac{w}{a_l})$ is the first kind of Chebyshev polynomial of the mth order. The continuity condition outside crack length $\mathbf{d}(x_l, 0) = \mathbf{v}^+(x_l, 0) - \mathbf{v}^-(x_l, 0) = 0$ $(|x_l| \geq a_l)$ results in,

$$\int_{-a_l}^{a_l}\mathbf{\Gamma}^{l'}(w)dw = 0 \tag{4.2.14}$$

From the orthogonality conditions of the Chebyshev polynomials, Equation (4.2.14) reduces to $\mathbf{c}^l_0 = 0$ in Equation (4.2.13).

Substituting (4.2.13) into (4.2.12), the following nonlinear algebraic equations can

be obtained,

$$\sum_{m=1}^{\infty} \mathbf{c}_m^l \frac{\sin(m\cos^{-1}\frac{x_l}{a_l})}{\sin(\cos^{-1}\frac{x_l}{a_l})} + \sum_{k\neq l}^{N}\sum_{m=1}^{\infty}\int_{-a_k}^{a_k}\Big[\cos\theta_{lk}\mathbf{S}^{lk}(\mathbf{B}_1^k+\mathbf{B}_2^k) - \sin\theta_{lk}\mathbf{S}^{lk}(\mathbf{C}_1^k+\mathbf{C}_2^k)\Big]$$
$$\mathbf{c}_m^k T_m(\frac{w}{a_k})/\sqrt{1-(\frac{w}{a_k})^2}dw - \sum_{m=1}^{\infty}\mathbf{M}^l c_m^l \frac{a_l}{m}\sin(m\cos^{-1}\frac{x_l}{a_l}) = -\mathbf{t}^{l(0)}(x_l) \quad (l=1,2...N) \tag{4.2.15}$$

where

$$\mathbf{M}^l = \begin{bmatrix} 0 & 0 & 0 \\ 0 & 0 & 0 \\ 0 & 0 & 0 \\ h_{31}^l\frac{\epsilon_0}{d_2^l} & h_{32}^l\frac{\epsilon_0}{d_2^l} & h_{33}^l\frac{\epsilon_0}{d_2^l} \end{bmatrix} \tag{4.2.16}$$

$$d_2^l = -\sum_{m=1}^{\infty}[h_{21}^l c_{1m}^l + h_{22}^l c_{2m}^l + h_{23}^l c_{3m}^l]\frac{a_l}{m}\sin(m\cos^{-1}\frac{x_l}{a_l}) \tag{4.2.17}$$

The unknown vectors $\mathbf{c}_m^l$ can be determined by solving Equation (4.2.15), from which the electromechanical behaviour of interacting cracks can be predicted. To solve this equation, a collocation method is used. It is assumed that equation (4.2.15) is satisfied, for each crack, at M collocation points $x_{ln} = a_l\cos\frac{(n-1)\pi}{M-1}$ $(n=1,2,...M)$ and the Chebyshev polynomials are truncated at Mth term. The governing equations are then reduced to a system of algebraic equations. The mechanical and electric behaviour of interacting dielectric cracks can be determined by solving these equations.

4.2.2 Fracture parameters

Similar to the single crack problem, the singular stress and electric displacement $\mathbf{t}$, at a distance $r_l = |x_l| - a_l$ ahead of the tip of crack l, can be expressed as,

$$\mathbf{t}^l(r_l) = \frac{\mathbf{k}^l}{\sqrt{2\pi r_l}} \ (l = 1, 2...N) \tag{4.2.18}$$

and the jumps of the displacement and electric potential across the crack surfaces are

$$\mathbf{d}^l(x_l) = \sqrt{\frac{2(a_l - x_l)}{\pi}}\mathbf{H}^l\mathbf{k}^l \quad |x_l| \leq a_l \ (l = 1, 2...N) \tag{4.2.19}$$

where $\mathbf{k}^l = \{K_{II}^l, K_I^l, K_D^l\}^T$ with K_I^l, K_{II}^l, and K_D^l being the stress intensity factors of mode I and mode II, and the electric displacement intensity factor for crack l, respectively. Based on the general solution for the electroelastic fields provided in the previous subsection, the stress intensity factors and electric displacement intensity factor can be determined as,

at the right tip of crack,

$$\mathbf{k}^l = \sqrt{\pi a_l}\sum_{m=1}^{\infty}\mathbf{c}_m^l \quad (l = 1, 2...N) \tag{4.2.20}$$

at the left tip of crack,

$$\mathbf{k}^l = \sqrt{\pi a_l}\sum_{m=1}^{\infty}(-1)^m\mathbf{c}_m^l \quad (l = 1, 2...N) \tag{4.2.21}$$

From equations (4.2.18) and (4.2.19), the energy release rate is expressed, as

$$G^l = \lim_{\delta \to 0+}\frac{1}{2\delta}\int_{a_l}^{a_l+\delta}(\mathbf{t}^l)^T(x_l)\mathbf{d}^l(x_l - \delta)dx_l = \frac{1}{4}(\mathbf{k}^l)^T\mathbf{H}^l\mathbf{k}^l \tag{4.2.22}$$

As discussed in Chapter 3, the usage of energy release rate in predicting the fracture of cracked piezoelectric media has a drawback. Using this fracture criterion,

it is predicted that the electric field always impedes the crack propagation, which is in contradict with the existing experimental results (McHenry and Koepke, 1983; Tobin and Pak, 1993; Park and Sun, 1994 for examples). As mentioned by Park and Sun (1995a, b), total energy release rate may not be a suitable fracture criterion for piezoelectric materials. To describe the mechanical deformation, it is interesting to consider the property of the crack opening displacement (COD) defined in Chapter 3. In the current case, the COD intensity factor K_{COD} can be used to describe the opening deformation of the crack surfaces, which is given by,

$$K^l_{COD} = \lim_{x_l \to a_l} \frac{d^l_2}{\sqrt{a_l - x_l}} = \sqrt{\frac{2}{\pi}} \{h^l_{21}\ h^l_{22}\ h^l_{23}\} \mathbf{k}^l \ (l = 1, 2...N) \tag{4.2.23}$$

4.3 Solution Technique

To solve the nonlinear Equation (4.2.15), an iteration process has been proposed as,

$$\sum_{m=1}^{\infty} \mathbf{c}_m^{l(n+1)} \frac{\sin(m \cos^{-1} \frac{x_l}{a_l})}{\sin(\cos^{-1} \frac{x_l}{a_l})} + \sum_{k \neq l}^{N} \sum_{m=1}^{M} \int_{-a_k}^{a_k} \Big[\cos\theta_{lk} \mathbf{S}^{lk} (\mathbf{B}^k_1 + \mathbf{B}^k_2) - \sin\theta_{lk} \mathbf{S}^{lk} (\mathbf{C}^k_1 + \mathbf{C}^k_2) \Big]$$
$$\mathbf{c}_m^{k(n)} T_m(\frac{w}{a_k}) / \sqrt{1 - (\frac{w}{a_k})^2} dw - \sum_{m=1}^{M} \mathbf{M}^l \mathbf{c}_m^{l(n)} \frac{a_l}{m} \sin(m \cos^{-1} \frac{x_l}{a_l}) = -\mathbf{t}^{l(0)} \ (l = 1, 2...N) \tag{4.3.1}$$

where n is the the step number of the interaction. Numerical simulation indicates that the solution of the problem is not unique, i.e. both open crack mode and closed crack (crack surface overlapping) mode can be numerically obtained for each crack. For the case where two cracks are involved, four different modes can be predicted, i.e. both cracks are open; the first open and the second overlapping; the first overlapping and the second open; both overlapping. More complicated deformation modes can be

observed when more cracks are involved in interaction, i.e. for N cracks, 2^N solutions exist. An overlapping crack may indicate the closure of the crack. In the current problem, the cracked piezoelectric medium is assumed to subject a tensile mechanical load $\sigma_{22}^{\infty} > 0$ and an electric displacement D_2^{∞} at infinity. It is indicated in Equation (4.2.9) that each crack is subjected to a tensile normal stress along crack surfaces for crack orientation $\theta \in [0, 90]$. The closed crack mode is believed to be physically impossible under these loading conditions. This is because as soon as a crack is closed, the electric potential will be continuous across the crack surfaces. As a result, electric field will have no effect on this crack, and the applied tensile stress perpendicular to the crack will result in a crack opening. With this in mind, only the open crack mode is considered in the current discussion.

To clearly identify the open crack mode, a simplified solution is developed considering only one term c_{31}^l in the Chebyshev polynomial expansion of c_{3j}^l in Equation (4.3.1), while M terms of $c_{1j}^l, c_{2j}^l (j = 1, 2...M)$ are still used. This treatment enables the determination of different response modes analytically. Correspondingly, M collocation points along the surfaces of each crack are used for the mechanical boundary conditions, however, only the central point is used for the electric boundary condition.

The accuracy of this single-term solution mentioned above is verified by considering the interaction of two parallel cracks of the same length ($2a = 2mm$), shown in figures 4.2~4.4, subjected to applied electromechanical loads σ_{22}^{∞} and D_2^{∞}, for the case where the distance between these two cracks is $1.0a$ and $\sigma_{22}^{\infty} = 20MPa$. Figure 4.2 shows the comparison between the maximum crack opening at the centre of the

crack determined by the single-term solution and that by the complete solution obtained from Equation (4.3.1) using 13 terms in the Chebyshev polynomial expansion. Figure 4.3 shows the corresponding comparison between the normalized stress intensity factors $k_I = K_I/K_I^S$ at the right tip of the crack determined by single-term and complete solutions, with superscript S representing the result from the single crack problem. Good agreement between these two solutions can be observed. The variation of $\overline{D}_2$ along the crack surface obtained by the complete solution is depicted in Figure 4.4, showing that $\overline{D}_2$ keeps almost constant. It is interesting to mention that a constant $\overline{D}_2$ distribution along the crack surface can be predicted by the first term of Chebyshev polynomial expansion. The results indicate that since the variation of electric displacement along the surfaces of each crack is not significant, this treatment can provide reasonable solutions for interacting crack problems. Based on these results, the single-term solution will be used in the following discussion. 13 terms in Chebyshev polynomial expansion, which can provide reasonably accurate solution of the problem, will be used.

4.4 Fracture Behaviour of Interacting Cracks

The piezoelectric material used in the current Chapter for numerical calculation is assumed to be piezoceramics $PZT-4$, with the corresponding material constants in the global coordinate system oxy being given in Chapter 3. In this section, the fracture behaviour of interacting cracks are described by the stress intensity factors, the energy release rate, the electric displacement intensity factor and the crack opening

displacement (COD) intensity factor. The effect of crack orientation and dimension, and the distance between cracks are considered to study the interaction. The effect of the electric boundary condition is also demonstrated by using different crack models.

4.4.1 Interacting effect

Firstly, we restrict our attention on the effect of crack dimension upon crack interaction. Figure 4.5 shows the normalized stress intensity factor $k_I = K_I/K_I^S$, electric displacement intensity factor $k_D = K_D/K_D^S$ and COD intensity factor $k_{COD} = K_{COD}/K_{COD}^S$ at the inner tips of two collinear cracks for different crack-length ration with the distance between the cracks being $d = 0.5a_1$ ($a_1 = 1mm$). The superscript 'S' represents the corresponding intensity factors for single crack problem. The whole system is subjected to electromechanical loads $\sigma_{22}^{\infty} = 20MPa$ and $D_2^{\infty} = 0.001C/m^2$ at infinity. Amplification effect for both electric and mechanical fields for these cracks is observed, i.e. all the normalized intensity factors are greater than one. The intensity factors of crack 1 increase with increasing crack-length ratio, while the corresponding factors of crack 2 decrease. These results are similar to that for traditional materials, where only the mechanical field is involved. The interaction effect between two parallel cracks subjected to the same external loads is shown in Figure 4.6, in which the distance d between the cracks is assumed to be a_1 ($a_1 = 1mm$) and the cracks are centrally aligned. It can be clearly identified that in this configuration the crack interaction is dominated by shielding effect with all intensity factors for both cracks being less than 1. With the increase of the length of the second crack a_2, this shielding effect on the first crack increases, but the effect on the second one decreases.

The effect of the distance between cracks is also investigated. The interaction between three equally spaced parallel cracks of the same size ($2a = 2mm$) is studied firstly. The system is subjected to remote electromechanical loads $\sigma_{22}^{\infty} = 20MPa$ and $D_2^{\infty} = 0.001C/m^2$. Figure 4.7 shows the normalized stress intensity factors $k_I = K_I/K_I^S$ and $k_{II} = K_{II}/K_I^S$ for three cracks for different distance d between the adjacent cracks. The shielding effect on stress intensity factor K_I exists for all these cracks, e.g. all normalized intensity factors k_I are less than 1, which is similar to that in traditional materials. K_{II} can be observed due to the interaction effect. The normalized stress intensity factor $k_{II}^{(1)}$ is approximately 25% of $k_I^{(1)}$ when the distance between the cracks is $0.4a$. This interacting effect is also investigated by considering three cracks subjected to $\sigma_{22}^{\infty} = 20MPa$ and $D_2^{\infty} = 0.001C/m^2$ remotely as shown in Figure 4.8 with all these cracks having the same length $2a$ and their orientation angles being $0°, 45°$ and $135°$, respectively. The variation of the normalized intensity factors of the central crack with d/a is given in this figure. It is observed that the central crack is subjected to a shielding effect, which decreases with the increasing crack distance. The intensity factors at the inner tip of the orientated cracks, normalized by the corresponding results of single oriented crack, are given in Figure 4.9. It is evident that the oriented crack experience amplification effect from the central crack.

The effect of crack orientation upon the crack interaction is further considered. Figure 4.10 shows the normalized intensity factors $k_I^{in} = K_I^{in}/K_I^S$, $k_{II}^{in} = K_{II}^{in}/K_I^S$, $k_D^{in} = K_D^{in}/K_D^S$ and $k_{COD}^{in} = K_{COD}^{in}/K_{COD}^S$ at the inner tip of crack 1 with the variation of orientation angle θ of crack 2. The whole medium is remotely subjected to the same electromechanical loads as in previous cases. The ratio between the crack lengths is

$a_2/a_1 = 0.5$ ($a_1 = 1mm$) and the distance between the centres of the cracks is $1.6a_1$, i.e. $d/a_1 = 0.1$ when these two cracks become collinear. Amplification effects on K_I^{in}, K_D^{in} and K_{COD}^{in} are observed when the crack orientation $\theta < 57°$, while shielding effect is present when $\theta > 57°$. It is also observed that the presence of crack 2 introduces Mode II (shear) deformation as evidenced by $k_{II}^{in} \neq 0$ for the cases where these two cracks are not collinear or perpendicular to each other. k_{II}^{in} is sensitive to the orientation of crack 2 and reaches its maximum value at $\theta = 45°$.

4.4.2 Effect of electric boundary condition

The effect of electric boundary condition upon the above mentioned fracture parameters are studied. Figure 4.11 shows the normalized electric displacement intensity factor $k_D = K_D/K_D^S$ at the inner tips of two collinear cracks of the same length under an electromechanical load $\sigma_{22}^{\infty} = 20MPa, D_2^{\infty} = 0.001C/m^2$. The corresponding results k_D^I for electrically impermeable crack and k_D^P for electrically permeable crack are also provided in this figure for comparison. The influence of the electric boundary condition upon the amplification effect can be clearly observed. Figure 4.12 shows the comparison between results of k_D from current, impermeable and permeable crack models at the right tip of a crack interacting with an oriented crack, under the same loading condition as that discussed in Figure 4.10. For small $\theta(< 30°$ for example), the result from the current model is between that from the impermeable and permeable models. When θ approaches 90°, the current result is very close to that predicted by the permeable model. This may be caused by the shielding effect of crack 2 to crack 1, which reduces the crack opening at crack 1. This effect of electric boundary

condition is also evidenced by the total energy release rate. Figure 4.13 shows the energy release rate of one of the two parallel cracks with varying electric field E_2^∞, when the medium is subjected to $\sigma_{22}^\infty = 20MPa$. The resulting energy release rate G is bounded by G^I and G^P for the applied electric field considered, with G^I and G^P corresponding to the electrically impermeable and permeable boundary conditions along the crack surfaces. It can be observed from this figure that neither G^I nor G^P can be used to provide a reasonable prediction of the energy release rate.

To show the transition between the traditionally permeable and impermeable crack models, for the case of interacting cracks described in Figure 4.8, K_D and K_{COD} of the central crack based on different crack models are plotted in Figure 4.14 and Figure 4.15, respectively, with the system being subjected to an electric load $E_2^\infty = 500V/mm$. The closest distance between the central crack and other cracks is $d = a$. It shows that both K_D and K_{COD} from the current model are always between the corresponding results from the electrically impermeable and permeable crack models. The results from the current model are closer to that from the electrically permeable model when the stress level is low, but approach that from the electrically impermeable model with increasing stress level. This phenomenon indicates the importance of considering crack opening deformation in the electric boundary condition since neither the impermeable nor the permeable crack models can accurately simulate the electric boundary condition along the crack surfaces.

4.4.3 Effect of electric field upon crack propagation

To predict the effect of applied electric field upon crack deformation and crack initiation, it is interesting to consider the property of the COD intensity factor. Figure 4.16 shows the variation of K_{COD} with the applied electric field E_2^∞ for the parallel crack problem studied in Figure 4.2. The whole medium is subjected to a mechanical load $\sigma_{22}^\infty = 20MPa$ and the distance between these two centrally aligned cracks is $d = 1.0a$. The corresponding results K_{COD}^I and K_{COD}^P using electrically impermeable and permeable crack models are also provided in these figures for comparison. For an applied mechanical load $\sigma_{22}^\infty = 20MPa$, the variation of K_{COD} of the central crack with the applied electric field intensity E_2^∞ for the crack geometry given in Figure 4.8 is also depicted in Figure 4.17. It can be observed from these two figures that K_{COD} increases monotonically with increasing electric field. If K_{COD} is used as a fracture parameter to evaluate crack initiation, it is indicated that a positive electric field will enhance crack propagation, while a negative one will impede it, as predicted by Park and Sun (1995a, b) using strain energy release rate as the fracture criterion. To show the effect of electric boundary condition, K_{COD} intensity factors from impermeable and permeable models are also provided in this figure for comparison. It shows that electric field direction has no effect on crack propagation based on permeable model. However, significant effect on K_{COD} can be observed when the current model or impermeable crack model are used.

4.5 Conclusions

A theoretical study is conducted to evaluate the effects of the interaction between multiple cracks and loading-dependent boundary condition on the fracture behaviour of cracked piezoelectric materials. In addition to the well-known shielding/amplification effect caused by multiple cracks, the current study indicates that the nonlinear electric boundary condition plays a significant role in determining the fracture behaviour of interacting cracks. The existence of multiple deformation modes and the discrepancy between the current crack model and traditional ones indicate that the commonly used permeable and impermeable crack models may not be suitable for predicting the fracture behaviour of cracked piezoelectric medium and the dielectric property of cracks should be considered when significant crack opening is expected.

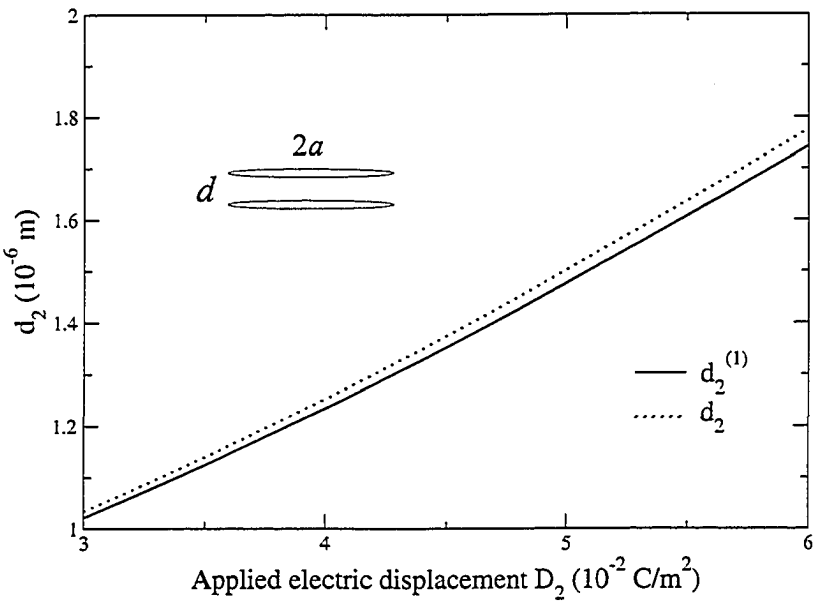

Figure 4.2: The maximum crack opening of two parallel cracks

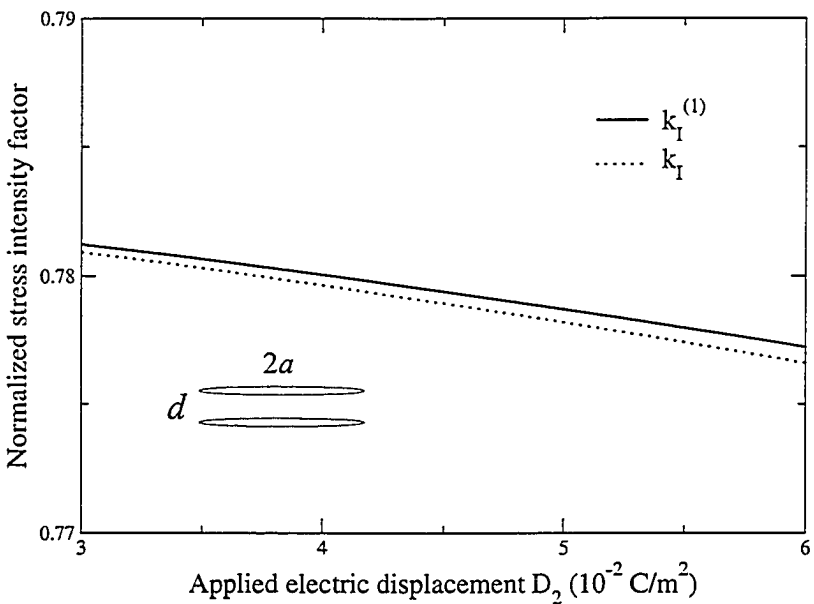

Figure 4.3: The normalized k_I for two parallel crack problem

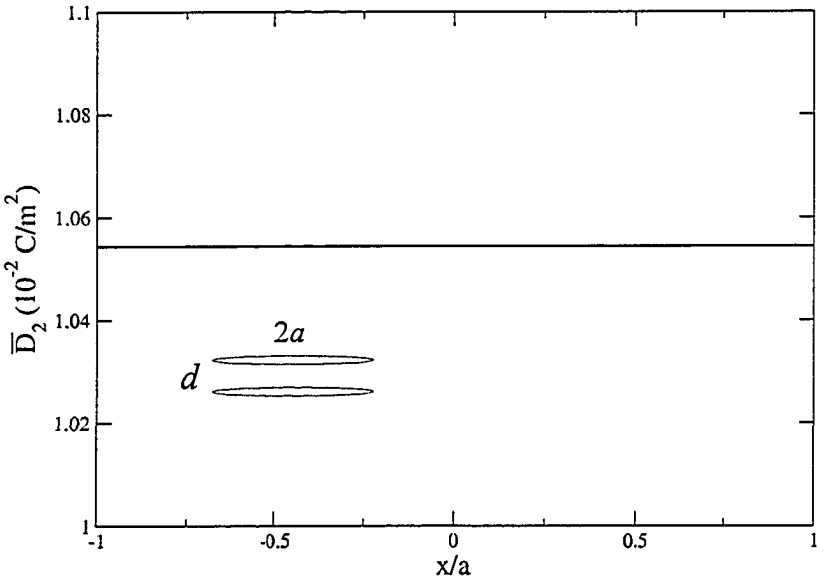

Figure 4.4: The electric displacement distribution along the crack surface for two parallel crack problem

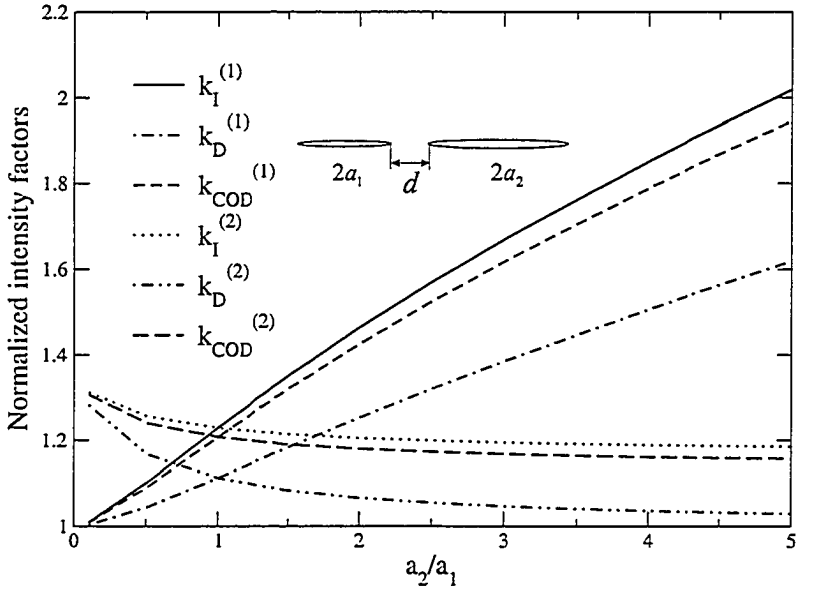

Figure 4.5: The normalized intensity factors at the inner tips of two collinear cracks

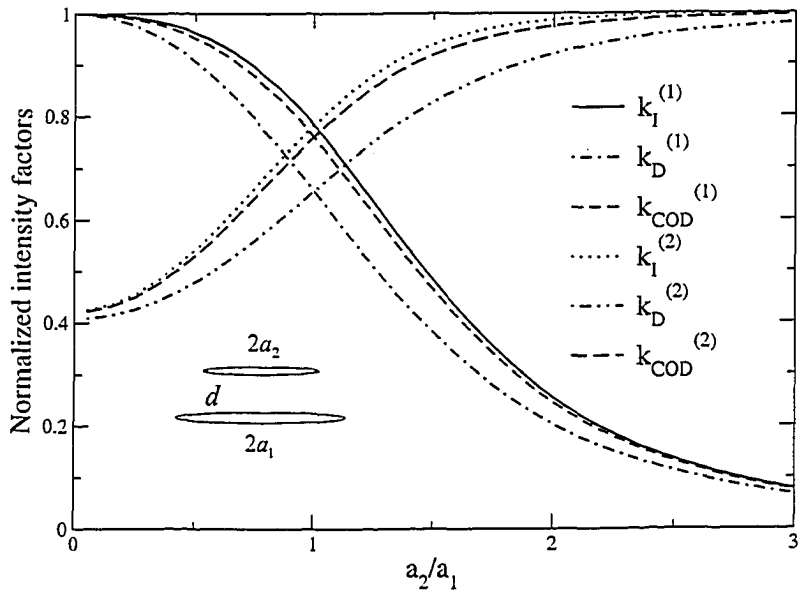

Figure 4.6: The normalized intensity factors for two parallel cracks

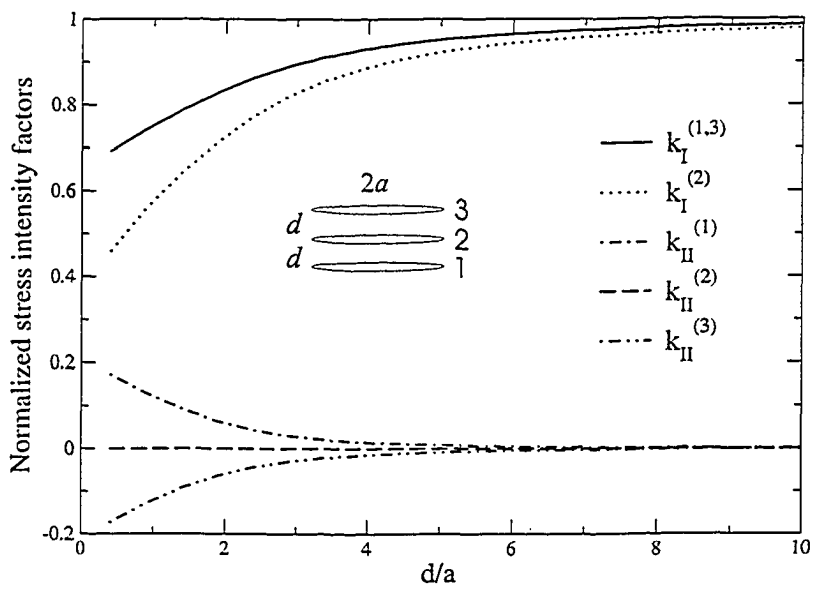

Figure 4.7: The variation of the normalized stress intensity factors of interacting parallel cracks with d/a

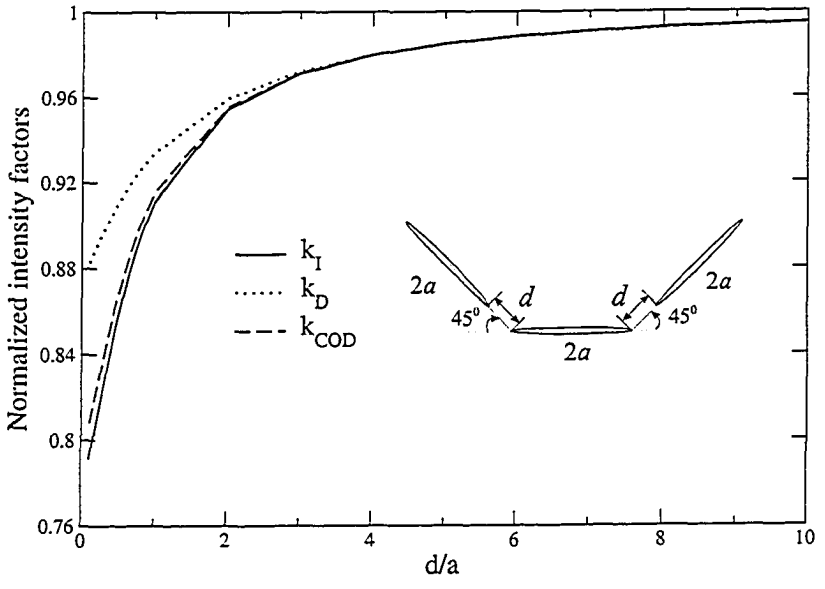

Figure 4.8: The variation of the normalized intensity factors of the central crack with d/a

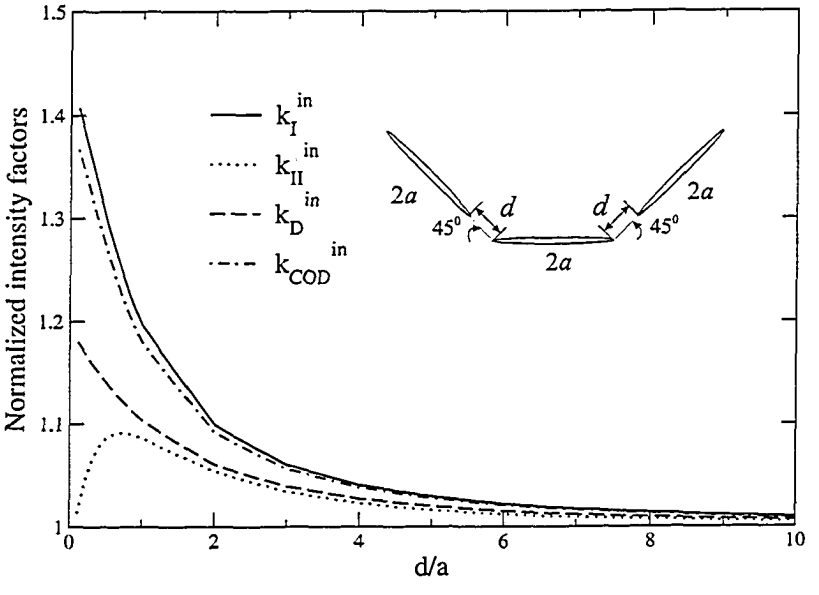

Figure 4.9: The variation of the normalized intensity factors at the inner tips of oriented cracks with d/a

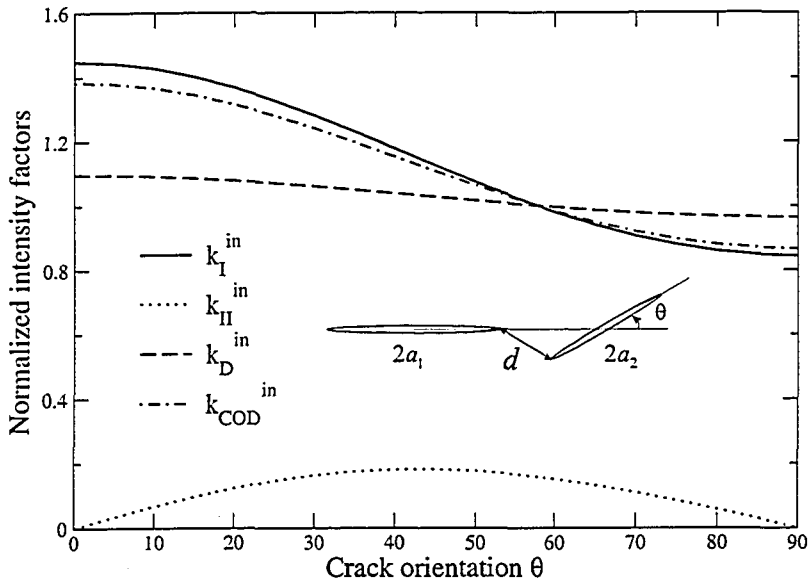

Figure 4.10: The variation of the normalized intensity factors at the inner tip of crack 1 with the orientation of crack 2

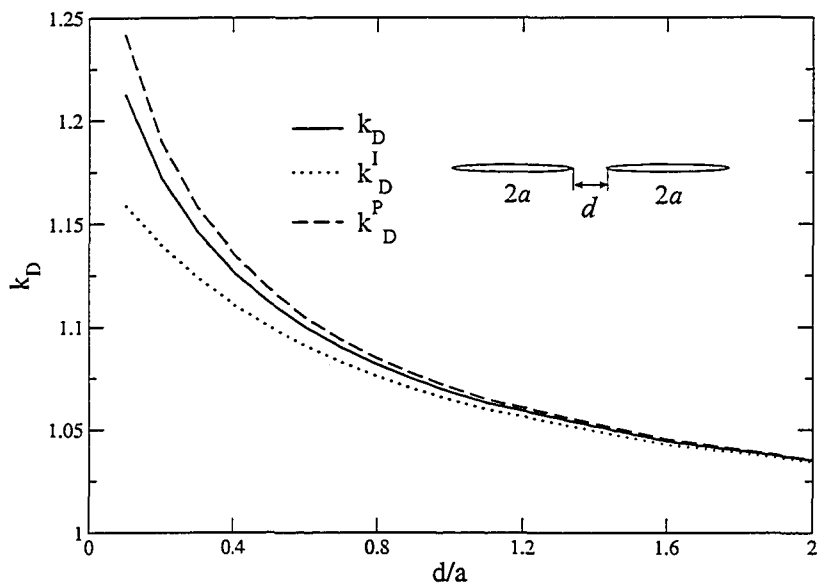

Figure 4.11: The normalized electric displacement intensity at the inner tip of two collinear cracks for different crack models

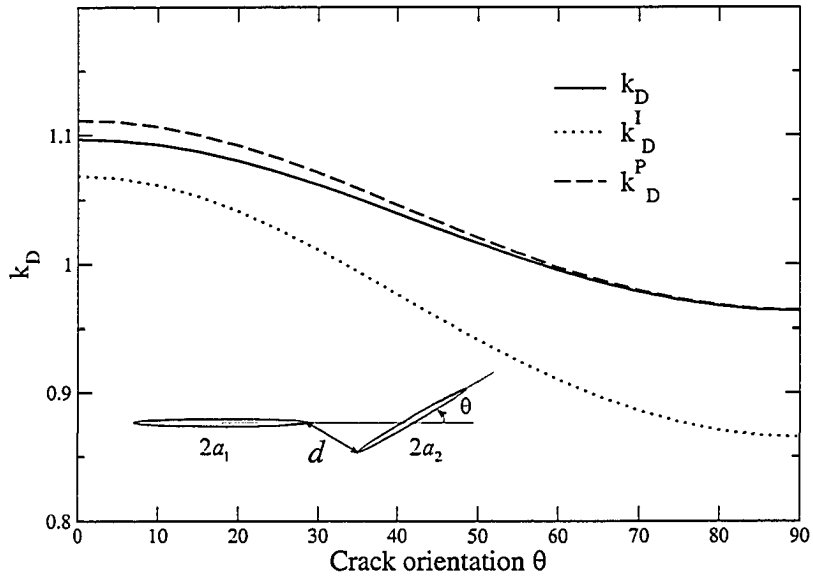

Figure 4.12: The variation of k_D at the inner tip of crack 1 with the orientation of crack 2 for different crack models

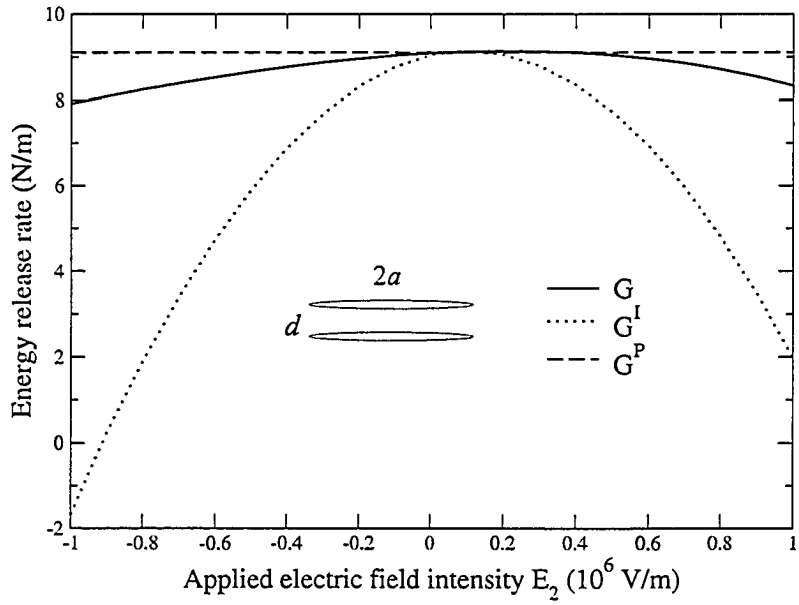

Figure 4.13: The energy release rate of two parallel crack problem for different crack models

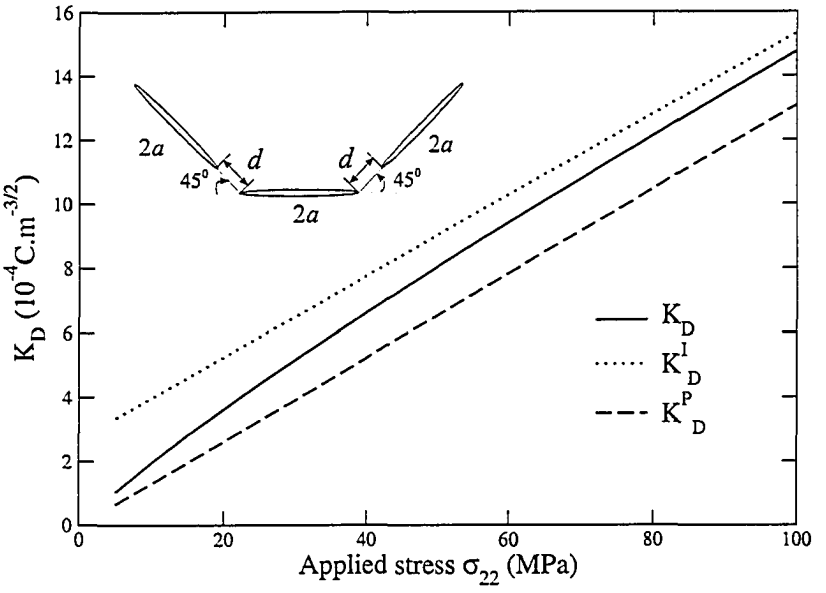

Figure 4.14: The variation of K_D for the central crack with σ_{22}^{∞} for different crack models

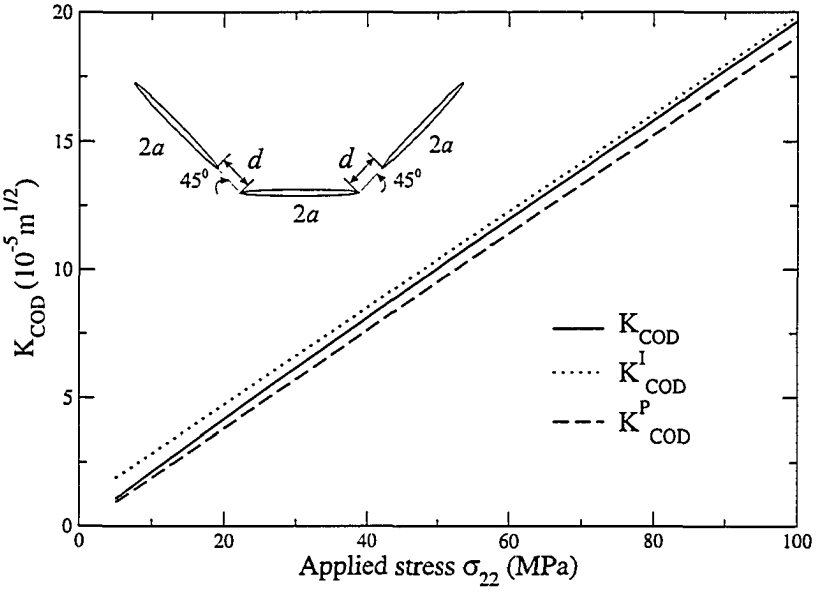

Figure 4.15: The variation of K_{COD} for the central crack with σ_{22}^{∞} for different crack models

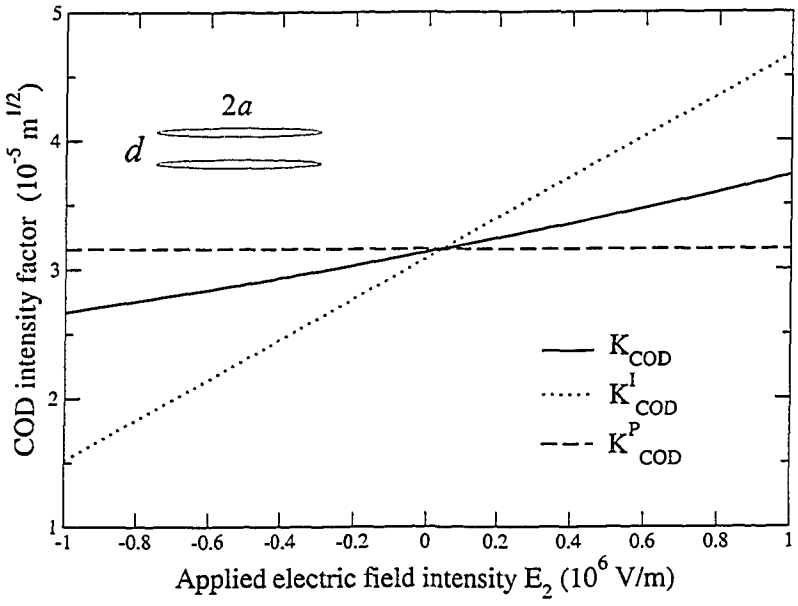

Figure 4.16: The variation of K_{COD} for two parallel crack problem with E_2^∞ for different crack models

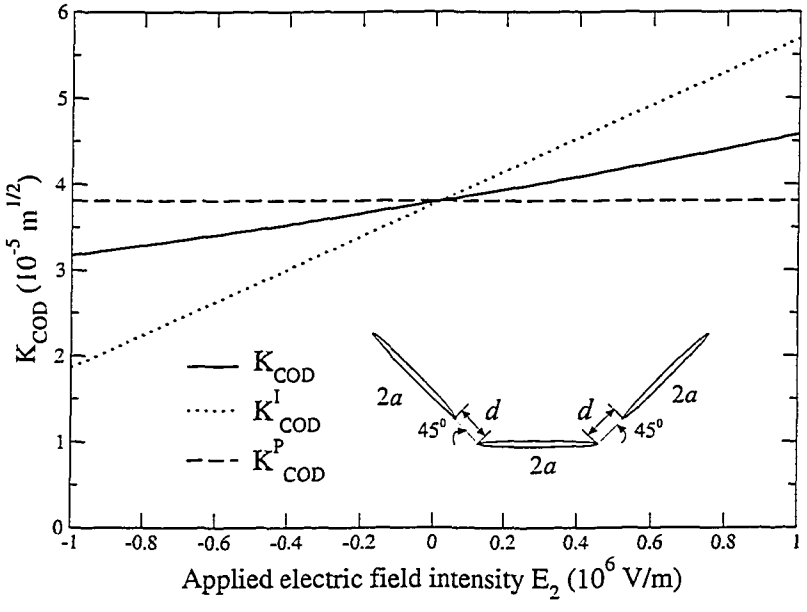

Figure 4.17: The variation of K_{COD} for the central crack with E_2^∞ for different crack models

Chapter 5

Micromechanics Study of the Effective Electroelastic Property of Cracked Piezoelectric Materials

This chapter presents a study of the effective electroelastic property of piezoelectric materials with parallel or randomly distributed cracks. The theoretical formulation is derived using the dilute model of distributed cracks based on the solution of a single dielectric crack problem, in which the electric boundary condition along the crack surfaces is governed by the crack opening displacement. It is observed that the effective electroelastic property of such cracked piezoelectric media is nonlinear and sensitive to loading conditions. Numerical simulations are conducted to show the effects of crack distribution and electric boundary condition upon the effective electroelastic property. The transition between the commonly used electrically permeable and impermeable crack models is studied.

5.1 Statement of the Problem

Existing studies of the effective electroelastic property of cracked piezoelectric materials are mostly based on the traditionally impermeable and permeable crack models. The effect of the dielectric medium filling the cracks upon the effective eletroelastic properties is still unknown. It is, therefore, the objective of this chapter to provide a theoretical study of the effective electroelastic property of cracked piezoelectric materials based on the deformation-dependent boundary condition discussed in Chapter 2.

The plane problem envisaged in this chapter is to determine the effective electroelastic property of a piezoelectric medium weakened by arbitrarily distributed or parallel cracks by micromechanics analysis. Micromechanics method provides the overall behaviour of cracked materials through an analysis using a representative volume element (RVE). Assume that the microcracked piezoelectric medium can be modelled by a RVE of volume Ω with unit thickness in z direction and area A in oxy plane as shown in Figure 5.1. The effective electroelastic property of this cracked medium can be derived by considering the relation between the volume averages of two electroelastic field variables $\overline{\mathbf{\Phi}}$ and $\overline{\mathbf{Z}}$,

$$\overline{\mathbf{\Phi}} = \frac{1}{\Omega}\int \mathbf{\Phi} d\Omega \tag{5.1.1}$$

$$\overline{\mathbf{Z}} = \frac{1}{\Omega}\int \mathbf{Z} d\Omega \tag{5.1.2}$$

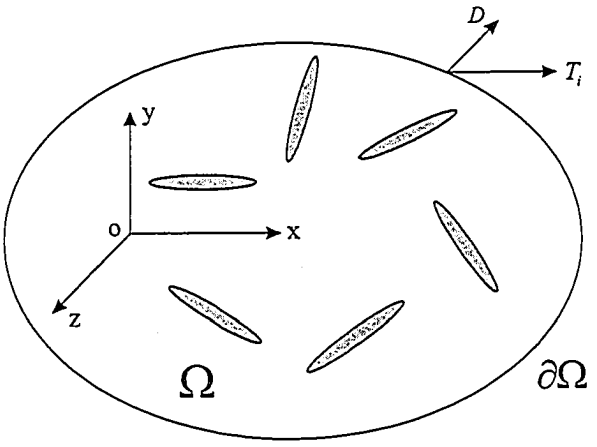

Figure 5.1: The RVE model

where the stress and electric displacement field $\mathbf{\Phi}$, and the strain and electric field $\mathbf{Z}$ are defined as,

$$\mathbf{\Phi} = \{\Phi_{11}, \Phi_{22}, \Phi_{21}, \Phi_{31}, \Phi_{32}\}^T \tag{5.1.3}$$

$$\mathbf{Z} = \{Z_{11}, Z_{22}, 2Z_{21}, Z_{31}, Z_{32}\}^T \tag{5.1.4}$$

with the notation introduced by Barnett and Lothe (1975), these two field variables are identified as,

$$\Phi_{Ij} = \begin{cases} \sigma_{Ij} & I,j = 1,2 \\ D_j & I = 3, j = 1,2 \end{cases} \tag{5.1.5}$$

$$Z_{Ij} = \begin{cases} (u_{I,j} + u_{j,I})/2 & I,j = 1,2 \\ V_{,j} & I = 3, j = 1,2 \end{cases} \tag{5.1.6}$$

σ_{Ij}, u_I, D_j and V are the stress, the displacement, the electric displacement and electric potential, respectively. These two volume-averaged electromechanical fields

$\overline{\Phi}$ and $\overline{\mathbf{Z}}$ are related as,

$$\overline{\mathbf{Z}} = \mathbf{S}\overline{\Phi} \tag{5.1.7}$$

with $\mathbf{S}$ being the generalized electroelastic compliance matrix of the effective medium, which may depend on $\overline{\Phi}$.

Suppose the boundary $\partial\Omega$ of the RVE is subjected to traction T_i and electric displacement D, which correspond to a uniform stress and electric displacement field $\Phi^0 = \{\sigma^0_{11}, \sigma^0_{22}, \sigma^0_{21}, D^0_1, D^0_2\}$ with $T_i = \sigma^0_{ij}\overline{n}_j$, $D = D^0_j\overline{n}_j$ and $\overline{n}_j$ being the components of outward normal of $\partial\Omega$. The averaged stress and electric displacement in the cracked medium can be obtained using the average scheme (5.1.1) as,

$$\overline{\Phi} = \Phi^0 \tag{5.1.8}$$

If the RVE is homogeneous without cracks, then the corresponding average strain and electric field intensity field associated with the average stress and electric displacement Φ^0 would be,

$$\mathbf{Z}^m = \mathbf{S}^m\Phi^0 \tag{5.1.9}$$

where $\mathbf{S}^m$ is the generalized compliance matrix of the host medium, with the superscript m representing the host matrix. The presence of cracks disturbs the uniform electroelastic fields. In general cases, the averaged strain and electric field $\overline{\mathbf{Z}}$ can be decomposed into two parts as discussed for traditional cracked media by Nemat-Nasser and Hori (1993),

$$\overline{\mathbf{Z}} = \mathbf{Z}^m + \mathbf{Z}^c \tag{5.1.10}$$

where superscript c denotes the variable due to the existence of cracks. $\mathbf{Z}^m$ is defined by Equation (5.1.9), and $\mathbf{Z}^c$ is the additional strain and electric field caused by the presence of cracks. The components of $\mathbf{Z}^c$ can be determined by the displacement and electric potential jumps across crack surfaces (Nemat-Nasser and Hori, 1993; Yu and Qin, 1996b). $\mathbf{Z}^c$ can be generally expressed as,

$$\mathbf{Z}^c = \mathbf{S}^c \mathbf{\Phi}^0 \tag{5.1.11}$$

where $\mathbf{S}^c$ is a matrix to be determined through the crack surface deformation. Using Equations (5.1.7)-(5.1.11), the effective compliance of cracked piezoelectric medium becomes,

$$\mathbf{S} = \mathbf{S}^m + \mathbf{S}^c \tag{5.1.12}$$

5.2 Effective Electroelastic Property of Cracked Piezoelectric Materials

There are two important issues in the determination of matrix $\mathbf{S}^c$ of cracked media through the use of micromechanics models, the crack model and the interaction of cracks. In the current work , 'real' electric boundary condition along crack surfaces will be considered using a dielectric crack model, and a dilute scheme will be used to treat the crack interaction.

5.2.1 The solution of a dielectric crack

Consider the plane strain problem of a typical crack in an infinite piezoelectric medium as shown in Figure 5.2. The poling direction of the medium is along the y-axis in

the global coordinate system, and the whole medium is subjected to remotely applied electromechanical loads $(\mathrm{t}^{\infty}, \mathrm{s}^{\infty})$ with $\mathrm{t}^{\infty} = \{\sigma_{21}^{\infty}\ \sigma_{22}^{\infty}\ D_2^{\infty}\}^T$ and $\mathrm{s}^{\infty} = \{\sigma_{11}^{\infty}\ \sigma_{12}^{\infty}\ D_1^{\infty}\}^T$. A local Cartesian coordinate system $o_k x_k y_k$ is used to describe this crack, with the origin being the crack centre and y_k-axis perpendicular to the crack surfaces. The crack length is $2a_k$ and the crack orientation is measured from x-axis to x_k-axis by θ_k.

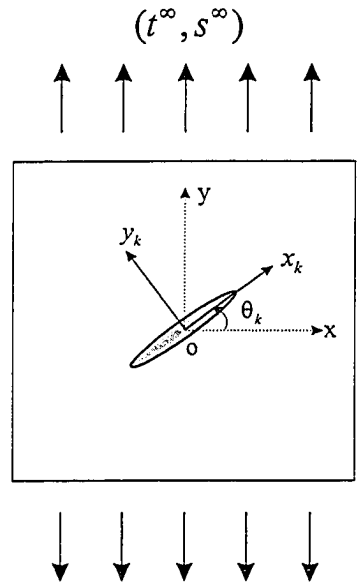

Figure 5.2: The simplified crack model for calculating the jumps of displacements and electric potential across crack surfaces

As mentioned in Section 5.1, the additional strain and electric field intensity $\mathbf{Z}^c$ caused by the existence of this crack can be determined from the jumps of displacements and electric potential across crack surfaces, which will be derived from the

single crack solution. Therefore, the crack model is of great importance in determining the effective electroelastic property of cracked piezoelectric media. In the current study, a dielectric crack model, proposed in Chapter 2, with 'real' electric boundary condition along crack surfaces will be used to represent the behaviour of the crack. Based on the solution of an arbitrarily oriented crack provided in Chapter 3, the jumps of displacements and electric potential across the crack surfaces can be derived from Equation (3.2.16) in the local coordinate system $o_k x_k y_k$ as,

$$\mathbf{d}(x_k,0)=\left\{\begin{array}{c}\triangle u_1\\ \triangle u_2\\ \triangle V\end{array}\right\}=-\left\{\begin{array}{c}h_{11}^k c_1^k+h_{12}^k c_2^k+h_{13}^k c_3^k\\ h_{21}^k c_1^k+h_{22}^k c_2^k+h_{23}^k c_3^k\\ h_{31}^k c_1^k+h_{32}^k c_2^k+h_{33}^k c_3^k\end{array}\right\}\sqrt{a_k^2-x_k^2} \tag{5.2.1}$$

where $h_{ij}^k(i,j=1,2,3)$ are components of matrix $\mathbf{H}^k$ related to material constants and crack orientation, which can be derived explicitly from Equations (4.2.7) and (4.2.8).

The unknown parameters c_i^k $(i=1,2,3)$ are determined from the remotely applied electromechanical loads $(\mathbf{t}^\infty,\mathbf{s}^\infty)$,

$$\left\{\begin{array}{l}c_1^k=-\sigma_{21}^k\\ c_2^k=-\sigma_{22}^k\\ c_3^{k(1)}=\dfrac{1}{2h_{23}^k}(A_1+B);\ c_3^{k(2)}=\dfrac{1}{2h_{23}^k}(A_1-B)\end{array}\right. \tag{5.2.2}$$

where

$$\begin{cases} A_1 = h_{21}^k \sigma_{21}^k + h_{22}^k \sigma_{22}^k - h_{23}^k D_2^k - \epsilon_0 h_{33}^k \\ A_2 = h_{21}^k \sigma_{21}^k + h_{22}^k \sigma_{22}^k + h_{23}^k D_2^k + \epsilon_0 h_{33}^k \\ C = 4\epsilon_0[((h_{23}^k)^2 - h_{22}^k h_{33}^k)\sigma_{22}^k + (h_{23}^k h_{31}^k - h_{21}^k h_{33}^k)\sigma_{21}^k] \\ B = \sqrt{A_2^2 + C} \end{cases} \tag{5.2.3}$$

and $\mathbf{t}^k = \{\sigma_{21}^k \ \sigma_{22}^k \ D_2^k\}^T$ is given by,

$$\mathbf{t}^k = \cos\theta_k \mathbf{S}^k \mathbf{t}^\infty - \sin\theta_k \mathbf{S}^k \mathbf{s}^\infty \tag{5.2.4}$$

with $\mathbf{S}^k$ being given by Equation (4.2.8).

As discussed in Chapter 3, multiple solutions for (5.2.2) indicates that the open or closed crack mode of crack may occur depending on the loading condition. When the crack is closed, the mechanical and electric boundary conditions will result in the following solutions,

$$\begin{cases} c_1^k = -\sigma_{21}^k \\ c_2^k = \sigma_{21}^k \dfrac{h_{31}^k h_{23}^k - h_{21}^k h_{33}^k}{h_{32}^k h_{23}^k - h_{22}^k h_{33}^k} \\ c_3^k = \sigma_{21}^k \dfrac{h_{32}^k h_{21}^k - h_{31}^k h_{22}^k}{h_{32}^k h_{23}^k - h_{22}^k h_{33}^k} \end{cases} \tag{5.2.5}$$

with $d_2^k(x_k, 0) = 0$ and $d_3^k(x_k, 0) = 0$.

5.2.2 Effective electroelastic property

In this study, the crack interaction is simplified using a dilute model, i.e. a microcrack is assumed to be surrounded by a pristine matrix. The crack surface deformation

can then be determined directly from the single crack solution given in the previous subsection. The strain and electric field caused by the existence of crack k can be expressed in terms of the jumps of the displacement and the electric potential across crack surfaces, similar to that obtained by Nemat-Nasser and Hori (1993) and Yu and Qin (1996b) for traditional cracked materials and for piezoelectric materials with impermeable cracks, as

$$Z_{Ij}^k = \frac{1}{2A}\int_{-a_k}^{a_k}\{[1+H(I-3)]d_I^k n_j^k + H(2-j)d_j^k n_I^k\}ds \tag{5.2.6}$$

where Z_{Ij} is defined in Equation (5.1.4), d_I^k are the jumps of the displacement and the electric potential across crack surfaces given in Equation (5.2.1), n_I are elements of the outer normal vector of crack surface, $\mathbf{n}^k = \{0,1,0\}^T$, and $H(i)$ is Heaviside step function. Based on Equation (5.2.1), Equation (5.2.6) can be rewritten as,

$$Z_{Ij}^k = \frac{\pi a_k^2}{4A}\{[1+H(I-3)]\triangle U_I^k n_j^k + H(2-j)\triangle U_j^k n_I^k\} \tag{5.2.7}$$

where

$$\triangle U_I^k = -\sum_{l=1}^{3} h_{Il}^k c_l^k \quad (I,l=1,2,3) \tag{5.2.8}$$

which contains the nonlinear effect of loading represented by c_l^k. It should be noted that all the quantities in Equation (5.2.7) are expressed in the local coordinate system. To determine the contribution of crack k to the strain and electric field of the whole medium in the global coordinate system, a transformation is conducted,

$$\mathbf{Z}^{k(c)} = \mathbf{T}^k\mathbf{Z}^k \tag{5.2.9}$$

where the components of $\mathbf{Z}^{k(c)}$ depend on both θ_k and applied loads $(\mathbf{t}^0, \mathbf{s}^0)$ with the transformation matrix $\mathbf{T}^k$ being given by,

$$\mathbf{T}^k = \begin{bmatrix} \cos^2\theta_k & \sin^2\theta_k & -\sin\theta_k\cos\theta_k & 0 & 0 \\ \sin^2\theta_k & \cos^2\theta_k & \sin\theta_k\cos\theta_k & 0 & 0 \\ 2\sin\theta_k\cos\theta_k & -2\sin\theta_k\cos\theta_k & \cos^2\theta_k - \sin^2\theta_k & 0 & 0 \\ 0 & 0 & 0 & \cos\theta_k & -\sin\theta_k \\ 0 & 0 & 0 & \sin\theta_k & \cos\theta_k \end{bmatrix} \tag{5.2.10}$$

As discussed by Tsukrov and Kachanov (2000), for certain simple cases where the cracks have random distribution or parallel distribution with arbitrary orientation, the total contribution of these cracks to the strain and electric field can be determined from the conventional scalar crack density ρ introduced by Bristow (1960),

$$\rho = \pi \sum_{k=1}^{n} N_k a_k^2 / A \tag{5.2.11}$$

with N_k being the number of cracks of length $2a_k$ in the RVE. Correspondingly, the total contribution of these cracks to the strain and electric field of this RVE can be expressed by integration over the orientation angle, as

$$\begin{Bmatrix} Z_{11}^c \\ Z_{22}^c \\ 2Z_{21}^c \\ Z_{31}^c \\ Z_{32}^c \end{Bmatrix} = \frac{\rho}{4\pi} \int_0^{2\pi} T^k \begin{Bmatrix} 0 \\ -h_{21}^k c_1^k - h_{22}^k c_2^k - h_{23}^k c_3^k \\ -h_{11}^k c_1^k - h_{12}^k c_2^k - h_{13}^k c_3^k \\ 0 \\ -h_{31}^k c_1^k - h_{32}^k c_2^k - h_{33}^k c_3^k \end{Bmatrix} d\theta_k \tag{5.2.12}$$

with c_1^k, c_2^k and c_3^k being given in (5.2.2) or (5.2.5). Substituting (5.2.12) into (5.1.11), $\mathbf{S}^c$ can be determined.

For a typical piezoceramic material with the poling direction along y, the generalized compliance matrix of the pristine medium $\mathbf{S}^m$ is derived from constitutive

equations (2.1.7) and (2.1.8) as,

$$\mathbf{S}^m = \begin{bmatrix} f_{11} & f_{12} & 0 & 0 & p_{21} \\ f_{12} & f_{22} & 0 & 0 & p_{22} \\ 0 & 0 & f_{33} & p_{13} & 0 \\ 0 & 0 & p_{13} & k_{11} & 0 \\ p_{21} & p_{22} & 0 & 0 & k_{22} \end{bmatrix} = \begin{bmatrix} c_{11} & c_{12} & 0 & 0 & e_{21} \\ c_{12} & c_{22} & 0 & 0 & e_{22} \\ 0 & 0 & c_{66} & e_{16} & 0 \\ 0 & 0 & e_{16} & -\epsilon_{11} & 0 \\ e_{21} & e_{22} & 0 & 0 & -\epsilon_{22} \end{bmatrix}^{-1} \tag{5.2.13}$$

The generalized compliance of the cracked medium defined by (5.1.12) can be obtained from equations (5.1.11), (5.1.12) (5.2.12) and (5.2.13) as,

$$\mathbf{S} = \mathbf{S}^m + \mathbf{S}^c = \begin{bmatrix} s_{11} & s_{12} & s_{13} & s_{14} & s_{15} \\ s_{21} & s_{22} & s_{23} & s_{24} & s_{25} \\ s_{31} & s_{32} & s_{33} & s_{34} & s_{35} \\ s_{41} & s_{42} & s_{43} & s_{44} & s_{45} \\ s_{51} & s_{52} & s_{53} & s_{54} & s_{55} \end{bmatrix} \tag{5.2.14}$$

5.3 Results and Discussion

First, we restrict our attention to the verification of the current solution. For isotropic elastic media weakened by randomly distributed cracks, an analytical solution can be obtained, which predicts the normalized $c_{22}^* = 1/(1+\rho)$. The result is supported by numerical calculations and is identical to that obtained by Kachanov (1992). To verify the current solution for piezoelectric media and evaluate the suitability of the dilute model (DIL) used, existing results of normalized stiffness $c_{22}^* = c_{22}/c_{22}^m$ for $BaTiO_3$ weakened by parallel cracks (Qin et al., 1998) are compared in Figure 5.3 with the result of the present solution based on the impermeable crack model. Excellent agreement is observed. Results from self-consistent (SC) method and finite element (FE) method are also included in Figure 5.3. The comparison shows that, for the current problem, the dilute model provides reasonable prediction of the effective

property of the cracked medium for the crack densities considered, as evidenced by the good agreement between the current result and that of the finite element method. Comparison is also made in Figure 5.4 between the current solution, based on the impermeable crack model, and that of a $PZT-5^{+}$ weakened by distributed spherical voids (Dunn and Taya, 1993b) with the crack density being assumed to be equal to the volume fraction of voids. A good agreement is observed for low crack densities.

The following discussion will be focussed on the numerical results of the effective electroelastic properties of cracked piezoelectric media under different mechanical and electric loads. Both randomly distributed and parallel cracks are considered in the determination of the effective electroelastic property. Attention is also paid to the transition between traditional impermeable and permeable models under different loading conditions. $PZT-4$ with material properties given in Chapter 3 will be used as the cracked medium for numerical simulation.

5.3.1 Nonlinear effective property

(i) Applied σ_{11}^{0}

First, let the representative volume element (RVE) under consideration be subjected to a tensile stress along x-axis in the global coordinate system, i.e. $\Phi_{11}^{0}=\sigma_{11}^{0}$ and the other stresses and electric displacements are zero. Under this loading condition, the corresponding components s_{i1} $(i=1\sim 5)$ in the effective compliance matrix $\mathbf{S}$ can be determined. Figure 5.5 shows the effect of crack density upon the normalized effective parameter $s_{11}^{*}=s_{11}/f_{11}$ for different crack distributions with $\sigma_{11}^{0}=50MPa$. In this figure, the angle in the legend represents the direction of parallel cracks. It

is observed that s_{11}^* increases linearly with the crack density. The effect of the crack distribution is clearly identified, while identical results are obtained for the cases of randomly distributed cracks and parallel cracks with orientation angle $\theta = 45°$. The coupling between shear strain and normal stress is also introduced as shown by $s_{31}^* = s_{31}/f_{12}$ in Figure 5.6 when the parallel cracks are not perpendicular/parallel to the poling direction of the material. It is observed from this figure that s_{31}^* induced by parallel cracks are symmetric about $\theta = 45°$. It is interesting to note that for applied σ_{11}^0, which is perpendicular to the poling direction of the material, effective parameters s_{i1} $(i = 1 \sim 5)$ are all independent of the applied load. Numerical results indicate that $s_{21} = f_{12}, s_{41} = 0, s_{51} = p_{21}$.

(ii) Applied σ_{22}^0

When only tensile stress σ_{22}^0 along the poling direction is applied, s_{i2} $(i = 1 \sim 5)$ can be determined. The variation of the normalized effective parameter $s_{22}^* = s_{22}/f_{22}$ with the applied σ_{22}^0 is plotted in Figure 5.7 with the crack density being $\rho = 0.3\pi$. As expected, cracks perpendicular to the loading direction ($\theta = 0°$) result in the highest compliance s_{22}^*. For all the parallel and random crack cases, decrease of s_{22}^* with increasing σ_{22}^0 is observed, showing nonlinearity of the problem. But this effect becomes insignificant for large orientation angles ($\theta = 60°$ for example). The result for random cracks is very close to that for $\theta = 45°$. Figure 5.8 shows the normalized effective parameter $s_{52}^* = s_{52}/p_{22}$ for the same crack density. Significant increase of s_{52}^* with increasing σ_{22}^0 can be observed for both parallel and random cracks. The coupling between shear strain and normal stress exists represented by $s_{32} \neq 0$ for

parallel cracks not perpendicular/parallel to the poling direction of the material. The resulting s_{32} is load-dependent. The normalized parameter $s_{42}^* = s_{42}/p_{22}$ is given in Figure 5.9 for $\sigma_{22}^{\infty} = 50MPa$. The existence of a nonzero s_{42} indicates electromechanical coupling caused by the cracks. This coupling coefficient decreases with the increase of crack orientation with $s_{42} = 0$ when cracks are parallel or perpendicular to the poling direction of the material or the cracks are randomly distributed. Under this loading condition, $s_{12} = f_{12}$.

(iii) Applied σ_{21}^0

Under this loading condition, the corresponding s_{i3} $(i = 1 \sim 5)$ can be determined. The effect of applied σ_{21}^0 upon these normalized effective parameters, i.e. $s_{13}^* = s_{13}/f_{33}, s_{23}^* = s_{23}/f_{33}, s_{33}^* = s_{33}/f_{33}, s_{43}^* = s_{43}/p_{13}, s_{53}^* = s_{53}/p_{13}$ for randomly distributed cracks with crack density being $\delta = 0.3\pi$ is shown in Figure 5.10. The coupling between normal strain and shear stress exists for the case of randomly distributed cracks with $s_{13}^* \neq 0$ and $s_{23}^* \neq 0$. The coupling between electric field intensity and shear stress is also evidenced by $s_{53}^* \neq 0$. It is observed that all these parameters are not sensitive to the applied σ_{21}^0.

(iv) Applied D_1^0

When only D_1^0 is applied, the solution can be used to identify $s_{i4}(i = 1 \sim 5)$. It is found that under this loading condition s_{14}, s_{24} and s_{54} can be ignored. For the applied electric load considered, $4 \times 10^{-2} C/m^2 \leq D_1^0 \leq 1 \times 10^{-1} C/m^2$, s_{34} and s_{44} are not sensitive to the loading level, i.e. $s_{34} = p_{13}, s_{44} = k_{11}$.

(v) Applied D_2^0

For the case where only electric displacement D_2^0 along the poling direction is applied, s_{i5} $(i = 1 \sim 5)$ in the generalized effective compliance matrix can be determined. Numerical results indicate that s_{15}, s_{35} and s_{45} can be approximated by $s_{15} = p_{21}, s_{35} = 0, s_{45} = 0$ for randomly distributed cracks. However, s_{25} and s_{55} are sensitive to the applied electric load. When the crack density $\rho = 0.3\pi$, the variation of the normalized $s_{25}^* = s_{25}/p_{22}$ and $s_{55}^* = s_{55}/k_{22}$ with applied D_2^0 is shown in Figure 5.11 and Figure 5.12, respectively. Significant nonlinearity can be observed, as evidenced by the increase of s_{25}^* and s_{55}^* with increasing D_2^0. With the increase of crack orientation, crack closure may also occur. For parallel cracks, when $\theta = 60°$, all cracks become closed and correspondingly $s_{25}^* = 1$ and $s_{55}^* = 1$. For parallel cracks with $\theta = 30°$ and $\theta = 45°$, the cracks are initially closed, resulting in $s_{25}^* = 1$ and $s_{55}^* = 1$. The cracks eventually become open with increasing D_2^0.

5.3.2 Effect of the electric boundary condition

The electric boundary condition along crack surfaces is an important issue in determining the effective property of cracked piezoelectric materials. The normalized effective parameters s_{22}^* and s_{55}^* for random cracks obtained using the current model are compared in Figure 5.13 and Figure 5.14, respectively, with that using electrically impermeable and permeable crack models for crack density $\rho = 0.3\pi$. It shows in these figures that the results based on the current dielectric crack model are always

between the results from impermeable and permeable crack models, and are closer to the results of the electrically permeable model when the applied loading level is low, but approaches those of the impermeable model with the increase of the loading level. Figure 5.15 shows the effect of crack density upon the normalized effective s_{52}^* for different crack models under a tensile stress $\sigma_{22}^0 = 50Mpa$. s_{52}^* increases with increasing crack density for both the current and the impermeable crack models, although crack density shows no effect on s_{52}^* based on the permeable crack model. For an applied $D_2^0 = 5 \times 10^{-2} C/m^2$, the variation of normalized s_{25}^* with crack density for different crack models is provided in Figure 5.16 for comparison. Similar phenomena to what predicted in Figure 5.15 can be observed. It should be noted that effective s_{52}^* and s_{25}^* for the dielectric crack model are load-dependent, which will cause the unsymmetry of the generalized effective compliance matrix, as evidenced by the difference between s_{52}^* and s_{25}^* under specific loading conditions in Figure 5.15 and Figure 5.16. Significant discrepancy between the current model and the impermeable and permeable ones indicates that the dielectric medium filling the crack and the crack opening displacement should be considered in determining the effective electroelastic property of this type of materials.

5.4 Conclusions

The effective electroelastic property of piezoelectric media weakened by parallel or randomly distributed cracks is predicted based on a dilute scheme and the solution of a single dielectric crack model, in which the electric boundary condition along crack

surfaces is governed by crack deformation. Attention is focused on the parameters that control the effective electroelastic properties, the nonlinearity of these effective parameters and the transition between permeable and impermeable crack models under different loads. The current study indicates that the commonly used permeable and impermeable crack models represent two limiting cases which may not be suitable for predicting the effective property of cracked piezoelectric media in some cases.

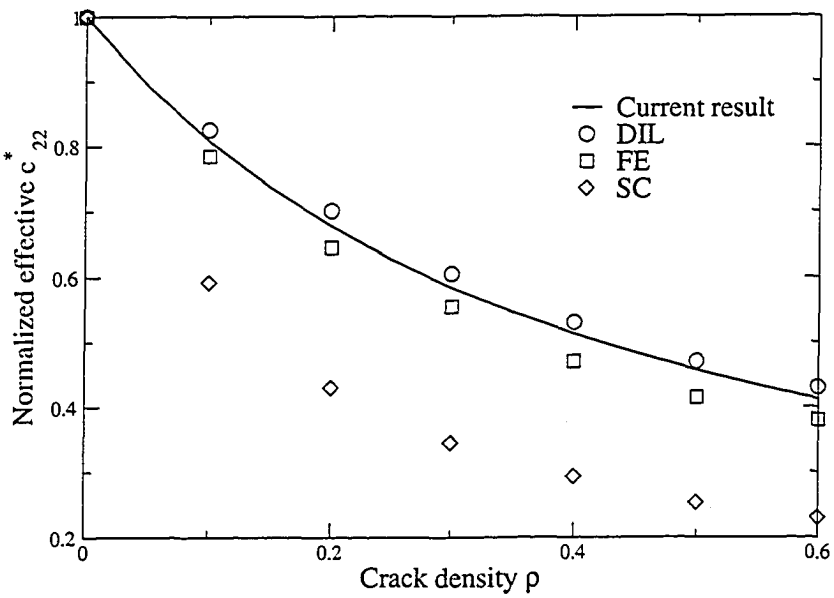

Figure 5.3: Comparison for the normalized effective c_{22}^*

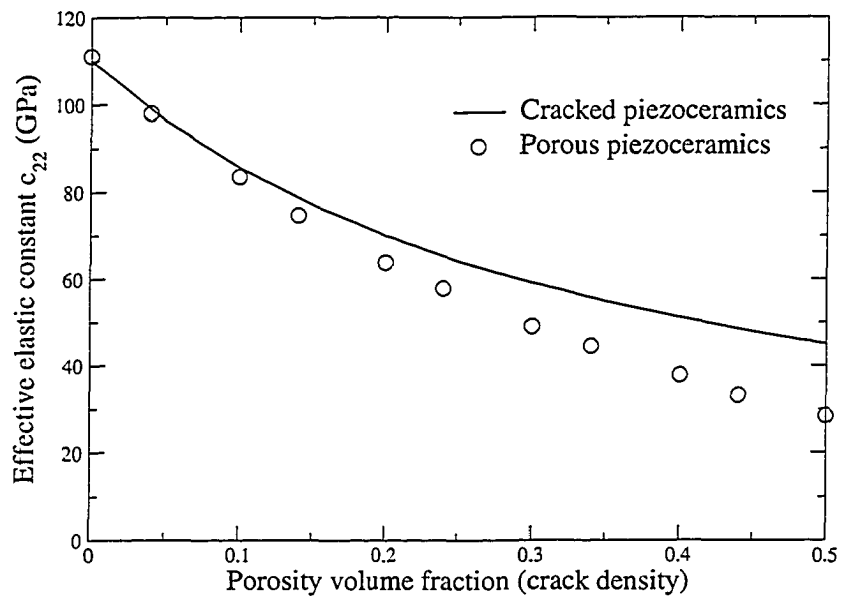

Figure 5.4: Comparison between cracked and porous piezoceramics

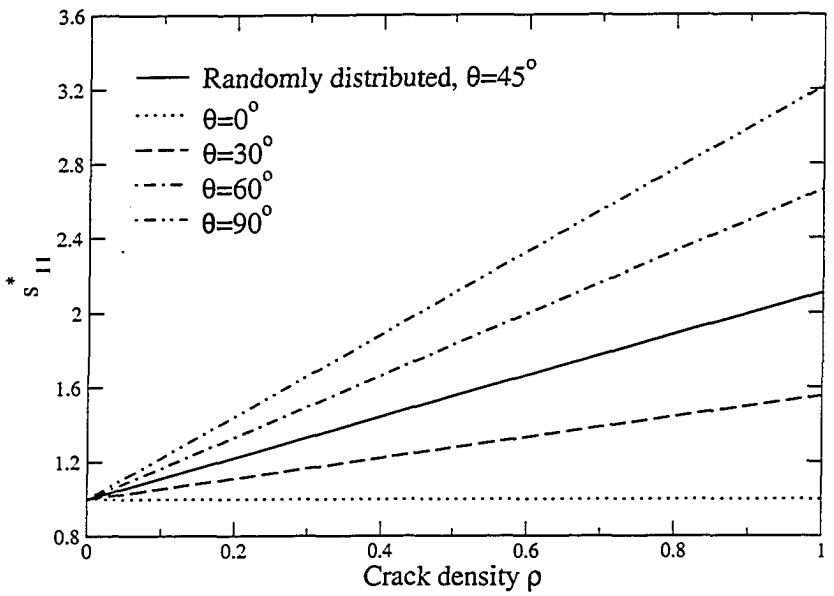

Figure 5.5: The variation of s^*_{11} with crack density

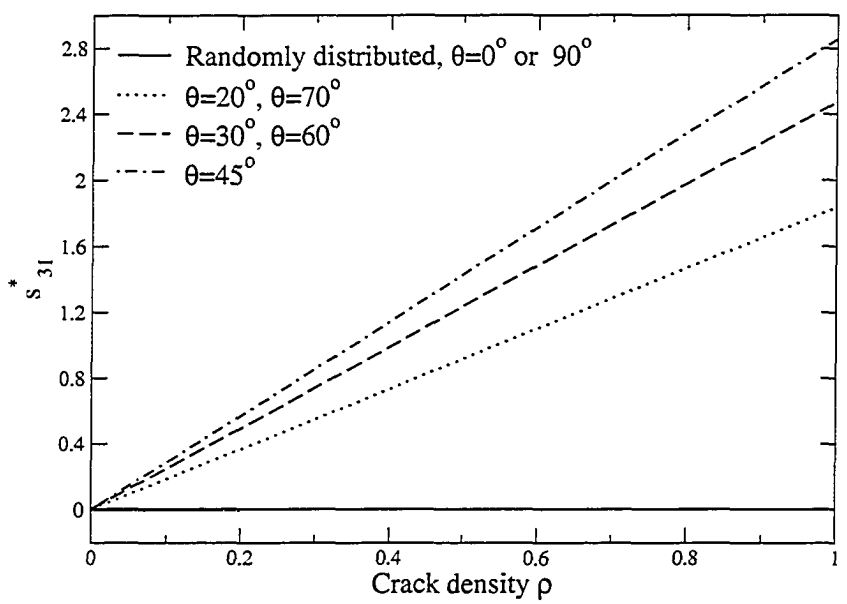

Figure 5.6: The variation of s^*_{31} with crack density

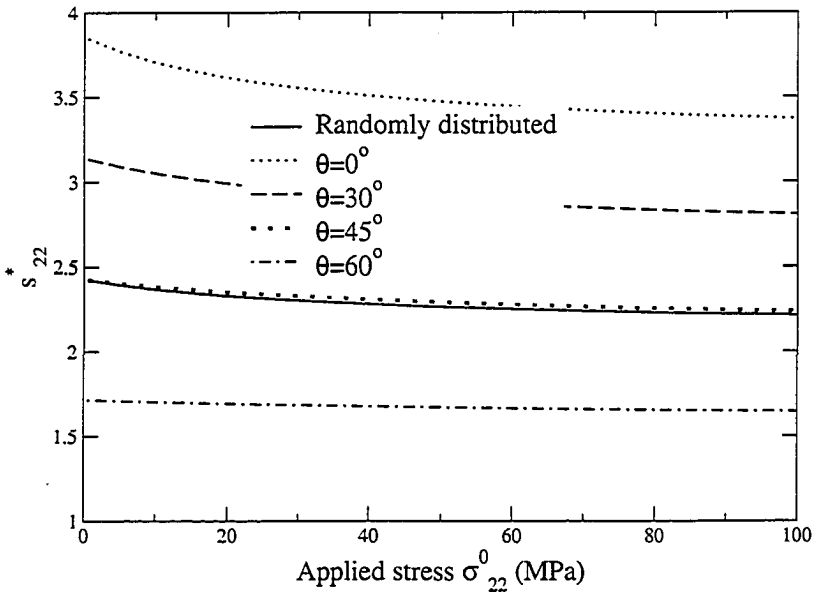

Figure 5.7: The normalized effective s^*_{22} under tensile stress σ^0_{22}

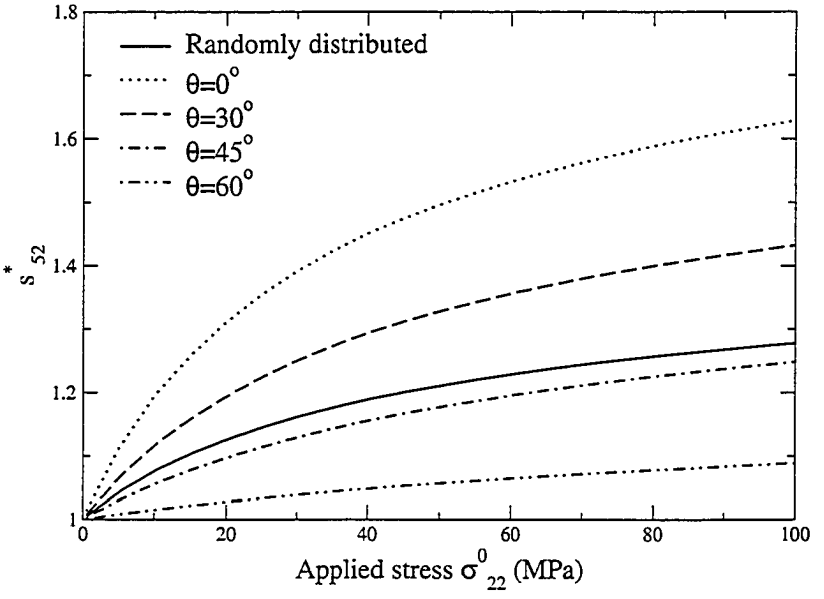

Figure 5.8: The normalized effective s^*_{52} under tensile stress σ^0_{22}

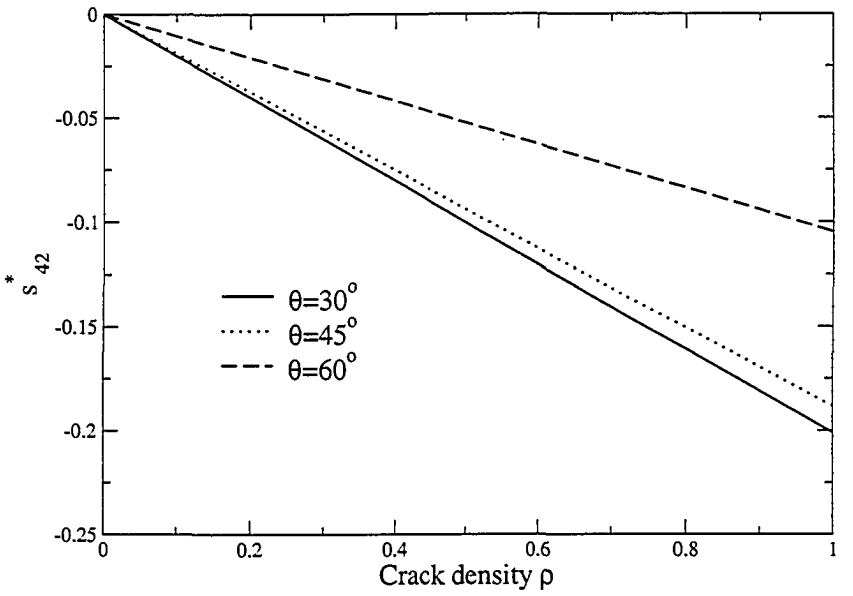

Figure 5.9: The variation of s^*_{42} with crack density

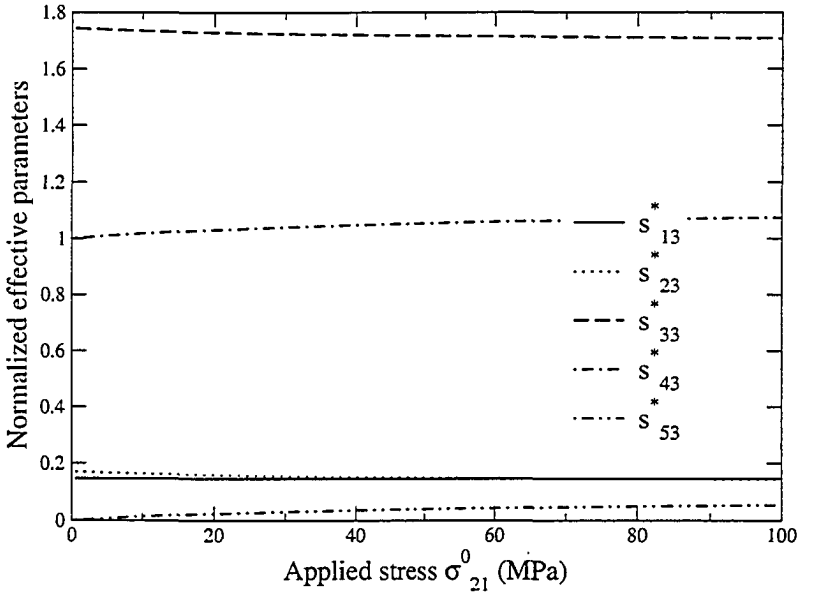

Figure 5.10: The normalized effective parameters under shear stress σ^0_{21}

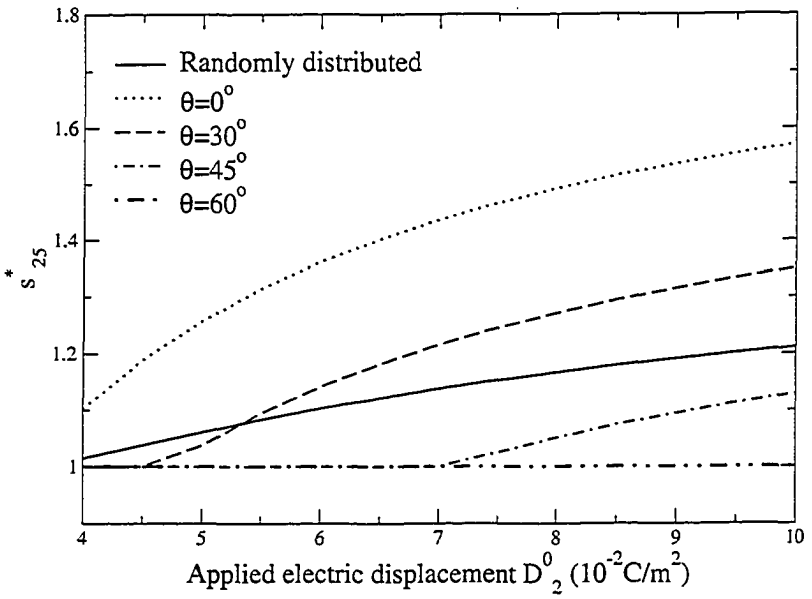

Figure 5.11: The normalized effective s^*_{25} under electric loading D^0_2

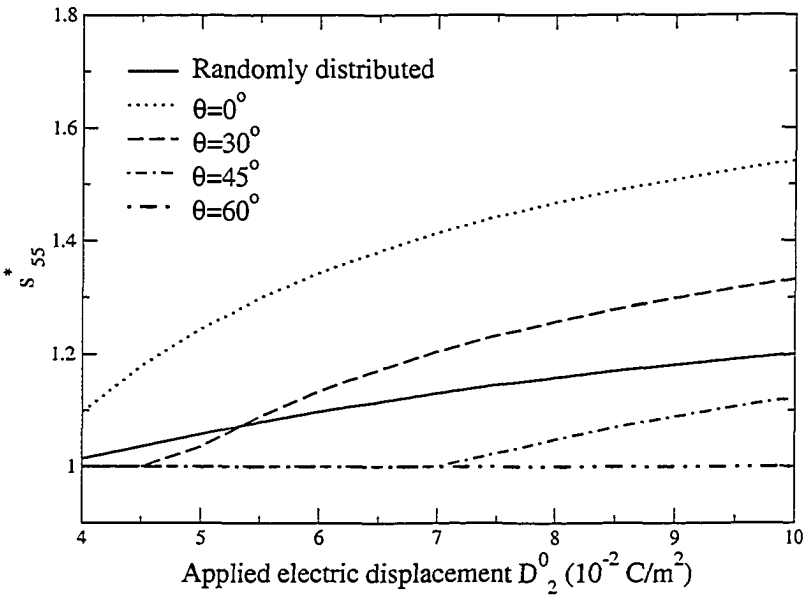

Figure 5.12: The normalized effective s^*_{55} under electric loading D^0_2

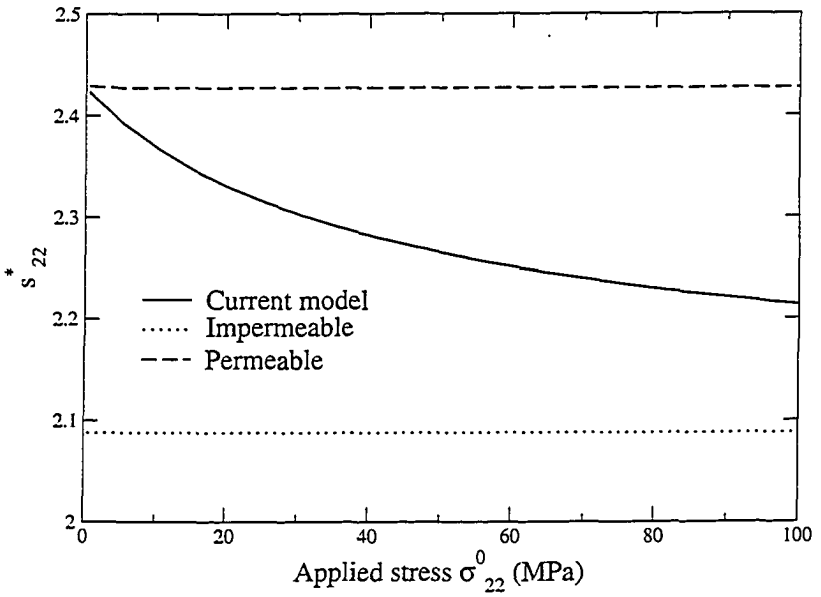

Figure 5.13: The variation of s^*_{22} with σ^0_{22} for different crack models

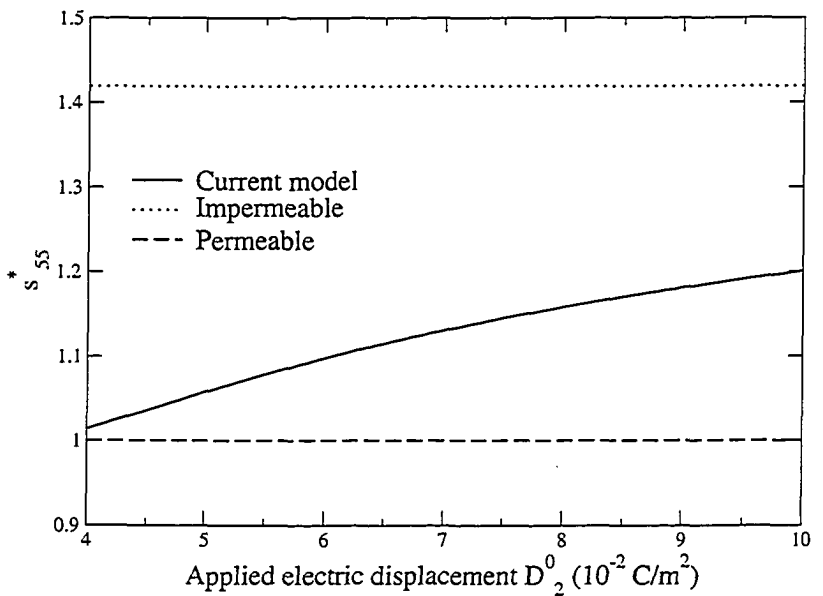

Figure 5.14: The variation of s^*_{55} with D^0_2 for different crack models

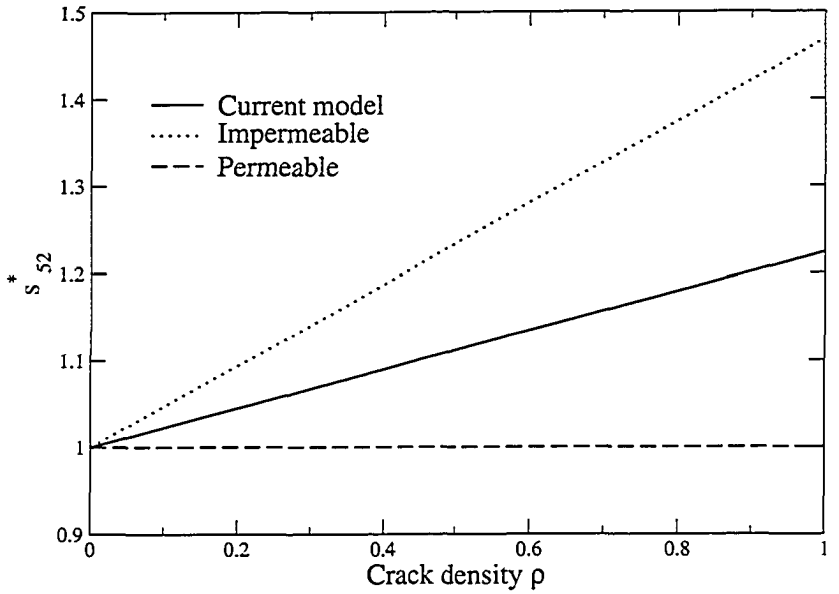

Figure 5.15: The variation of s^*_{52} with crack density for different crack models

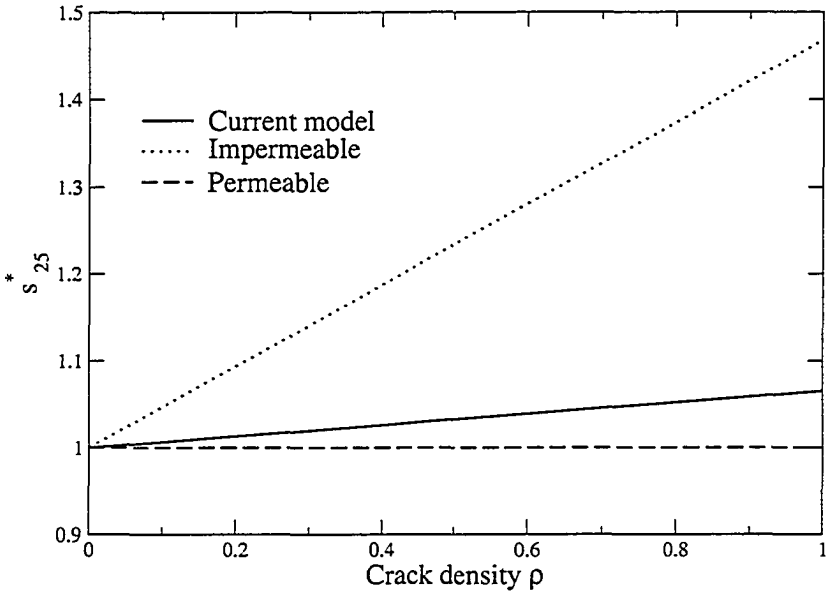

Figure 5.16: The variation of s^*_{25} with crack density for different crack models

Chapter 6

Limitation of the Current Dielectric Crack Model

Numerical simulations in previous chapters indicate that the fracture behaviour of cracked piezoelectric materials is very sensitive to the electric boundary condition along crack surfaces, which is governed by the deformation of the crack surfaces. For the dielectric crack model considered, the crack is assumed to be a slit crack without initial crack surface separation, and the electric boundary condition is totally governed by the crack opening displacement caused by the applied electromechanical loads. However, this is an ideal assumption ignoring the possible initial separation of the crack surfaces. The existence of the initial crack surface separation may have significant effect upon the electric boundary condition. It is, therefore, the objective of this chapter to study the relation between the dielectric crack model and the intermediate model with the electric boundary condition being governed by the initial crack surface separation.

6.1 Statement of the Problem

Consider the plane strain problem of an infinitely extended piezoelectric material containing a crack of length $2a$ as shown in Fig. 6.1. To investigate the effect of the initial separation of crack surfaces, the air (or vacuum) inside the crack is modelled as a thin dielectric layer with negligible elastic constant. The thickness of this layer is assumed to be h. A Cartesian coordinate system oxy is used to characterize the crack with the crack center being at the origin of the coordinate system, and crack surfaces being parallel to the x-axis. The poling direction of this piezoelectric material is assumed to be parallel to the y-axis direction. The medium is subjected to electromechanical loads $\mathbf{t}^0 = \{\sigma_{21}^0 \ \sigma_{22}^0 \ D_2^0\}^T$ at infinity. The original problem (a) in Figure 6.1 is decomposed into two sub-problems (b) and (c). The problem (c), in which we are interested, is subjected to both electric and mechanical loads along crack surfaces.

Similar to the traditional crack problem, the following traction-free condition along crack surfaces should be satisfied,

$$\sigma_{2i}^+ = \sigma_{2i}^- = \sigma_{2i}, \quad \sigma_{2i}(x,0) = -\sigma_{2i}^0 \ \ (i=1,2), \ |x| \le a \tag{6.1.1}$$

with superscripts $+$ and $-$ representing the upper and lower crack surfaces, respectively.

The electric boundary condition along crack surfaces can be expressed as (Parton and Kudryavtsev, 1988; Dascalu and Homentcovschi, 2002),

$$D_2^+ = D_2^- = D_2, \quad D_2(x,0) + \frac{\epsilon_0}{h}(V^+(x,0) - V^-(x,0)) = -D_2^0 \tag{6.1.2}$$

with V being the electric potential along crack surfaces and ϵ_0 being the dielectric constant of the air (vacuum) inside the crack. When $\frac{\epsilon_0}{h}$ is very "large" or "small", the crack reduces to permeable and impermeable ones, respectively.

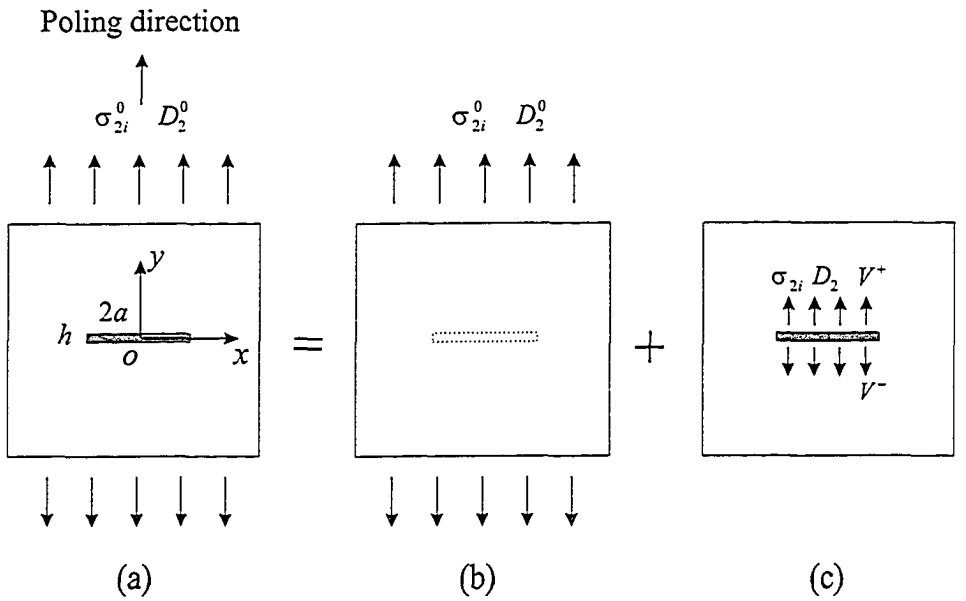

Figure 6.1: The intermediate crack model and the decomposition of the problem

6.2 Formulation of the Problem

As discussed in Chapter 3, the stress and electric displacement fields along crack line can be represented in terms of the dislocation density function $\mathbf{d}'$ defined by Equation

(3.2.3),

$$\mathbf{t}(x,0) = \frac{\mathbf{H}^{-1}}{\pi}\int_{-a}^{a}\frac{\mathbf{d}'(w,0)}{w-x}dw \tag{6.2.1}$$

where the elements of material constant matrix $\mathbf{H}$ are given in the Appendix of Chapter 3.

Substituting Equation (6.2.1) into equations (6.1.1) and (6.1.2), the following singular integral equations for boundary conditions can be obtained,

$$\frac{1}{\pi}\int_{-a}^{a}\frac{\mathbf{\Gamma}'(w,0)}{w-x}dw + \mathbf{KH\Gamma}(x,0) = -\mathbf{t}^0(x,0) \tag{6.2.2}$$

where $\mathbf{K}$ is a 3×3 matrix with only one non-vanishing element of $k_{33} = \epsilon_0/h$, and

$$\mathbf{\Gamma}' = \mathbf{H}^{-1}\mathbf{d}' \tag{6.2.3}$$

Equation (6.2.2) is a singular integral equation, which can be solved by expanding $\mathbf{\Gamma}'$ using Chebyshev polynomials, as,

$$\mathbf{\Gamma}'(w,0) = \sum_{j=0}^{\infty}\mathbf{c}_j\frac{T_j(w/a)}{\sqrt{1-(w/a)^2}} \tag{6.2.4}$$

where $T_j(w/a)$ are Chebyshev polynomials of the first kind and $\mathbf{c}_j = \{c_1^j\ c_2^j\ c_3^j\}^T$ is an unknown vector to be determined. From the orthogonality condition of Chebyshev polynomials, the continuity condition $\mathbf{d}(x,0) = \mathbf{v}^+(x,0) - \mathbf{v}^-(x,0)$ leads to $\mathbf{c}_0 = 0$. Substituting Equation (6.2.4) into (6.2.2), the following algebraic equation for $\mathbf{c}_j$ is obtained,

$$\sum_{j=1}^{\infty}\mathbf{c}_j U_{j-1}(\frac{x}{a}) + \mathbf{KH}\sum_{j=1}^{\infty}\mathbf{c}_j\frac{a}{j}(-1)\sin(j\cos^{-1}\frac{x}{a}) = -\mathbf{t}^0(x,0), \quad |x|\le a \tag{6.2.5}$$

where $U_j(x/a)$ represents Chebyshev polynomials of the second kind.

If the Chebyshev polynomials in Equation (6.2.5) are truncated to the Nth term and the boundary condition are satisfied at N collocation points given by,

$$x_l = a\cos\left(\frac{l-1}{N-1}\pi\right), \quad l = 1, 2...N \tag{6.2.6}$$

then Equation (6.2.5) reduces to the following linear algebraic equations,

$$\sum_{j=1}^{N} \mathbf{c}_j \frac{\sin\left(\frac{j(l-1)\pi}{N-1}\right)}{\sin\left(\frac{(l-1)\pi}{N-1}\right)} - \mathbf{KH}\sum_{j=1}^{N} \mathbf{c}_j \frac{a}{j}\sin\left(\frac{j(l-1)\pi}{N-1}\right) = -\mathbf{t}^0(x_l, 0), \quad |x_l| \le a \tag{6.2.7}$$

After solving these algebraic equations, the electroelastic fields can be obtained for this intermediate crack model. Correspondingly, fracture parameters defined in Chapter 3 are derived as,

Stress and electric displacement intensity factors,

$$\mathbf{k} = \begin{Bmatrix} K_{II} \\ K_I \\ K_D \end{Bmatrix} = -\sqrt{\pi a} \begin{Bmatrix} \sum_{j=1}^{N} c_2^j \\ \sum_{j=1}^{N} c_1^j \\ \sum_{j=1}^{N} c_3^j \end{Bmatrix} \tag{6.2.8}$$

Crack opening displacement (COD) intensity factor,

$$K_{COD} = \sqrt{\frac{2}{\pi}}\{h_{21}\ h_{22}\ h_{23}\}\mathbf{k} \tag{6.2.9}$$

with h_{21}, h_{22} and h_{23} being the elements of matrix $\mathbf{H}$.

These fracture parameters will be used to study the effect of the initial crack surface separation upon the fracture behaviour of cracked piezoelectric media and show the relation between different crack models.

6.3 Effect of the Initial Crack Surface Separation

As indicated by Equation (6.1.2), the intermediate crack model provides a way to evaluate the effect of the initial crack surface separation, but ignores the effect of the deformation of the crack surface. Whether the crack opening displacement or the initial crack surface separation is dominant depends on the applied electromechanical loading level. Therefore, the validity of this intermediate crack model or that of the nonlinear dielectric crack model is studied by comparing the initial crack surface separation and the crack opening displacement.

Figure 6.2 provides the normalized crack opening displacement $d_2/a(a = 1mm)$ with the variation of the applied stress σ_{22}^0 for different initial crack surface separation with $E_2^0 = 500V/mm$. The normalized crack opening displacement for the nonlinear dielectric crack model is also provided for comparison. This figure indicates that the effect of the initial crack surface separation upon the crack surface deformation is insignificant, i.e. the crack opening displacement derived from the intermediate and nonlinear dielectric crack models are comparable for a wide range of applied loading. It is interesting to compare the initial crack surface separation with the opening displacement of the crack caused by the applied loads. For very small initial crack surface separation, $h/a = 10^{-4}$ for example, the crack surface deformation is more important in formulating the electric boundary condition along the crack surfaces, as evidenced by the fact that the crack opening displacement is much higher than the initial crack surface separation even for small applied stress ($\sigma_{22}^0 = 2MPa$ for example). For the case where $h/a = 10^{-3}$, the crack opening displacement due to the applied loading is

lower or comparable with the initial crack surface separation until σ_{22}^0 approaches approximately $20MPa$, indicating the importance of considering the initial crack surface separation. For high initial crack surface separation, $h/a = 10^{-2}$, the crack surface condition is dominant by the initial crack surface separation. It is concluded from this figure that whether to apply the nonlinear dielectric crack model or the intermediate crack model depends on both the applied electromechanical loads and the initial crack surface separation. The comparison of electric displacement intensity factor K_D for these two crack models and traditional permeable and impermeable models is plot in Figure 6.3. It indicates that there is significant discrepancy between these two models when the initial crack surface separation is large ($h/a = 10^{-2}$), especially for low loading level as predicted. The result for this intermediate crack model is very close to that of the impermeable model, while the result of the nonlinear dielectric crack model approaches that of the impermeable model only when the loading is very high. The application of the nonlinear dielectric crack model is limited for the cases where the initial crack surface separation is very big or the applied loading level is very low.

When the applied stress level is very low, the crack opening displacement caused by this loading is compared with the initial crack surface separation in Figure 6.4. It is clearly identified that for this specific case the initial crack surface separation is dominant and, therefore, important to formulate the electric boundary condition. The electric displacement intensity factors K_D are plot in Figure 6.5 to show the effect of the initial crack surface separation upon the electric boundary condition and fracture behaviour. This figure demonstrates the importance of considering the initial crack

surface separation in formulating the electric boundary condition for some loading conditions.

To predict the effect of applied electric field E_2^0 on the crack deformation, the variation of COD intensity factor K_{COD} with applied electric field is graphed in Figure 6.6 under different crack surface conditions for the case of very low tensile stress level ($\sigma_{22} = 1MPa$). It can be observed that K_{COD} increases monotonically with increasing electric field for the intermediate crack model and nonlinear dielectric model, indicating that applied positive electric field tends to enhance crack propagation, while negative electric field will impede it. It should be noted that K_{COD} is negative when the electric field is negative, which implies that negative applied electric field inclines to decrease the crack surface separation based on this intermediate crack. However, the crack still keeps open, which is clearly identified in Figure 6.7. For example, when $h/a = 10^{-2}$ or $h/a = 10^{-3}$, the negative crack opening displacement caused by applied electromechanical loads is less than the initial crack surface separation, which results in a opening crack.

6.4 Conclusions

The effect of initial crack surface separation upon the electric boundary condition is studied based on an intermediate crack model. It can be observed that this initial crack surface separation may play a significant role in predicting the fracture behaviour of cracked piezoelectric materials in some cases. This study indicates that the application of the nonlinear dielectric crack model is limited when the crack

surface condition is dominant by the initial crack surface separation over the crack surface deformation.

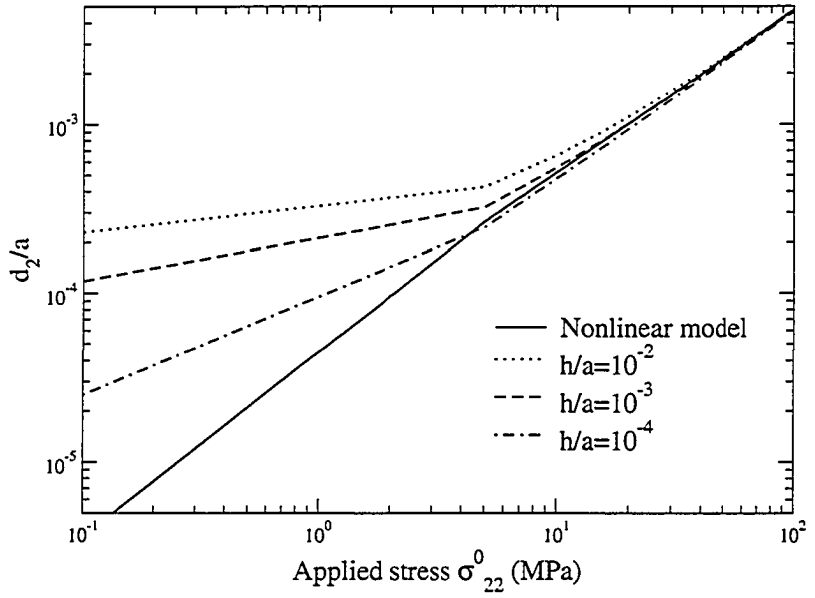

Figure 6.2: The normalized crack opening displacement for different crack models

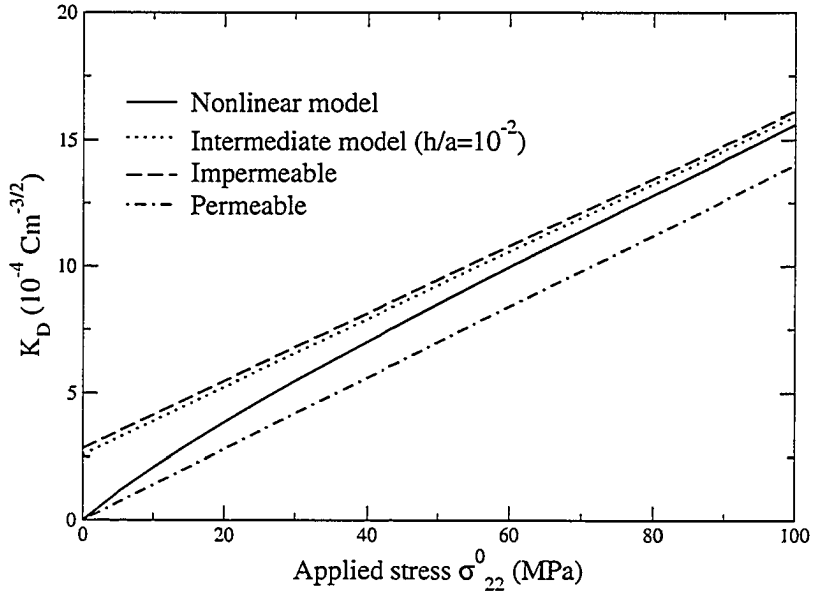

Figure 6.3: The variation of K_D with applied tensile stress

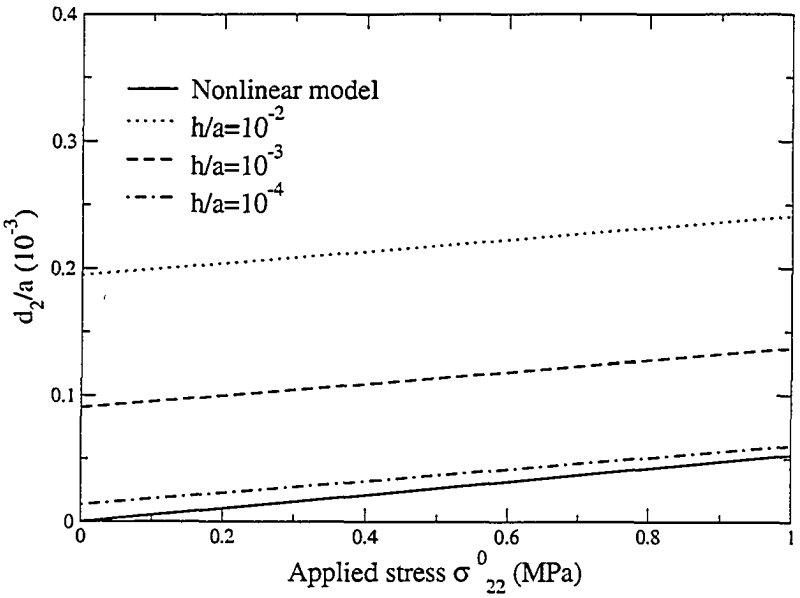

Figure 6.4: The normalized crack opening displacement for different crack models subjected to low tensile stress

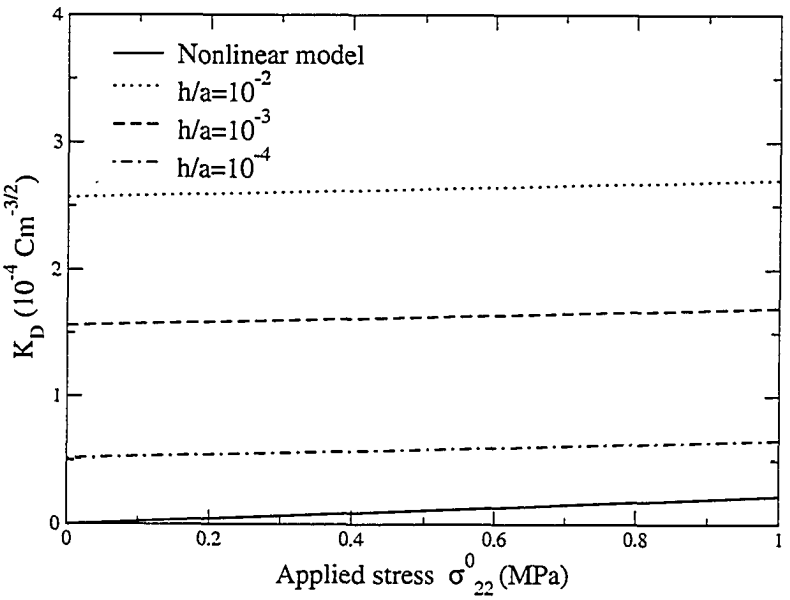

Figure 6.5: The variation of K_D for different crack models subjected to low tensile stress

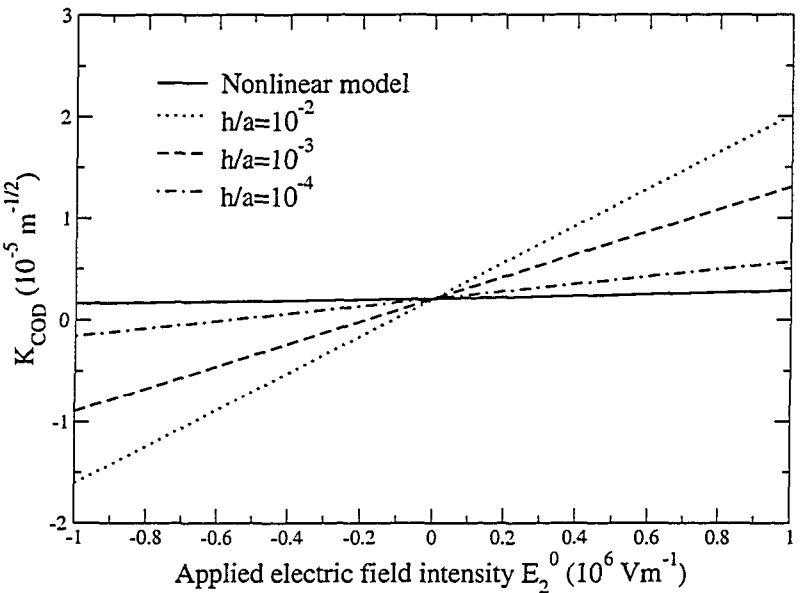

Figure 6.6: The variation of K_{COD} with E_2^0 for different crack models under low tensile stress

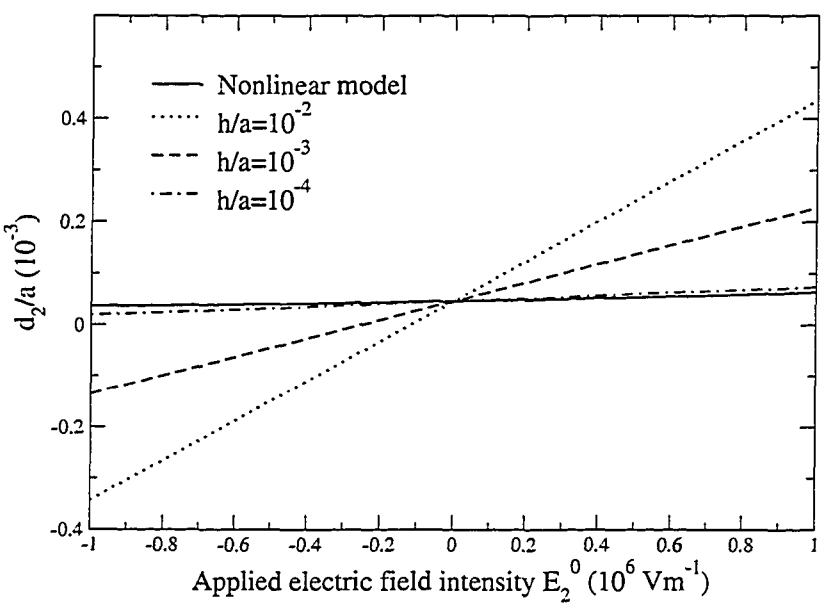

Figure 6.7: The variation of d_2/a with E_2^0 for different crack models under low tensile stress

Chapter 7

Conclusions and Suggestions for Future Study

7.1 Contributions and Conclusions

This dissertation provides a systematical theoretical study of the nonlinear fracture behaviour of cracked piezoelectric materials subjected to different electromechanical loads. The contributions of this work are summarized as the follows:

(i) A dielectric crack model, using the 'real' electric boundary condition containing the effects of both normal and tangential displacements of the crack surfaces, is proposed. Based on this deformation-dependent crack model, the electroelastic fields of cracked piezoelectric materials are obtained by using Fourier transform technique.

(ii) Based on the proposed dielectric crack model, numerical simulations are conducted to study the problems of an arbitrarily oriented crack, interacting dielectric cracks and the effective electroelastic property of cracked piezoelectric materials. The results demonstrate how the 'real' electric boundary condition

affects the fracture behaviour of cracked piezoelectric materials.

(iii) Unlike the results from the traditional impermeable and permeable crack models, nonlinear response and multiple deformation modes of the dielectric crack are predicted in response to different loading conditions.

(iv) To evaluate the effect of applied electric field upon the crack propagation, a COD intensity factor K_{COD} which describes the mechanical deformation of the crack, is introduced. By using K_{COD} as a fracture parameter, it can be concluded that an applied positive electric field (perpendicular to crack surfaces) tends to enhance crack propagation, while an applied negative electric field will impede it. This prediction agrees with the experimental results given by Park and Sun (1994; 1995a, b), and avoids the confusion when energy release rate is used, which predicts that the applied electric field will always impede crack growth.

(v) The relation between existing crack models and the current model is studied to demonstrate the importance of taking into account of the crack deformation in formulating the electric boundary condition along the crack surfaces.

Specific conclusions can be drawn from the results obtained in this work,

(i) It is found that the crack opening displacement has a significant effect upon the electric boundary condition along the crack surfaces. As a result, the fracture behaviour of cracked piezoelectric materials is deformation-dependent and sensitive to applied electromechanical loading.

(ii) With the change of applied loads (or crack opening displacement), the transition between the electrically permeable and impermeable crack models is clearly observed. Numerical results indicate that the commonly used permeable and impermeable crack models represent two limiting cases of physical problems, which may not be suitable for predicting the fracture behaviour of cracked piezoelectric media in some cases.

7.2 Future Studies

The methodology introduced in this work can be extended to a wide class of problems dealing with cracked materials with electromechanical coupling. Based on the results and discussions in this work, additional investigations are suggested to be further conducted.

(i) The current study is limited to the cases where the cracked piezoelectric medium is subjected to static electromechanical loading conditions. In spite of the fact that piezoelectric materials are mostly being used or considered for use in situations involving dynamic loading, the dynamic fracture behaviour of cracked piezoelectric materials has received much less attention. Existing work has been focussed mostly on the traditional impermeable and permeable crack models. Further investigation on the dynamic fracture behaviour of dielectric cracks in piezoelectric materials will be an important issue for the design and application of piezoelectric materials in smart structures and systems. Due to the

complexity caused by the dynamic formulation and the electromechanical coupling, appropriate mathematical treatment of the nonlinear electric boundary condition is required for numerical simulations.

(ii) With the widespread use of piezoelectric materials in structural applications, the reliability of these materials may inevitably depend on the ambient temperature or thermal disturbance. As a result, it would be important to incorporate the thermal effect into the electromechanical coupling to study the fracture behaviour of piezoelectric materials. The existing studies on cracked piezoelectric materials with consideration of thermal effect are limited to using traditional crack models. How the 'real' electric boundary condition affect the coupling among mechanical, electric and thermal fields of cracked piezoelectric materials is still unknown and needs further investigations.

(iii) Some piezoelectric materials are known to exhibit strong electric nonlinearity when subjected to high electromechanical loading. Therefore, it is necessary to consider the nonlinear behaviour at the crack tip, an area with high electroelastic concentration. The nonlinear behaviour associated with both the crack deformation discussed in this work and the material nonlinearity should be studied.

(iv) To overcome the unexplained discrepancies between theory and experiments, new fracture criteria need to be developed. Most existing fracture criteria are based on the assumption that the crack will propagate at a self-similar way. However, the results in the current work indicate that crack orientation (or

poling direction) and applied electromechanical loading play significant roles in the fracture behaviour of cracked piezoelectric materials. As a result, how to predict the propagation of an arbitrarily oriented crack under combined electromechanical loads is much more complicated and new criteria are needed.

(v) Extensive experimental work is needed to study the nonlinear fracture behaviour of cracked piezoelectric materials and verify the corresponding fracture criteria to predict crack growth. Existing experimental studies are mostly limited to the cases where the poling direction has a specific orientation with the crack, i.e., perpendicular or parallel to crack surfaces. How the fracture behaviour of cracked piezoelectric materials vary with loading conditions and the poling direction should be further investigated.

Bibliography

[1] Aboudi, J. and Benveniste, Y., 1987, "The effective moduli of cracked bodies in plane deformations", *Engineering Fracture Mechanics*, 26: 171-184.

[2] Allik, H. and Hughes, T. J. R., 1970, "Finite element method for piezoelectric vibration", *International Journal of numerical methods in engineering*, 2: 151-157.

[3] Ashley, S., 1995, "Smart skis and other adaptive structures", *Mech. Engng*, 11: 76-81.

[4] Barnette, D. M. and Lothe, J., 1975, "Dislocations and line charges in anisotropic piezoelectric insulators", *Physica Status Solidi*, 67: 105-111.

[5] Barsoum, R. G. S., 1997, "Active materials and adaptive structures", *Smart Materials and Structures*, 6: 117-122.

[6] Benveniste, Y., 1986, "On the Mori-Tanaka's method in cracked bodies", *Mechanics Research Communication*, 13: 193-201.

[7] Beom, H. G., 2003, "Permeable cracks between two dissimilar piezoelectric materials", *International Journal of Solids and Structures*, 40: 6669-6679.

[8] Bibly, B. A. and Eshelby, J. D., 1968, "Dislocation and theory of fracture", *Fracture An Advanced Treaties*, Liebowitz, H. ed. Academic Press, New York, 1: 99-182.

[9] Bristow, J.R., 1960, "Microcracks and the static and dynamic elastic constants of annealed and heavily cold-worked metals", *British Journal of Applied Physics*, 11: 81-85.

[10] Buchanan, J. P., 1956, "Handbook of Piezoelectric Crystals for Radio Equipment Designers", Wright Air Development Center, National Technical Information Services Springfield Virginia.

[11] Budiansky, Y. and O'Connell, R. J., 1976, "Elastic moduli of a cracked solid", *International Journal of Solids and Structures*, 12: 81-92.

[12] Cady, W.G., 1922, "The piezoelectric resonator", *Proceedings of I.R.E.*, 10: 83-114.

[13] Cady, W.G., 1946, "Piezoelectricity", McGraw-Hill Book Co. Inc., New York, New York.

[14] Chen, T., 1994, "Micromechanical estimates of the overall thermoelectricelastic moduli of multiple fibrous composites", *International Journal of Solids and Structures*, 31: 3099-3111.

[15] Chen, Y. H. and Han, J. J., 1999a, "Macrocrack-Microcrack interaction in piezoelectric materials, Part I: Basic formulations and J-analysis", *Journal of Applied Mechanics, Transactions of the ASME*, 66: 514-520.

[16] Chen, Y. H. and Han, J. J., 1999b, "Macrocrack-Microcrack interaction in piezoelectric materials, Part II: Numerical results and discussions", *Journal of Applied Mechanics, Transactions of the ASME*, 66: 522-527.

[17] Chen, Z. T. and Yu, S. W., 1997, "Antiplane dynamic fracture mechanics in piezoelectric materials", *International Journal of Fracture*, 85: L3-L12.

[18] Chen, Z. T. and Karihaloo, B. L., 1999, "Dynamic response of a cracked piezoelectric ceramic under arbitrary electro-mechanical impact", *International Journal of Solids and Structures*, 36: 5125-5133.

[19] Chen, Z. T. and Worswick, M. J., 2000, "Antiplane mechanical and in-plane electric time-dependent load applied to two coplanar cracks in piezoelectric ceramic material", *Theoretical and Applied Fracture Mechanics*, 33: 173-184.

[20] Cherepanov, G. P., 1979, "Mechanics of Brittle Fracture", McGraw-Hill, New York, New York.

[21] Chung, M. Y. and Ting, T. C. T., 1996, "Piezoelectric solid with an elliptic inclusion or hole", *International Journal of Solids and Structures*, 33: 3343-3361.

[22] Curie, J. and Curie, P., 1880,"Development par compression de l'eletricite polaire dans les cristaux hemiedres a faces inclines", *Comptes Rendus Acad. Sci. Paris*, 91: 294-295.

[23] Curie, J. and Curie, P., 1884, "Contractions et dilations productes par des tensions electriques dans les cristaux hemiedres a faces inclines", *Comptes Rendus Acad. Sci. Paris*, 93: 1137-1139.

[24] Dascalu, C. and Homentcovschi, D., 2002, "An intermediate crack model for flaws in piezoelectric solids", *Acta Mechanica*, 154: 85-100.

[25] Deeg, W. E. F., 1980, "The Analysis of Dislocation, Crack, and Inclusion Problems in Piezoelectric Solids", Ph.D thesis, Stanford University.

[26] Ding, H. J., Wang, G. and Chen, W., 1998, "A boundary integral formulation and 2D fundamental solutions for piezoelectric media", *Computational Methods in Applied Mechanical Engineering*, 158: 65-80.

[27] Dosch, J., Lesieutre, G., Koopmann, G. and Davis, C., 1995, "Inertial piezoceramic actuators for smart structures", *SPIE*, 2447: 14-25.

[28] Dunn, M. L. and Taya, M., 1993a, "Micromechanics predictions of the effective electro-elastic moduli of piezoelectric composites", *International Journal of Solids and Structures*, 30: 161-175.

[29] Dunn, M. L. and Taya, M., 1993b, "Electromechanical properties of porous piezo-electric ceramics", *Journal of American Ceramics Society*, 76(7): 1697-1706.

[30] Dunn, M. L., 1994, "The effects of crack face boundary conditions on the fracture mechanics of piezoelectric solids", *Engineering Fracture Mechanics*, 48: 25-39.

[31] Erdogan, F., 1975, "Complex Function Technique. In: Continuum Physics", Vol. II, Academic Press, New York, New York.

[32] Freiman, S. W. and Pohanka, R. C., 1989, "Review of mechanically related failures of ceramic capacitors and capacitor materials", *Journal of American Ceramic Society*, 72: 2258-2263.

[33] Gandhi, M. V. and Thompson, B. S., 1992, "Smart Materials and Structures", Chapman & Hall, London.

[34] Gao, C. F. and Yu, J. H., 1998, "Two-dimensional analysis of a semi-infinite crack in piezoelectric media", *Mechanics Research Communications*, 25: 695-700.

[35] Gao, C. F. and Wang, M. Z., 2000, "Collinear permeable cracks between dissimilar piezoelectric materials", *International Journal of Solids and Structures*, 37: 4949-4967.

[36] Gao, C. F., Zhao, Y. T. and Wang, M. Z., 2001, "Moving antiplane crack between two dissimilar piezoelectric media", *International Journal of Solids and Structures*, 38: 9331-9345.

[37] Grekov, A. A., Kramarov, S. O. and Kuprienko, A. A., 1989, "Effective properties of a transversely isotropic piezocomposite with cylindrical inclusions", *Ferroelectrics*, 99: 115-126.

[38] Gu, B., Yu, S. W. and Feng, X. Q., 2002, "Transient response of an interface crack between dissimilar piezoelectric layers under mechanical impacts", *International Journal of Solids and Structures*, 39: 1743-1756.

[39] Han, X. L. and Wang, T. C., 1999. "Interacting multiple cracks in piezoelectric materials", *International Journal of Solids and Structure*, 36: 4183-4202.

[40] Hashin, Z., 1988, "The differential scheme and its application to cracked materials", *Journal of Mechanics and Physics of Solids*, 36: 719-734.

[41] Hori, H. and Nemat-Nasser, S., 1983, "Overall moduli of solids with microcracks: load-induced anisotropy", *Journal of Mechanics and Physics of Solids*, 33: 155-171.

[42] Horii, H. and Nemat-Nasser, S., 1987, "Interacting micro-crack near the tips in the process zone of a macro-crack", *Journal of the Mechanics and Physics of Solids*, 35: 601-629.

[43] Huang, Y. and Hu, K. X., Chandra, A., 1994, "A generalized self-consistent mechanics method for microcracked solids", *Journal of Mechanics and Physics of Solids*, 42: 1273-1291.

[44] Huang, H. M., Shi, H. J. and Yin, Y. J., 2002, "Multi-cracks problem for piezoelectric materials strip subjected to dynamic loading", *Mechanics Research Communications*, 29: 413-424.

[45] Hutchinson, J. W., 1987, "Crack tip shielding by micro-cracking in brittle solids", *Acta Metallurgica*, 35: 1605-1619.

[46] Irwin, G. R., 1957, "Analysis of stresses and strains near the end of a crack traversing a Plate", *Journal of Applied Mechanics*, 24: 361-364.

[47] Jain, A. K. and Sirkis, J. S., 1994, "Continuum damage mechanics in piezoelectric ceramics", *Adaptive Structures and Composite Materials: Analysis and Application*, AD45/MD54: 47-58.

[48] Kachanov, M., 1987, "Elastic solids with many cracks: a simple method of analysis", *International Journal of Solids and Structures*, 23: 23-44.

[49] Kachanov, M., 1992, "Effective elastic properties of cracked solids: critical review of some basic concepts", *Applied Mechanics Review*, 45: 304-335.

[50] Kachanov, M., 1993, "Elastic solids with many cracks and related problems", *Advanced Applied Mechanics*, 30: 259-428.

[51] Kumar, S. and Singh, R. N., 1996, "Crack propagation in piezoelectric materials under combined mechanical and electrical loadings", *Acta Metallurgica et Materialia*, 44: 173-200.

[52] Kumar, S. and Singh, R. N., 1997a, "Energy release rate and crack propagation in piezoelectric materials. Part I-Mechanical/electrical load", *Acta Materialia*, 45: 849-857.

[53] Kumar, S. and Singh, R. N., 1997b, "Energy release rate and crack propagation in piezoelectric materials. Part II-Combined mechanical and electrical loads", *Acta Materialia*, 45: 859-868.

[54] Kuo, C. M. and Barnett, D. M., 1991, "Stress singularities of interfacial cracks in bonded piezoelectric half-spaces", *Modern Theory of Anisotropic Elasticity and Applications (edited by J. J. Wu, Ting, T. C. T. and Barnett, D. M.)*: 33-50. SIAM Proceedings Series, Philadelphia, PA.

[55] Lekhnitskii, S. G., 1963. "Theory of Elasticity of an Anisotropic Elastic Body", Holden-Day, Inc., San Francisco.

[56] Li, S. and Mataga, P. A., 1996a, "Dynamic crack propagation in piezoelectric materials-Part I. Electrode solution", *Journal of the Mechanics and Physics of Solids*, 44(11): 1799-1830.

[57] Li, S. and Mataga, P. A., 1996b, "Dynamic crack propagation in piezoelectric materials-Part II. Vacuum solution", *Journal of the Mechanics and Physics of Solids*, 44(11): 1831-1866.

[58] Lippmann, H.G., 1881, "Sur le principle de la conversation de l'eletricite ou second principle de la theorie des phenomenes electriques", *Comptes Rendus Acad. Sci*, Paris, 92: 1049-1050.

[59] Lu, P. and Mahrenholtz, O., 1994, "A variational boundary element formulation for piezoelectricity", *Mechanics Research Communication*, 21: 605-611.

[60] Mason, W.P., 1934, "Electrical wave filters employing quartz crystals as elements", *Bell Syst. Tech. J.*, XIII, 405-452.

[61] Mason, W.P., 1950, "Piezoelectric Crystals and Their Application to Ultrasonics", D. Van Nostrand Company, INC., New York.

[62] McHenry, K. D. and Koepke, B. G., 1983, "Electric field effects on subcritical growth in PZT", *Fracture Mechanics of Ceramics*, 5: 337-352.

[63] McMeeking, R. M., 1989, "Electrostrictive stresses near crack-like flaws", *Journal of Applied Mathematics and Physics*, 40: 615-627.

[64] McMeeking, R. M., 1990, "A J-integral for the analysis of electrically induced mechanical stress at cracks in elastic dielectrics", *International Journal of Engineering Science*, 28(7): 605-613.

[65] McMeeking, R. M, 1999, "Crack tip energy release rate for a piezoelectric compact tension specimen", *Engineering Fracture Mechanics*, 64: 217-244.

[66] Meguid, S. A. and Wang, X. D., 1995, "On the dynamic interaction between a microdefect and a main crack", *Proceedings of Royal Society of London, A*, 448: 449-464.

[67] Meguid, S. A. and Wang, X. D., 1998, "Dynamic antiplane behaviour of interacting cracks in a piezoelectric medium", *International Journal of Fracture*, 91(4): 391-403.

[68] Mehta, K. and Virkar, A. V., 1990, "Fracture mechanisms in ferroelectric-ferroelastic lead zirconate titanate (Zr:Ti=0.54:0.46) ceramics ", *Journal of American Ceramic Society*, 73: 567-574.

[69] Mikhailov, G. K. and Parton, V. Z., 1990, "Electromagnetoelasticity", Hemisphere, New York.

[70] Mori, T. and Tanaka, K., 1973, "Average stress in matrix and average elastic energy of materials with misfitting inclusions", *Acta Metallurgica*, 21: 571-574.

[71] Narita, F. and Shindo, Y., 1998, "Anti-plane shear crack growth rate of piezoelectric ceramic body with finite width", *Theoretical and Applied Fracture Mechanics*, 30: 127-132.

[72] Nemat-Nasser, S. and Hori, M., 1993, "Micromechanics: Overall Properties of Heterogeneous Materials", Amsterdam, North-Holland.

[73] Norris, A. N., 1985, "A differential scheme the effective moduli of composites", *Mechanics of Materials*, 4: 1-16.

[74] Pak, Y. E. and Herrmann, G., 1986, "Conservation law and the material momentum tensor for the elastic dielectric", *International Journal of Engineering Science*, 24(8): 1365-1374.

[75] Pak, Y. E., 1990, "Crack extension force in a piezoelectric material", *Journal of Applied Mechanics*, 57: 647-653.

[76] Pak, Y. E., 1992, "Linear electro-elastic fracture mechanics of piezoelectric materials", *International Journal of Fracture*, 54: 79-100.

[77] Pak, Y. E. and Goloubeva, E., 1995, "Influence of cracks on electroelastic properties of piezoelectric materials", *Adaptive Material System, ASME*, AMD-Vol. 206: 33-43.

[78] Park, S. and Sun, C. T., 1994, "Crack extension in piezoelectric materials", *SPIE*, 2189: 357-368.

[79] Park, S. B. and Sun, C. T., 1995a, "Effect of electric fields on fracture of piezoelectric ceramics", *International Journal of Fracture*, 70: 203-216.

[80] Park, S. and Sun, C. T., 1995b, "Fracture criteria for piezoelectric ceramics", *Journal of the American Ceramic Society*, 78: 1475-1480.

[81] Park, S. B. and Carman, G. P., 1997, "Minimizing stress levels in piezoelectric media containing elliptical voids", *Journal of Applied Mechanics*, 64: 466-470.

[82] Park, S. B., Park, S. S., Carman, G. P. and Hahn, H. T., 1998, "Measuring strain distribution during mesoscopic domain reorientation in a ferroelectric material", *Journal of Engineering Materials and Technology*, 120: 1-6.

[83] Parton, V. Z., 1976, "Fracture mechanics of piezoelectric materials", *Acta Astronaut*, 3: 671-683.

[84] Parton, V. Z. and Kudryavtsev, B.A., 1988, "Electromagnetoelasticity: Piezoelectrics and Electrically Conductive Solids", Gordon and Breach Science Publishers, New York

[85] Pierce, G.W., 1925, "Piezoelectric crystal oscillators applied to the precision measurement of the velocity of sound in air and CO_2 at high frequencies", *Proceedings of the American Academy of Arts and Science*, 60: 269-302.

[86] Pohanka, R. C. and Smith, P. L., 1988," Electronic Ceramics, Properties, Devices and Applications", (edited by Levinson, L. N.), Chapter 2, Marcel Dekker, New York.

[87] Polovinkina, I. B. and Ulitko, A. F., 1978, "On the equilibrium of piezoceramic bodies containing cracks", *TN* 18: 10-17.

[88] Qin, Q., Mai, Y. and Yu, S., 1998, "Effective moduli for thermopiezoelectric materials with microcracks", *International Journal of Fracture*, 91: 359-371.

[89] Qin, Q. H., 1999. "Thermopiezoelectric interaction of macro- and microcracks in piezoelectric medium", *Theoretical and Applied Fracture Mechanics*, 32: 129-135.

[90] Qin, Q. H. and Mai, Y. W., 1999, "A new thermoelectroelastic solution for piezoelectric materials with various openings", *Acta Mechanica*, 138: 97-111.

[91] Qin, Q. H., 2001, "Fracture Mechanics of Piezoelectric Materials", WIT press, Southampton, Boston.

[92] Rice, J. R., 1968, "A path independent integral and the approximate analysis of strain concentration by notches and cracks", *Journal of Applied Mechanics*, 35: 379-386.

[93] Rogacheva, N. N., 1994, "The Theory of Piezoelectric Shells and Plates", CRC Press, Boca Raton.

[94] Rubinstein, A. A., 1986, "Macrocrack-microdefect interaction", *ASME Journal of Applied Mechanics*, 53: 505-510.

[95] Shindo, Y., Ozawa, E. and Nowacki, J. P., 1990, "Singular stress and electric fields of a cracked piezoelectric strip", *Applied Electromagnetic Materials*, 1: 77-87.

[96] Shindo, Y, and Ozawa, E., 1990, "Dynamic analysis of a cracked piezoelectric material", *Mechanical Modeling of New Electromagnetic Materials* (Edited by Hsieh, R. K. T.), Elsevier, Amsterdam, 297-304.

[97] Shindo, Y. Katsura, H. and Yan, W., 1996, "Dynamic stress intensity factor of a cracked dielectric medium in a uniform electric field", *Acta Mechanica*, 117: 1-10.

[98] Singh, R. N. and Wang, H., 1995, "Adaptive materials system", *Proceedings of AMD, ASME*, 206: 85-95.

[99] Sosa, H. A. and Pak, Y. E., 1990, "Three dimensional eigenfunction analysis of a crack in a piezoelectric material", *International Journal of Solids and Structures*, 26(1): 1-15.

[100] Sosa, H., 1991, "Plane problems in piezoelectric media with defects", *International Journal of Solids and Structures*, 28: 491-505.

[101] Sosa, H., 1992, "On the fracture mechanics of piezoelectric solids", *International Journal of Solids and Structures*, 29: 2613-2622.

[102] Sosa, H. and Khutoryansky, N., 1996, "New developments concerning piezoelectric materials with defects", *International Journal of Solids and Structures*, 33(23): 3399-3414.

[103] Stroh, A. N., 1958, "Dislocations and cracks in anisotropic elasticity", *Philosophy Magazine*, 7: 625-646.

[104] Sunar, M. and Rao, S. S., 1999, "Recent advances in sensing and control of flexible structures via piezoelectric materials technology", *Applied Mechanics Review*, 52: 1-16.

[105] Suo, Z., 1991, "Mechanics concepts for failure in ferroelectric ceramics", *Smart Structures and Materials, ASME, edited by G. K. Haritos and A. V. Srinvassan, New York*, AD, 23: 1-6

[106] Suo, Z., Kuo, C. M., Barnett, D. M. and Willis, J.R., 1992, "Fracture mechanics for pieozoelectric ceramics", *Journal of Mechanics and Physics of Solids*, 40: 739-765.

[107] Tiersten, H. F., 1964, "Linear Piezoelectric Plate Vibrations", Plenum Press, New York, New York.

[108] Tobin, A. and Pak, Y.E., 1993, "Effect of electric fields on fracture behaviour of PZT ceramics", *SPIE North American Conference on Smart Structures and Materials*, Albuquerque, New Mexico, Feb. 1-4.

[109] Tsukrov, I. and Kachanov, M., 2000, "Effective moduli of an anisotropic material with elliptical holes of arbitrarily orientational distribution", *International Journal of Solids and Structures*, 37: 5919-5941.

[110] Varadan, V. K., Wu, Z., Bao, X. Q. and Varadan, V. V., 1993, "Light weight robot using piezoelectric motor, sensor and actuator", *Adaptive Structures and Material Systems*, AD, 35: 141-148.

[111] Voigt, W., 1890, "General theory of the piezo and pyroelectric properties of crystals", *Abh. Gott.*, 36: 1-5.

[112] Waanders, J. W., 1991, "Piezoelectric Ceramics: Properties and Applications", N. V. Philips' Gloeilampenfabrieken, Endhoven, NE and APC International Ltd., Mackeyville, PA.

[113] Wang, X. D. and Meguid, S. A., 2000a, "Effect of electromechanical coupling on the dynamic interaction of cracks in piezoelectric materials", *Acta Mechanica*, 143: 1-15.

[114] Wang, X. D. and Meguid, S. A., 2000b, "Modelling and analysis of the dynamic behaviour of piezoelectric materials containing interacting cracks", *Mechanics of Materials*, 32: 723-737.

[115] Wang, X. D., 2001, "On the dynamic behaviour of interacting interfacial cracks in piezoelectric media", *International Journal of Solids and Structures*, 38: 815-831.

[116] Wang, X. Y. and Yu, S. W., 2000, "Transient response of a crack in piezoelectric strip subjected to the mechanical and electrical impacts: mode-III problem", *International Journal of Solids and Structures*, 32: 5795-5808.

[117] Wang, X. Y. and Yu, S. W., 2001, "Transient response of a crack in piezoelectric strip subjected to the mechanical and electrical impacts: mode-I problem", *Mechanics of Materials*, 33: 11-20.

[118] Wang, Z. K. and Huang, S. H., 1995, "Fields near elliptical crack tip in piezoelectric ceramics", *Engineering Fracture Mechanics*, 51: 447-456.

[119] Weng, G., 1990, "The theoretical connection between Mori-Tanaka's theory and the Hashin-Shtrikman-Walpole bounds", *International Journal of Engineering Science*, 28: 1111-1120.

[120] Williams, M. L., 1957, "On the stress distribution at the base of a stationary crack", *Journal of Applied Mechanics*, 24: 109-114.

[121] Winzer, S. R., Shanker, N. and Ritter, A. P., 1989, "Designing cofired multilayer electrostrictive actuators for reliability", *Journal of the American Ceramic Society*, 72: 2246-2257.

[122] Wood, R.W. and Loomis, A.L., 1927, "The physical and biological effects of intense audible sound on living organisms and cells", *Phil. Mag.*, 4: 417-433.

[123] Xu, X. L. and Rajapakse, R. K. N. D., 1999, "Analytical solution for an arbitrarily oriented void/crack and fracture of piezoceramics", *Acta Materials*, 47(6): 1735-1747.

[124] Xu, X. L. and Rajapakse, R. K. N. D., 2001, "On a plane crack in piezoelectric solids", *International Journal of Solids and Structures*, 38: 7643-7658.

[125] Yang, F., 2001, "Fracture mechanics for a mode I crack in piezoelectric materials", *International Journal of Solids and Structures*, 38: 3813-3830.

[126] Yu, S. W. and Qin, Q. H., 1996a, "Damage analysis of thermopiezoelectric properties: Part I-Crack tip singularites", *Theoretical and Applied Fracture Mechanics*, 25: 263-277.

[127] Yu, S. W. and Qin, Q. H., 1996b, "Damage analysis of thermopiezoelectric properties: Part II. Effective crack model", *Theoretical and Applied Fracture Mechanics*, 25: 279-288.

[128] Zhang, T. Y. and Tong, P., 1996, "Fracture mechanics for a mode-III crack in a piezoelectric material", *International Journal of Solids and Structure*, 33: 343-359.

[129] Zhang, T.Y., Qian, C.F. and Tong, P., 1998, "Linear electro-elastic analysis of a cavity or a crack in a piezoelectric material", *International Journal of Solids and Structures*, 35: 2121-2149.

[130] Zimmerman, R. W., 1991, "Elastic moduli of a solid containing spherical inclusions", *Mechanics of Materials*, 12: 17-24.

List of Publications

[1] Wang, X. D. and Jiang, L. Y., 2004, "The nonlinear fracture behaviour of an arbitrarily oriented dielectric crack in piezoelectric materials", *Acta Mechanica* (accepted).

[2] Wang, X.D. and Jiang, L.Y., 2003, "The effective electroelastic property of piezoelectric media with dielectric cracks", *International Journal of Solids and Structures*, 40(20): 5287-5303.

[3] Wang, X.D. and Jiang, L.Y., 2002, "Fracture behaviour of cracks in piezoelectric media with electromechanically coupled boundary conditions", *Proceedings of the Royal Society of London, Series A*, 458: 2545-2560.

[4] Wang, X.D. and Jiang, L.Y., 2002, "Nonlinear behaviour of interacting dielectric cracks in piezoelectric materials", *International Journal of Solids and Structures*, 39: 585-560.

[5] Meguid, S.A., Wang, X.D., and Jiang, L.Y., 2002, "On the dynamic propagation of a finite crack in functionally graded materials", *Engineering Fracture Mechanics*, 69: 1753-1768.

[6] Jiang, L.Y. and Wang, X.D., 2001, "On the dynamic crack propagation in

an interphase with spatially varying elastic properties under inplane loading",
International Journal of Fracture, 114: 225-244.